

UNCLASSIFIED

AD NUMBER
AD907814
NEW LIMITATION CHANGE
TO Approved for public release, distribution unlimited
FROM Distribution authorized to U.S. Gov't. agencies only; Test and Evaluation; 29 DEC 1972. Other requests shall be referred to Air Flight Dynamics Lab., Wright-Patterson AFB, OH 45433.
AUTHORITY
AFWAL ltr, 11 Feb 1980

THIS PAGE IS UNCLASSIFIED

THIS REPORT HAS BEEN DELIMITED  
AND CLEARED FOR PUBLIC RELEASE  
UNDER DOD DIRECTIVE 5200.20 AND  
NO RESTRICTIONS ARE IMPOSED UPON  
ITS USE AND DISCLOSURE.

DISTRIBUTION STATEMENT A

APPROVED FOR PUBLIC RELEASE;  
DISTRIBUTION UNLIMITED.

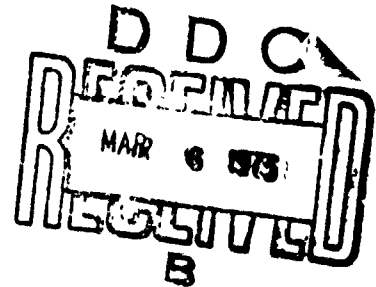
AD 907814 L

AFFDL-TR-72-147- VOL. I

**PROPULSION SYSTEM  
INSTALLATION CORRECTIONS**

**VOLUME I:  
ENGINEERS MANUAL**

**W. H. BALL  
THE BOEING COMPANY**



**TECHNICAL REPORT AFFDL-TR-72-147-VOL. I  
DECEMBER 1972**

Distribution limited to U. S. Government agencies only,  
test and evaluation, statement applied 29 December 1972.  
Other requests for this document must be referred to Air  
Force Flight Dynamics Laboratory (PTB), Wright-Patterson  
Air Force Base, Ohio 45433

**AIR FORCE FLIGHT DYNAMICS LABORATORY  
AIR FORCE SYSTEMS COMMAND  
WRIGHT-PATTERSON AIR FORCE BASE, OHIO 45433**

## NOTICE

When Government drawings, specifications, or other data are used for any purpose other than in connection with a definitely related Government procurement operation, the United States Government thereby incurs no responsibility nor any obligation whatsoever; and the fact that the Government may have formulated, furnished, or in any way supplied the said drawings, specifications, or other data, is not to be regarded by implication or otherwise as in any manner licensing the holder or any other person or corporation, or conveying any rights or permission to manufacture, use, or sell any patented invention that may in any way be related thereto.

Copies of this report should not be returned unless return is required by security considerations, contractual obligations, or notice on a specific document.

**PROPULSION SYSTEM  
INSTALLATION CORRECTIONS  
VOLUME I:  
ENGINEERS MANUAL**

**W. H. BALL**

Distribution limited to U.S. Government agencies only,  
test and evaluation; statement applied 29 December 1972.  
Other requests for this document must be referred to Air  
Force Flight Dynamics Laboratory (PTB), Wright-Patterson  
Air Force Base, Ohio 45433

## FOREWORD

This report was prepared by the Research and Engineering Division, Aerospace Group, of The Boeing Company under Air Force Contract F33615-72-C-1580, "Propulsion System Installation Corrections", Project 1366. The program was conducted under the direction of the Prototype Division, Air Force Flight Dynamics Laboratory, Air Force Systems Command. Mr. Gordon Tamplin was the Air Force Program Monitor.

The program was initiated on 31 December 1971 and draft copies of the final reports were submitted for approval on 31 October 1972.

Dr. P. A. Ross was Program Manager and Mr. W. H. Ball was principal investigator during the program. Significant contributions to the program were made by the following individuals: Mr. Joe Zeeben, engine performance; Dr. Franklin Marshall, inlet and exhaust system technology; Mr. John Petit, nozzle internal performance and nozzle/afterbody drag; and Mr. Gary Shurtleff, programming.

This report contains no classified information extracted from other classified reports.

Publication of this report does not constitute Air Force approval of the report's findings or conclusions. It is published only for the exchange and stimulation of ideas.



---

Lt. Col. Ernest J. Cross, Jr.  
Chief, Prototype Division  
Air Force Flight Dynamics Laboratory

## ABSTRACT

This report presents the results of a research program to develop a procedure for calculating propulsion system installation losses. These losses include inlet and nozzle internal losses and external drag losses for a wide variety of subsonic and supersonic aircraft configurations up to Mach 4.5. The calculation procedure, which was largely developed from existing engineering procedures and experimental data, is suitable for preliminary studies of advanced aircraft configurations. Engineering descriptions, equations, and flow charts are provided to help in adapting the calculation procedures to digital computer routines. Many of the calculation procedures have already been programmed on the CDC 6600 computer. Program listings and flow charts are provided for the calculation procedures that have been programmed. The work accomplished during the program is contained in four separate volumes. Volume I contains an engineering description of the calculation procedures. Volume II is a programmers manual containing flow charts, listings, and subroutine descriptions. Volume III contains sample calculations and sample input data. Volume IV contains bookkeeping definitions and data correlations.

## TABLE OF CONTENTS

SECTION		Page
I	INTRODUCTION	1
II	SUMMARY	4
III	PROPULSION SYSTEM PERFORMANCE	5
	3.1 General Description	5
	3.2 Calculations Using Tabulated Engine Data	9
	3.2.1 Thermodynamic Properties	11
	3.2.2 Energy Balance for Exhaust Gas Calculation	12
	3.2.3 Nozzle Gross Thrust Calculation	13
	3.2.4 Nozzle Pressure Ratio Calculation	15
	3.2.5 Inlet Recovery Correction	16
	3.3 Calculations Using Engine Cycle Match Deck	16
	3.4 Other Program Options	24
	3.4.1 Inlet and Nozzle Performance Maps	24
	3.4.2 Engine Manufacturers Nozzle Internal Performance	24
	3.4.3 Externally Generated $C_v$ Input	24
	3.4.4 Nozzle Internal Performance Subroutine	24
IV	INLET PERFORMANCE	25
	4.1 General Description	25
	4.2 Total Pressure Recovery	33
	4.2.1 Low Speed	33
	4.2.2 Subsonic and Transonic	42
	4.2.3 Supersonic	43

TABLE OF CONTENTS (Continued)

SECTION	Page	
4.3	Boundary Layer Bleed Drag	48
	4.3.1 Airflow	51
	4.3.2 Recovery	51
	4.3.3 Drag	51
4.4	Bypass Drag	68
4.5	Spillage Drag	71
	4.5.1 Theoretical Additive Drag	71
	4.5.2 $K_{ADD}$ Factors	74
4.6	Angle-of-Attack Effects	74
V	NOZZLE/AFTERBODY PERFORMANCE	86
5.1	Nozzle Internal Performance	86
	5.1.1 Convergent	86
	5.1.2 Convergent-Divergent	88
	5.1.3 Ejector	88
	5.1.4 Plug	91
5.2	Nozzle/Afterbody Drag	91
	5.2.1 Boattail Drag	92
	5.2.2 Interference Drag	101
	5.2.3 Base Drag	106
	5.2.4 Scrubbing Drag	110
5.3	Angle-of-Attack Effects	115
5.4	Installation Effects of Thrust Vector Control & Thrust Reversers	117

TABLE OF CONTENTS (Continued)

SECTION	Page
REFERENCES	122
APPENDIX	
ENGINEERING FLOW CHARTS	126

## LIST OF ILLUSTRATIONS

Figure No.	Title	Page
1	PITAP Procedure	2
2	PITAP Procedure Using Performance Maps	6
3	PITAP Procedure Using Program Subroutines	7
4	PITAP Procedure as an Independent Program	8
5	Output Format for PITAP (Cycle match deck version)	19
6	Inlet Performance Procedure	26
7	Inlet Performance Elements	27
8	Inlet Subprogram	29
9	Performance Calculation for an External-Compression Inlet	30
10	Performance Calculation for a Mixed-Compression Inlet	31
11	Nomenclature for Low-Speed Inlet Lip Losses	34
12	Corrected Airflow Parameter	36
13	Isentropic Area Ratio	38
14	Effective Inlet Throat Mach Number	39
15	Subsonic Diffuser Loss Factors	41
16	Diffuser Loss Coefficient for a Two-Dimensional Diffuser	44
17	Shock Loss Data	46
18	Shock Flow Deflections	47
19	Maximum Inviscid Total Pressure Recovery for Axisymmetric Inlets (External Compression)	49

LIST OF ILLUSTRATIONS (Continued)

Figure No.	Title	Page
20	Maximum Inviscid Total Pressure Recovery for Axisymmetric Inlets (External and Internal Compression)	50
21	Boundary Layer Bleed	52
22	Plenum Total Pressure Recovery	53
23	Effect of Turbulent Boundary Layer on Bypass Flap Angle	63
24	Bypass Door Pressure Coefficients	64
25	Bypass Airflow Total Pressure Recovery	69
26	Additive Drag of a Pitot Inlet	72
27	Additive Drag of a Two-Dimensional Inlet	73
28	Reference Ramp Drag	75
29	Additive Drag of an Axisymmetric Inlet	76
30	Pressure Drag on Cones in Transonic Flow	77
31	Mach Number Correction Factor for Two-Dimensional Wings	79
32	Effect of Angle-of-Attack on Inlet Local Mach Number (Two-Dimensional Wing)	80
33	Effect of Angle-of-Attack on Stream Tube Area for a Two-Dimensional Wing	81
34	Effect of Angle-of-Attack on Total Pressure Recovery Under a Two-Dimensional Wing	82
35	Effect of Angle-of-Attack on Local Inlet Mach Number for an Under-Fuselage Mounted Inlet	84
36	Effect of Angle-of-Attack on Local Inlet Total Pressure Recovery for an Under-Fuselage Mounted Inlet	85
37	Nozzle/Afterbody Calculation Procedure	87

## LIST OF ILLUSTRATIONS (Continued)

Figure No.	Title	Page
38	Conical Convergent/Divergent Nozzle Non-Isentropic Expansion Loss	89
39	Nozzle/Afterbody Drag Representation	93
40	Nozzle/Afterbody Drag Subprogram	94
41	Nozzle Boattail Pressure Drag Coefficients as $f(\beta)$	95
42	Boattail Drag Correction for Nozzle Pressure Ratios	96
43	Supersonic Boattail Drag Correlation	97
44	Nozzle/Afterbody Drag Coefficients as $f(A_9/A_{10})$	98
45	Definition of an Equivalent Nozzle	100
46	Nozzle Interference Drag Coefficient	102
47	Installation Effects for Plug and Convergent-Divergent Nozzles	103
48	Effect of Nozzle Pressure Ratio on Aft Fuselage Drag - Mach 0.95	105
49	Correlation of Incremental Base Pressure Due to Propulsive Jet as a Function of Jet to Base-to-Maximum Body Diameter Function	107
50	Annular Supersonic Base Pressure Correlations	109
51	Reference Base Pressure Ratio	111
52	Correlation of Base Pressure Data for Supersonic Flow	112
53	Velocity Regions for Scrubbing Drag Calculations	114

## LIST OF ILLUSTRATIONS (Continued)

Figure No.	Title	Page
54	Core Length and Velocity Decay Constants	116
55	Flow Chart for Inlet Performance	127
56	Inlet Functions	128
57	Flow Chart for Inlet Sizing Subroutine	129
58	Flow Chart for Scheduled-Bypass Mode	130
59	Flow Chart for Scheduled-Spillage Mode	131
60	Flow Chart for Low Speed Inlet Performance Calculation	132
61	Flow Chart for Subsonic and Transonic Inlet Internal Performance Calculation	133
62	Flow Chart for Shock Loss Calculation	134
63	Flow Chart for Boundary Layer Bleed Calculation.	135
64	Flow Chart for Momentum Drag Calculation	136
65	Flow Chart for Bypass Flap Drag Calculation	137
66	Flow Chart for Nozzle Internal Performance Subroutine	138

## LIST OF TABLES

Table	Title	Page
I	Calculation Procedure Options	3
II	Thermodynamic Subroutines	11
III	Engineering Assumptions for Boundary Layer Bleed and Bypass Exits	70
IV	Performance and Weight Changes Due to Thrust Vectoring and Reversing Installations	118

## SYMBOLS AND NOMENCLATURE

A	Area, in <sup>2</sup>
A <sub>C</sub>	Inlet capture area, in <sup>2</sup>
A <sub>O</sub>	Local stream tube area ahead of the inlet, in <sup>2</sup>
A <sub>O<sub>I</sub></sub>	Free-stream tube area of air entering the inlet, in <sup>2</sup>
<b>R</b>	Aspect ratio, dimensionless
B	Velocity decay exponent, dimensionless
C	Sonic velocity; ft/sec.
C <sub>D</sub>	Drag coefficient, $\frac{D}{qA_{REF}}$ , dimensionless
C-D	Convergent-divergent
C <sub>D<sub>ADD</sub></sub>	Additive drag coefficient, $C_{D_{ADD}} = \frac{D_{ADD}}{qA_C}$ , dimensionless
C <sub>D<sub>A<sub>MAX</sub></sub></sub>	Afterbody drag coefficient, $\frac{DRAG}{q A_{MAX}}$ , dimensionless
C <sub>D<sub>Base</sub></sub>	Base drag coefficient $\frac{(P_b - P_\infty) A_{BASE}}{qA_{MAX}}$ , dimensionless
C <sub>D<sub>S</sub></sub>	Scrubbing drag coefficient, $\frac{DRAG}{qA_{MAX}}$ , dimensionless
C <sub>f<sub>g</sub></sub>	Thrust coefficient, $\frac{F_g}{\frac{\dot{w}}{g} (V_{cp})}$ , dimensionless
C <sub>S</sub>	Stream thrust coefficient, dimensionless,
C <sub>V</sub>	Nozzle velocity coefficient, dimensionless
Conv.	Convergent
D	Drag, lb.; Hydraulic Diameter, $\frac{4A}{P}$ , in., diameter, in.

SYMBOLS AND NOMENCLATURE (Continued)

F	Thrust, lb.
$F_{g_i}$	Ideal gross thrust (fully expanded), lb.
f/a	Fuel/air ratio, dimensionless
g	Gravitational constant, ft/sec <sup>2</sup>
h	Enthalpy per unit mass, BTU/lb.; height, in.
$h_{fan}$	Enthalpy of fan discharge flow, BTU/lb.
$h_{pri}$	Enthalpy of primary exhaust flow after heat addition, BTU/lb.
$h_t$	Throat height, in <sup>2</sup>
K	Velocity decay coefficient, dimensionless
L	Length, in.
M	Mach number, dimensionless
P	Pressure, lb/in <sup>2</sup>
$P_r$	Relative pressure; the ratio of the pressures $p_a$ and $p_b$ corresponding to the temperatures $T_a$ and $T_b$ , respectively, along a given isentrope, dimensionless
$P_T$	Total pressure, lb/in <sup>2</sup>
Q	Effective heating value of fuel, BTU/lb.
q	Dynamic pressure, lb/in <sup>2</sup>
R, r	Radius, in.
S	Nozzle centerline spacing, in
T	Temperature, °R
V	Velocity, ft/sec

SYMBOLS AND NOMENCLATURE (Continued)

W	Mass flow, lb/sec
$W_{BX}$	Bleed air removed from engine, lb/sec.
$W_C, \frac{W \sqrt{\theta}}{\delta}$	Corrected airflow, lb/sec.
$W_f$	Weight flow rate of fuel, lb/sec.
$W_2$	Weight flow rate of air, primary plus secondary, lb/sec.
$W_8$	Primary nozzle airflow rate, lb/sec.
x	Length, in.
$\alpha$	Angle of attack; convergence angle of nozzle, degrees
$\gamma$	Ratio of specific heats, dimensionless
$\epsilon$	Diffuser loss coefficient, $\frac{\Delta P_T}{q}$ , dimensionless
$\eta_B$	Burner efficiency, dimensionless
$\nu$	Kinematic viscosity, ft <sup>2</sup> /sec.
$\rho$	Density, lb/ft <sup>3</sup>

SUBSCRIPTS

B	Burner
b, base	Base flow region
BP	Bypass
BLC	Boundary layer bleed
btail	Boattail
c	Core (nozzle); capture (inlet)
DES	Design conditions

SYMBOLS AND NOMENCLATURE (Continued)

SUBSCRIPTS

e	Boattail trailing edge
EFF	Based on effective area
ENG	Refers to engine demand
f	Fuel
g	gross
GEOM	Based on geometric area
int	Interference; internal
ip	Ideal, primary exhaust flow
jet	Exhaust flow jet
max	Maximum
min	Minimum
s	Scrubbing flow region
SPILL	Spillage
T	Total condition; throat station
$t_f$	Total condition, fan flow
T/O	Takeoff
$t_p$	Total condition, primary flow
o	Local conditions ahead of inlet
2	Compressor face station
8	Nozzle throat station
9	Nozzle exit station
18	Fan discharge throat station
$\infty$	Free-stream condition
x	Local

## SECTION I

### INTRODUCTION

The Propulsion Installation and Table Assembly Program (hereafter called PITAP) is designed to correct uninstalled engine data for propulsion related losses. The intended use of this program is for advanced aircraft configuration analyses. The degree of sophistication is consistent with the type of data now available for preliminary studies of advanced aircraft concepts.

PITAP consists of three main parts, related as shown in Figure 1. Portions of the PITAP procedure have already been programmed for the CDC 6600 computer and are now operational on the Air Force Computer System at WPAFB. The calculation procedures contained in the existing computer program are indicated in Figure 1 by a dashed line. The remaining procedures exist as documented methods suitable for computer programming. The existing computer program is suitable for calculating installed propulsion system performance corrected for the most frequently encountered installation losses. The programming of the remaining procedures will improve the flexibility of the program and provide greater capability for making tradeoff studies and more options in the types of input data required.

Several options are already available for the use of the existing program, depending on the desires of the user and the type and quantity of input data available. The various options are shown in Table I.

The procedure has the capability to correct for installation losses associated with most types of subsonic and supersonic aircraft designed for Mach Numbers from 0 to 4.5.

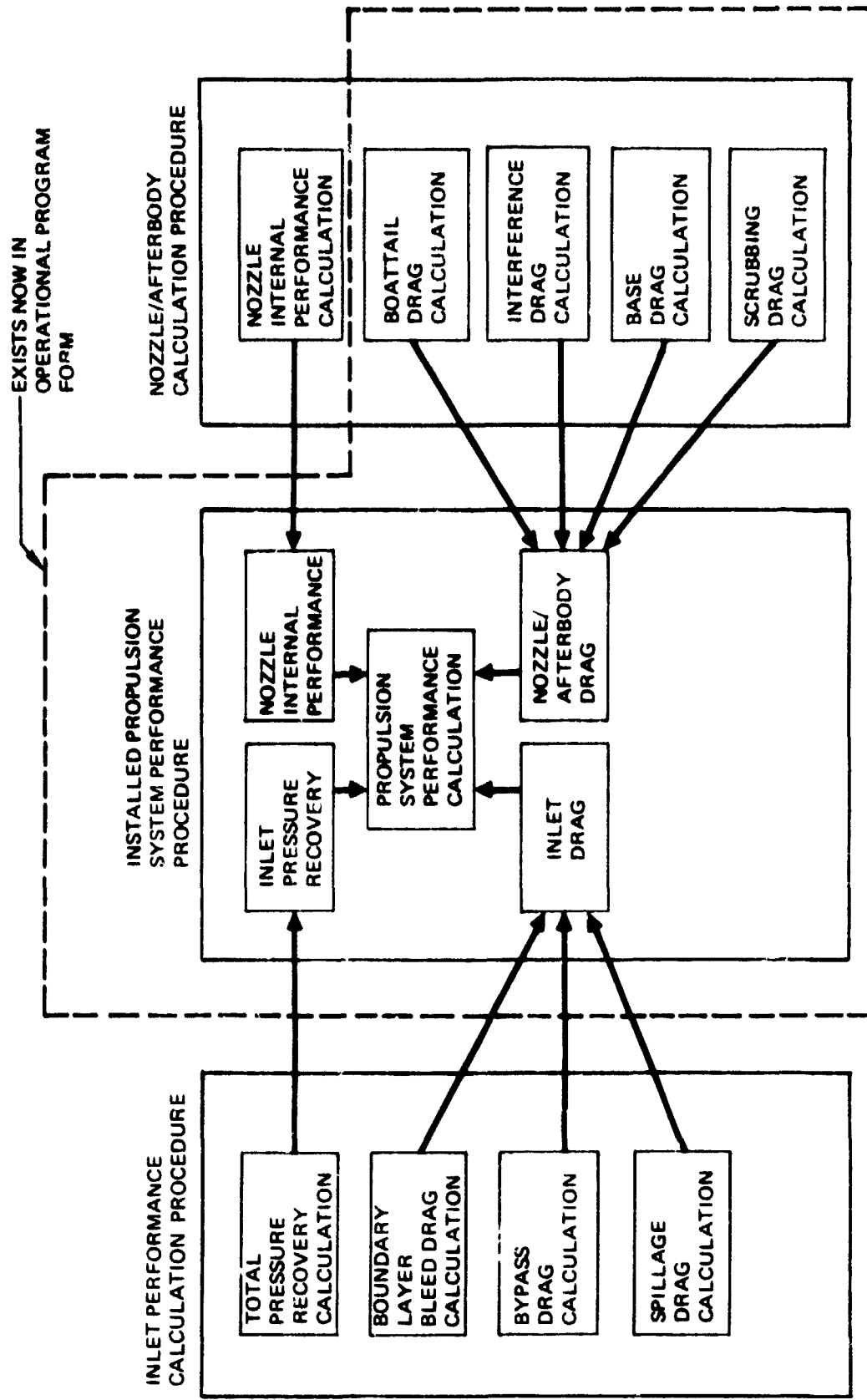


Figure 1: PITAP PROCEDURE

Table 1: CALCULATION PROCEDURE OPTIONS

		INPUT DATA			NOZZLE/ AFTERBODY DRAG	OUTPUT DATA
ENGINE PERFORMANCE DATA	INLET PRESSURE RECOVERY	INLET DRAG	NOZZLE INTERNAL PERFORMANCE			
Tabulated Data (Brochure)	Map of $P_{T2}/P_{T0}$ vs $W_2 \sqrt{\theta_2/\delta_2} A_C$	Map of $\Delta C_D$ vs $W_2 \sqrt{\theta_2/\delta_2} A_C$	Use nozzle internal performance built into engine manufacturers data	Map of $\Delta C_D$ vs $A_g/A_{10}$ and $P_g/P_0$	Installed Performance Parameters: $F_N, W_f, SFC,$ etc.	
		Buildup from predicted component contributions	Drop out engine manufacturers internal nozzle performance and substitute a constant $C_V$			
Engine Cycle Match Deck	Calculate from buildup of engineering methods using theoretical and semi-empirical prediction techniques for components		Drop out engine manufacturers internal nozzle performance and substitute a $C_V$ map.	Input geometric parameters and let coupled subprograms calculate $\Delta C_D$ vs $A_g/A_{Ref}$ and $P_{T8}/P_0$	Inlet and nozzle performance maps: $P_{T2}/P_{T0}$ vs $W \sqrt{\theta_2/\delta_2} A_C$ $\Delta C_D$ vs $W \sqrt{\theta_2/\delta_2} A_C$ $\Delta C_D$ vs $A_g/A_{10}$ and $P_g/P_0$	
			Drop out engine manufacturers internal nozzle performance by methods in PITAP			

## SECTION II

### SUMMARY

An analytical program was conducted to develop and document a calculation procedure that can be used to correct uninstalled propulsion system performance data for installation effects.

The program consisted of three phases: (I) Methods Survey and Data Collection, (II) Formulation of Correction Methods, and (III) Sample Calculations. During Phase I, data and methods were collected and reviewed to determine their usefulness in developing a general correction procedure. During Phase II, the correction methods were formulated and documented. Also, during Phase II, the main part calculation procedure was transmitted to the Air Force and has been made operational on the WPAFB CDC 6600 computer. This program can be used to make installed propulsion system performance calculations, using maps of inlet performance characteristics, tabulated engine data, built-in nozzle/afterbody drag routines, and the nozzle internal performance supplied by the engine manufacturer. The computerization of the additional calculation procedures documented during the study will expand the program capability and allow greater flexibility in types of input data. It will also permit calculations to be made of inlet and nozzle data where no experimental data exist, using existing engineering methods based on theoretical and semi-empirical data correlations. Phase III consisted of sample calculations to demonstrate the usefulness of the calculation procedure. Two configurations were used for these sample cases: an F-4J and a LWF type configuration.

The calculation procedure has been developed in the form of several modules to permit new data and methods to be added as they become available.

## SECTION III

### PROPULSION SYSTEM PERFORMANCE

#### 3.1 GENERAL DESCRIPTION

Installed propulsion system performance data represents the performance of an engine installed in a particular airplane configuration. Inlet and nozzle internal performance and drag are included, and bleed air and power are extracted from the engine for aircraft systems. These represent average values for aircraft "steady-state" performance calculations. Performance data is calculated for the entire engine-airframe flight envelope and engine power settings from maximum to idle.

PITAP can be used in several ways (Table I) to produce installed performance data, depending upon the form in which engine data is available. An engine computer program can be used directly with PITAP, or it can be used with maps generated by PITAP. PITAP can also be used with tabular data obtained from the engine computer program; i.e., each computer program is run separately. Figures 2, 3 and 4 show the various options that are possible with PITAP and an engine computer deck.

If a computer deck is available for an engine, the simplest procedure for obtaining installed performance is to use maps generated by PITAP (Figure 2). The engine main program can be altered to accept map inputs, and the output of the engine program is modified to include inlet and nozzle drag in the net thrust calculation. The engine deck main program can be altered to include a table assembly capability.

Figure 3 shows the relationship between PITAP and the engine program where either program can be used as a subroutine to produce installed data. Figure 4 shows PITAP being used as an independent program with a specified input format for engine data.

Several possibilities for use of PITAP have been described; however, there are really only two basic methods of using PITAP that affect the PITAP structure: (1) Using PITAP with tabulated engine performance data as input, and (2) Using PITAP with an engine cycle match deck providing engine performance data.

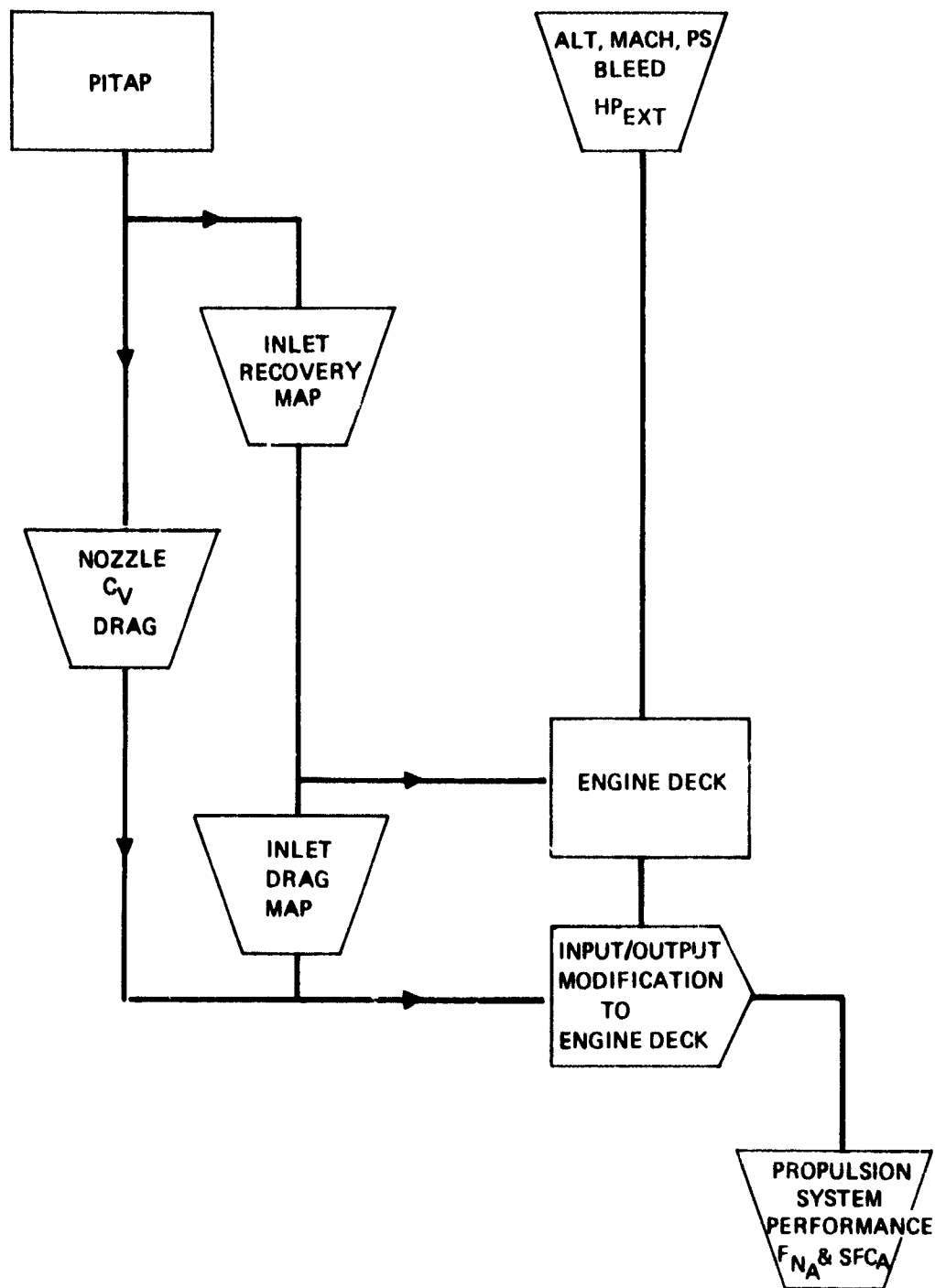


Figure 2: PITAP PROCEDURE USING PERFORMANCE MAPS

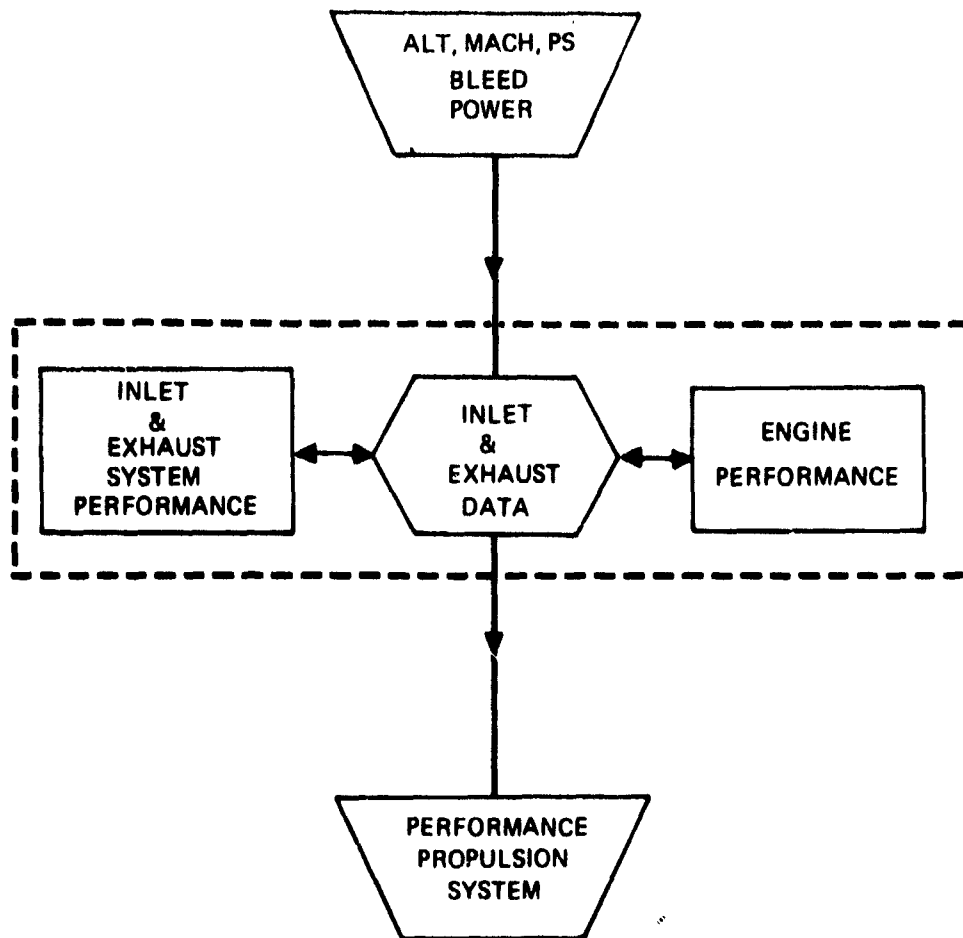
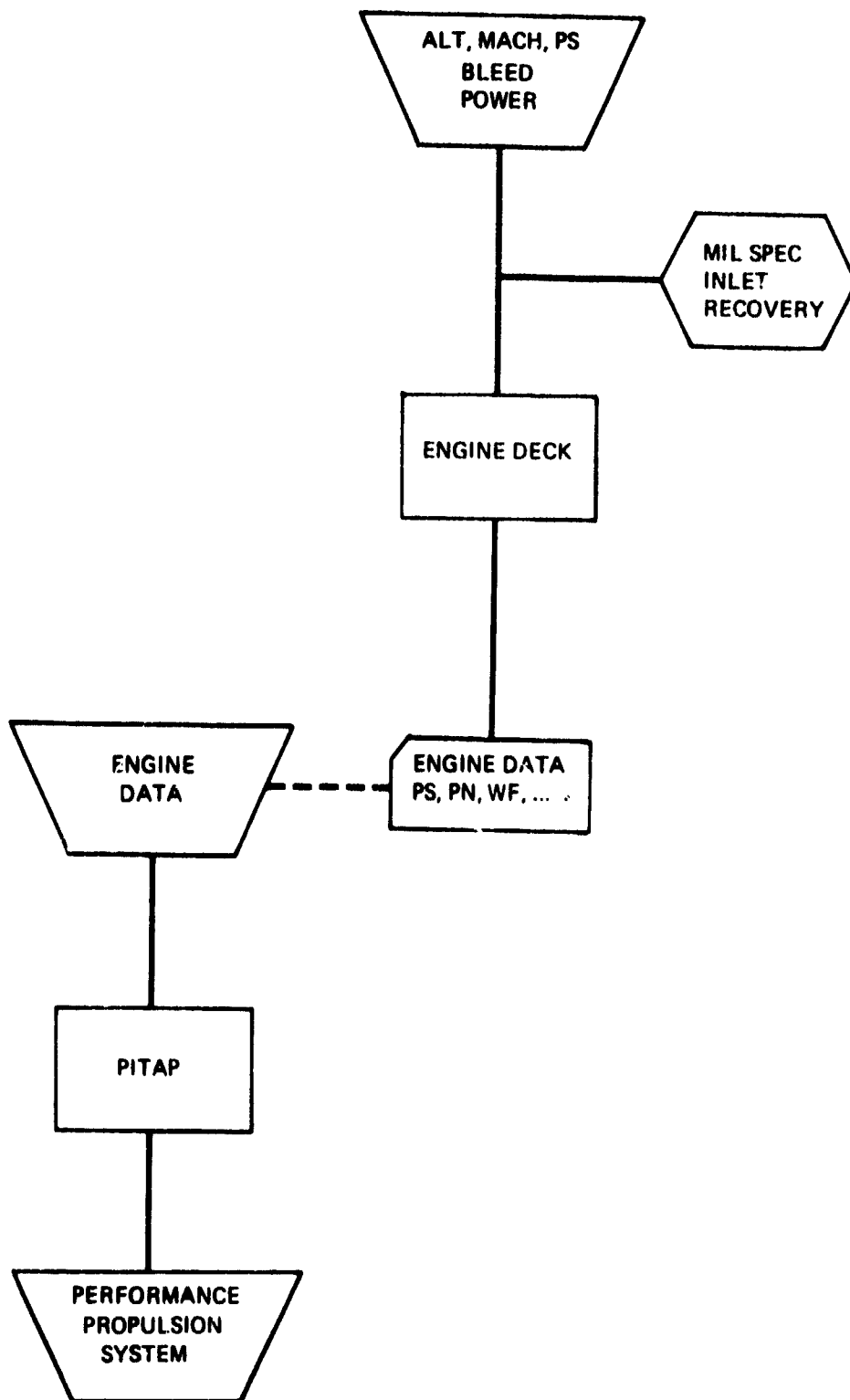


Figure 3. PITAP PROCEDURE USING PROGRAM SUBROUTINES



*Figure 4: PITAP PROCEDURE AS AN INDEPENDENT PROGRAM*

The engine data required for the tabulated version of the installation program are thrust, fuel flow, airflow, nozzle pressure ratio, throat and exit area and thrust coefficient. The installation program is designed for engine inputs with MIL 5008B inlet recovery and corrected mass flow. PITAP calculates inlet recovery and drag, and corrects the engine data for the desired recovery. The exhaust pressures and areas are required for nozzle drag calculation. The nozzle thrust coefficient is required if the nozzle performance is to be changed.

The tabulated version of the PITAP installation program can also be used if only thrust, fuel flow and air flow are available. Methods are included in the PITAP procedure to calculate nozzle pressure ratio, throat and exit areas. These methods are described in Section 3.4. The calculated exit areas and pressure ratio will be in error because the value of the exhaust nozzle coefficient is not known; however, the resultant error in nozzle drag calculation is still within the accuracy required for preliminary design performance calculations.

If PITAP is used with an engine computer program, the subroutines of PITAP which are used to make inlet recovery change calculations, nozzle calculations, and thermodynamic calculations are not required. This results in a smaller program with different logic.

Either version of the present programs can be used for installed performance calculation on turbojets, mixed flow and separate flow turbofans. Scrubbing drag calculation procedures are available as a separate program.

A more detailed discussion of the options available using the PITAP program is contained in Sections 3.2 and 3.4.

### 3.2 CALCULATIONS USING TABULATED ENGINE DATA

This is essentially the existing version of the PITAP program that is operational on the WPAFB computer. Tabular inlet input data are used to represent a series of inlet performance plots. The complete version of PITAP will eventually include procedures for calculating inlet performance plots. Generalized methods are included in the program to calculate C-D nozzle afterbody drag. The nozzle internal performance is the same as provided by the engine manufacturer. The required engine data is in the format of tables of thrust, fuel flow, corrected airflow nozzle total or static pressure ratio, throat area, exit area or velocity coefficient for each altitude, Mach number and power setting.

The engine section of the PITAP program calculates only the changes in internal performance due to changes in inlet recovery. Changes in inlet recovery produce a directly proportional change in nozzle pressure ratio, airflow, and fuel flow because the nozzle throat area does not change. Furthermore; it is assumed that engine data is calculated with MIL STD 5008B recovery and all inlet recovery changes are made relative to that value. Thermodynamic data from Keenan and Kaye tables has been "curve-fitted," and subroutines are provided to calculate the thermodynamic properties of the exhaust gases.

The calculation procedure is as follows: for each altitude, Mach number and power setting, the net thrust ( $F_N$ ), fuel flow ( $W_F$ ), corrected airflow ( $W \sqrt{\theta_2/\delta_2}$ ), nozzle throat area ( $A_g$ ), nozzle exit area ( $A_9$ ) and nozzle thrust coefficient ( $C_V$ ) are given.

Standard atmosphere and MIL Standard 5008B inlet recovery are used to calculate the airflow at the engine face and gross thrust is calculated for the given engine data before any changes in inlet recovery.

$$F_{g_{OLD}} = F_N + \frac{W_2 V_\infty}{g}$$

The desired inlet recovery is obtained from the inlet subprogram and the engine gross thrust ( $F_{g_1}$ ) is first calculated with MIL Standard recovery  $g_1$  and then with the calculated recovery ( $F_{g_2}$ ), the new value of gross thrust is then found by ratio  $g_2$

$$F_{g_{NEW}} = F_{g_{OLD}} \frac{F_{g_2}}{F_{g_1}}$$

The ratio procedure is used to minimize any inaccuracies that may be caused by assuming burner efficiency ( $\eta_B$ ) varies only with the fuel-air ratio for all engines.

The net thrust and fuel flow after correction for inlet recovery are:

$$F_{N_R} = F_{g_{NEW}} - \frac{W V_\infty}{g} \frac{R_F}{R_{F_{mil}}}$$

$$W_{F_R} = W_F \frac{R_F}{R_{F_{mil}}}$$

and the installed propulsion system thrust and SFC:

$$F_{N_A} = F_{N_R} - D_{INLET} - D_{NOZ} + D_{NOZ_{REF}}$$

$$SFC_A = \frac{W_{F_R}}{F_{N_A}}$$

Sections 3.2.1 through 3.2.5 describe the methods used to calculate the thermodynamic properties, exhaust gas properties, nozzle gross thrust, nozzle pressure ratio, and inlet recovery correction. These calculation methods are required only for the tabulated engine data input version of PITAP.

### 3.2.1 Thermodynamic Properties

Thermodynamic properties required for throat calculations are obtained using the functions shown in Table II. The functions listed in Table II and which appear in Sections 3.3 and 3.4 are "curve-fits" of Keenan and Kaye data (Reference 1). The gas tables are primarily used to calculate exhaust nozzle static pressures and jet velocities.

TABLE II

#### THERMODYNAMIC SUBROUTINES

H = HOFT (T,FOA)	Enthalpy as a function of temperature (degrees R) and fuel-air ratio
T = TOFH (H,FOA)	Temperature as a function of enthalpy and fuel-air ratio
PR = PROFH (H,FOA)	Relative pressure, (P <sub>r</sub> ) as a function of enthalpy and fuel/air <sup>r</sup> ratio
H = HOFPR (PR,FOA)	Enthalpy as a function of relative pressure and fuel-air ratio
C = COFH (H,FOA)	Sonic velocity as a function of total enthalpy and fuel-air ratio
C = COFHS (H,FOA)	Sonic velocity as a function of static enthalpy and fuel/air ratio

### 3.2.2 Energy Balance for Exhaust Gas Calculations

If the temperature at the engine compressor face, airflow, pressure ratio and fuel flow are known, the exhaust gas enthalpy ( $h$ ) and relative pressure ( $p_r$ ) can be calculated from the energy balance:

$$W_2 h_{T_2} + W_f Q \eta_B = W_{18} h_{T_{18}} + W_8 h_{T_8} + W_{BX} h_{T_{BX}}$$

(for either mixed or non-mixed flow engines)

For mixed flow fans or a turbojet:

$$W_8 = W_2 - W_{BX} + W_f$$

$$(f/a)_8 = W_f / (W_2 - W_{BX})$$

$$h_{T_8} = (W_2 h_{T_2} + W_f Q \eta_B) / W_8 \quad (W_{BX} h_{T_{BX}} \text{ is considered negligible})$$

$$(P_{r_T})_8 = f (h_{T_8}, f/a)_8$$

For a separate flow ducted fan (fan nozzle and primary nozzle):

$$h_{T_2} = f (T_{T_2}, f/a)_2; \text{ where } f/a = 0$$

$$(P_{r_T})_2 = f (h_{T_2}, f/a)_2; \text{ where } f/a = 0$$

$$(P_{r_T})_{18} = (P_{r_T})_2 (P_{T_{18}} / P_{T_2})$$

$$h_{T_{18}} = f (P_{r_T}, f/a)_{18}; \text{ where } f/a = 0$$

and

$$W_8 = W_2 - W_{18} - W_{BX} + W_f$$

$$h_{T_8} = (W_2 h_{T_2} - W_{18} h_{T_{18}} + W_f Q \eta_B) / W_8 \quad (W_{BX} h_{T_{BX}} \text{ is considered negligible})$$

$$(P_{r_T})_8 = f (h_{T_8}, f/a)_8$$

### 3.2.3 Nozzle Gross Thrust Calculation

The calculation procedure in this section applies to both mixed and non-mixed flow nozzles.

#### 3.2.3.1 Convergent Nozzle

The velocity at the throat for a convergent nozzle is a function of the total enthalpy (assuming the throat is choked).

$$C_8 = f(h_T, f/a)_8$$

and the static pressure is a function of the static enthalpy

$$h_8 = h_{T8} - \frac{(C_8)^2}{2gJ}$$

$$T_8 = f(h, f/a)_8$$

$$P_{r8} = f(h, f/a)_8$$

$$P_{T8}/P_8 = (P_{rT8})/P_{r8}; \quad P_{T8} \text{ is obtained from the tabulated engine input data as } f(P.S., \text{ alt.}, M_\infty) \text{ or it is calculated by the procedure described in Section 3.2.4.}$$

$$P_8 = P_{T8} / (P_{T8}/P_8)$$

The area of the throat is

$$A_8^* = \left(\frac{WRT}{PC}\right)_8$$

and the thrust is

$$F_g = \frac{W_8 V_8}{g} + A_8^* (P_8 - P_{\text{amb}})$$

#### 3.2.3.2 Convergent-Divergent Nozzle (fully expanded)

If the exhaust flow is fully expanded, the static pressure of the nozzle exit is equal to ambient, and the exit velocity is a function of the total to static enthalpy.

$$P_{r9} = P_{r8} (P_{\text{amb}}/P_8)$$

$$h_9 = f (P_r, f/a)_9$$

$$T_9 = f (h, f/a)_9$$

Since  $h_8 = h_9$

$$V_9 = \left( 2gJ (h_{T_8} - h_9) \right)^{1/2}$$

The exit area is

$$A_9 = W_9 R_8 T_9 / P_{amb} V_9$$

and the gross thrust is

$$F_g = \frac{W_9 V_9 C_V}{g}$$

### 3.2.3.3 Convergent-Divergent Nozzle (not fully expanded)

If the exit area of a convergent-divergent nozzle is less than required for full expansion, the exit static pressure will be higher than ambient. The throat conditions are known; therefore, a guessed exit velocity gives:

$$h_9 = h_{T_8} - V_9^2 / 2gJ$$

$$T_9 = f (h, f/a)_9$$

$$P_{r_9} = f (h, f/a)_9$$

$$P_9 = \frac{P_{r_9}}{P_{r_8}} (P_8)$$

$$W_9 = \frac{P_9}{R(T_9)} \quad A_9 V_9 = (\rho AV)_9 = \left( \frac{PAV}{RT} \right)_9$$

An iteration on  $V_9$  to make  $W_9 = W_8$  will result in the exit conditions for a given area.

The gross thrust is:

$$F_g = \left( \frac{WV}{g} + PA \right)_9 C_S - P_{amb} A_9$$

### 3.2.4 Nozzle Pressure Ratio Calculation

The exhaust nozzle pressure ratio can be calculated if thrust, fuel flow and airflow are known. The gross thrust is calculated as follows:

$$F_g = (F_{net} + F_{ram}) / C_V$$

$$F_{ram} = \frac{W_2 V_\infty}{g}$$

and the nozzle exit conditions are calculated by assuming that the flow is fully expanded.

$$W_8 = W_2 - W_{BX} + W_f$$

$$h_{T8} = h_{T2} + (Q\eta_B W_f / W_8)$$

$$T_{T8} = f (h_{T, f/a})_8$$

$$V_9 = F_g (g) / W_8$$

$$h_9 = h_{T8} - V_9^2 / 2gJ$$

$$P_{r9} = f (h, f/a)_9$$

$$(P_{rT})_8 = f (h_{T, f/a})_8$$

Since  $P_9 = P_{amb}$

$$P_{T8} / P_{amb} = (P_{rT})_8 P_{r9}$$

The pressure ratio calculation will be in error, an amount relative to the value of the thrust coefficient ( $C_V$ ), because this is usually unknown if pressure ratios and exhaust areas are not given.

### 3.2.5 Inlet Recovery Correction

The engine corrected airflow remains constant for any change in inlet recovery, and at any given power setting, the nozzle exhaust areas and burner fuel/air ratio remain constant. The engine performance for any change in inlet recovery is calculated by the following relations:

$$\begin{aligned} \text{RATIO} &= \text{RF/RFMIL; where RF/RFMIL} = \frac{(P_{T_2}/P_{T_\infty})}{(P_{T_2}/P_{T_\infty})_{\text{mil}}} \\ & \hspace{15em} 5008\text{B} \\ \text{W8RF} &= \text{W8 (RATIO)} \\ \text{WFRF} &= \text{WF (RATIO)} \\ \text{W2RF} &= \text{W2 (RATIO)} \\ \text{P8PORF} &= \text{P8/PO (RATIO)} \end{aligned}$$

After the above quantities are computed, the corrected quantities (W8RF, WFRF, W2RF, and P8PORF) are used in the subroutines described in Sections 3.2.1, 3.2.2, and 3.2.4 to compute a new gross thrust,  $F_{G_2}$ . This new gross thrust and the gross thrust,  $F_{G_1}$ , calculated using the same subroutines and the uncorrected (MIL 5008B) quantities (W8, WF, W2, P8PO) are used to compute a ratio,  $F_{G_2}/F_{G_1}$ . This ratio is then used as described in section 3.2 to obtain the new value of gross thrust,  $F_{G_{\text{NEW}}}$ .

### 3.3 CALCULATIONS USING ENGINE CYCLE MATCH DECK

This version of the PITAP program differs from the existing PITAP program in two specific areas. The first is in the input/output of the program and the second is that the thermodynamic functions, performance and thrust subroutines are not required. For this version of the PITAP program using the engine cycle match deck, the PITAP program is the main program and the engine cycle match deck is used as a subroutine.

The input/output of the engine program and PITAP are linked through the labeled common blocks of each program. The input for the engine program requires the following data:

$$\begin{aligned} \text{PS} &= \text{power setting or code} \\ T_2 &= \text{degrees R = inlet total temperature} \\ P_2 &= \text{lb/in}^2 = \text{inlet total pressure} \end{aligned}$$

$T_{amb}$	degrees R	=	free-stream static temperature
$P_{amb}$	lb/in <sup>2</sup>	=	free-stream static
ETAR	~	=	inlet recovery
WBFAN	lb/sec	=	fan bleed airflow
$W_{B_3}$	lb/sec	=	bleed air flow (high pressure) extraction
$W_{B_{2.X}}$	lb/sec	=	bleed airflow (intermediate)
HP	HP	=	horsepower extraction

Power setting, bleed and horsepower extraction are input, but inlet and ambient pressure conditions are calculated from the altitude and Mach input. The existing version of the PITAP Program obtains atmospheric properties from a subroutine which provides ambient temperature and pressure for ISA standard day as a function of pressure altitude. For non-standard day conditions, a different subroutine will be required. A special subroutine is provided with the engine program to interface with the inlet subroutine to obtain ram recovery.

It is recommended that power setting or power code inputs conform with ARP 681.B (PS = 100 is maximum augmented thrust, 50 is intermediate, 20 is idle, etc.)

Five tables are added to the current version of PITAP to input fan bleed, LP, IP and HP compressor bleed, and horsepower extraction as a function of altitude and flight Mach number.

The following input variables are required for variable cycle decks or engine description:

<u>Input Variables</u>		
<u>Symbol</u>	<u>Unit</u>	<u>Definition</u>
BRPDS	-	Design bypass ratio
P3P2DS	-	Design overall compressor pressure ratio
T4MAX	degrees F	Maximum turbine inlet temperature
W/DES	lb/sec	Design total airflow

Input Variables (Continued)

<u>Symbol</u>	<u>Unit</u>	<u>Definition</u>
PCW2C	-	Per cent corrected airflow desired at maximum height and Mach number
ALT MAX	ft	Altitude at maximum flight Mach number
MMach		Maximum Mach number
DASH M		Dash Mach Number
D ALT	ft	Dash altitude
LENG	in	Overall length
LNOZ	in	Nozzle length
DIA INL	in	Inlet flow path diameter
DMAX	in	Maximum engine diameter
WTENG	lb	Engine weight
WTNOZ	lb	Nozzle weight

The engine performance data is run for a matrix of Mach numbers, altitude and power settings.

The output format shown in Figure 5 uses 67 spaces on a printout page so that it can be cut to 8 1/2 x 11 size for storage, or it can be in CRT displays and remote teletype systems.

The output format has classification headings at the top and bottom of the page and is divided into five basic groups of data:

- a. Engine company, engine, and run identification
- b. Engine design description which is either input or calculated
- c. Engine data
- d. Installed performance - inlet and nozzle drag
- e. Special output: i.e.,  $FN/\delta$ ,  $SFC/\sqrt{\theta}$  etc.



### Output Parameters

<u>Symbol</u>	<u>Units</u>	<u>Definition</u>
Classification -		engine program security classification
Engine Co. Name -		engine co. name, engine identification and run title
BPRDS	-	design bypass ratio
P3P2DS	-	design overall compressor pressure ratio
T4MAX	degrees F	maximum turbine inlet temperature
WODES	lb/sec	design total airflow - sea level, standard day
PCW2C	-	percent of design corrected flow required at maximum $\theta_2$ condition
ALTMAX	ft	altitude of maximum Mach number
MMAX	-	maximum flight Mach number
DASHM	-	dash Mach number
DALT	ft	dash attitude
LENG	in	engine length (including nozzle)
LNOZ	in	nozzle length
DIAINL	in	inlet flow path diameter
DMAX	in	maximum engine diameter
WTENG	lb	engine weight (including nozzle)
WTNOZ	lb	nozzle weight
ALT	ft	altitude
MACH	-	Mach number
DELT	degrees F	temperature deviation from standard day
PS	-	power setting
PCODE	-	identification of power setting i.e., intermediate, max augmented, etc.

Output Parameters (Continued)

<u>Symbol</u>	<u>Units</u>	<u>Definition</u>
FN	lb	net thrust
SFC	lb/hr/lb	specific fuel consumption
FRAM	lb	ram drag
WFT	lb/hr	total fuel flow
FG	lb	gross thrust
PAMB	lb/in <sup>2</sup>	ambient pressure
P2	lb/in <sup>2</sup>	inlet total pressure
P12	lb/in <sup>2</sup>	fan discharge total pressure
P22	lb/in <sup>2</sup>	LP compressor discharge total pressure (port losses included)
P2x	lb/in <sup>2</sup>	IP compressor discharge total pressure (port losses included)
P3	lb/in <sup>2</sup>	HP compressor discharge total pressure (port losses included)
TAMB	degrees R	Ambient temperature
T2	degrees R	engine inlet total temperature
T12	degrees R	fan discharge total temperature
T22	degrees R	LP compressor discharge total temperature
T2X	degrees R	IP " " " "
T3	degrees R	HP " " " "
WBFAN	lb/sec	fan bleed air flow
WBLP	lb/sec	LP compressor bleed air flow
WBI	lb/sec	IP compressor bleed air flow
WBA	lb/sec	HP compressor bleed air flow
HPX	hp	horsepower extraction
DEX	in	nozzle exit diameter

Output Parameters (Continued)

<u>Symbols</u>	<u>Units</u>	<u>Definitions</u>
THETA	degrees	nozzle boattail angle
ETAR	-	inlet total pressure recovery ratio
W2C	lb/sec	engine corrected air flow
P8PO	-	exhaust nozzle pressure ratio
T8	degrees R	exhaust nozzle total temperature
W3	lb/sec	HP compressor air flow
W8	lb/sec	exhaust nozzle mass flow
WF4	lb/hr	burner fuel flow
WF8	lb/hr	total fuel flow
FGI8	lb	ideal gross thrust
CV8	-	nozzle thrust coefficient
DRAG	-	nozzle external drag
AE8	in <sup>2</sup>	nozzle throat effective area
A8	in <sup>2</sup>	nozzle throat area
AE9	in <sup>2</sup>	nozzle exit effective area
A9	in <sup>2</sup>	nozzle exit area
P180PO	-	fan nozzle pressure ratios
T18	degrees R	fan nozzle exhaust temperature
W12	lb/sec	fan duct air flow
W18	lb/sec	fan nozzle mass flow
WF18	lb/hr	fan duct reheat fuel flow
FGI18	lb	fan nozzle ideal gross thrust
CV18	-	fan nozzle thrust coefficient
AE18	in <sup>2</sup>	fan nozzle throat effective area

Output Parameters (Continued)

<u>Symbols</u>	<u>Units</u>	<u>Definitions</u>
A18	in <sup>2</sup>	fan nozzle throat area
AE19	in <sup>2</sup>	fan nozzle exit effective area
A19	in <sup>2</sup>	fan nozzle exit area
FNA	lb	propulsion system net thrust
SFCA	lb/hr/lb	propulsion system specific fuel consumption
DINLET	lb	inlet drag
DNOZ	lb	nozzle drag
AC	in <sup>2</sup>	inlet capture area
AOE/AC	-	engine mass flow ratio
AOI/AC	-	inlet capture mass flow ratio
AO/AC	-	inlet mass flow ratio
CPSPL	-	coefficient of inlet spillage drag
CDBCD	-	coefficient of inlet bleed drag
CDBYP	-	coefficient of inlet bypass drag
CDINL	-	coefficient of inlet total drag
AMAX	in <sup>2</sup>	maximum area of the exhaust system
LBT	in	length of exhaust system
DNOZR	lb	reference nozzle drag
CDBT	-	coefficient nozzle boattail drag
CDBASE	-	coefficient nozzle base drag
CDINT	-	coefficient nozzle interference drag
BETA	degrees	boattail angle
FN/DELTA	lb	corrected net thrust
SFC/RTHETA	lb/hr/lb	corrected specific fuel consumed
Q	lb/ft <sup>2</sup>	free-stream dynamic pressure

### 3.4 OTHER PROGRAM OPTIONS

#### 3.4.1 Inlet and Nozzle Performance Maps

A subroutine has been programmed that can call and control the existing subroutines required to generate inlet performance "maps" from tabulated inlet input data (representing inlet performance "plots"). The program listing for this subroutine is included in Volume II. A subroutine also exists to generate nozzle data, using the internal program procedures, but the output needs to be revised to adequately output the map data in the desired format.

#### 3.4.2 Engine Manufacturers Nozzle Internal Performance

The existing PITAP program (described in Volume II) uses this procedure.

#### 3.4.3 Externally-Generated $C_V$ Input

This option to the basic program procedure makes it possible to drop out the engine manufacturers nozzle internal performance ( $C_V$ ) and substitute a different  $C_V$ , which can be either a constant value or a map.

This is accomplished by changes to the existing Main Program routine (TEM 333) and subroutine COMPUTE. The changes consist of the following:

1. The main program is changed to accommodate reading in and storing the new coefficient or map.
2. Subroutine COMPUTE is changed to call the stored coefficients and insert them instead of the engine nozzle coefficient.

The changes are not extensive and the logic for them is included in Volume II.

#### 3.4.4 Nozzle Internal Performance Subroutine

This involves modifying the Main Program and Subroutine COMPUTE to eliminate use of the engine nozzle loss coefficient and building in the logic to call and use a subroutine which has the nozzle internal loss calculation procedures built into it. The nozzle internal loss calculation methods are described in Section V of this document. Engineering logic diagrams are provided in the Appendix to show how this should be done.

## SECTION IV

### INLET PERFORMANCE

The major installation losses that must be accounted for in correcting uninstalled propulsion system data for inlet effects are: (1) total pressure recovery, (2) boundary layer bleed drag, (3) bypass drag, and (4) spillage drag. This section describes the methods used to calculate these corrections. A general description of the existing computerized methods is presented first. The existing computer program uses input "maps", representing inlet recovery and drag as a function of mass flow, to calculate installation corrections.

Following a description of the engineering procedures in the computer program, engineering methods are discussed which can be used to obtain input data when no input "maps" are available. Several of the engineering methods have been programmed for the CDC 6600 computer and programming flow charts and listings for these are included in Volume II.

Figure 6 presents a diagram showing how the inlet calculation procedures relate to the installed propulsion system procedures.

#### 4.1 GENERAL DESCRIPTION

Corrections to uninstalled propulsion system performance to account for inlet recovery, bleed drag, bypass drag, and spillage drag can be accomplished using several different types of input data.

The basic propulsion system calculation procedure uses "maps" of total pressure recovery and inlet drag as a function of engine corrected airflow divided by capture area (Item 3 in Figure 7). These maps directly provide the recovery and drag for use in installed propulsion system calculations. Corrected airflow is the parameter used to match the inlet performance to the engine.

However, most wind tunnel test data are obtained in the form of individual inlet performance "plots" such as those shown in Item 2 of Figure 7. A separate subprogram is used to convert these performance plots into performance maps. This subprogram, (INLTMAP) is described in Volume II.

If wind tunnel test data are not available for which to obtain inlet performance plots, these plots are built up by theoretical and semi-empirical calculation procedures (Item 1 of Figure 7), that are described in this report.

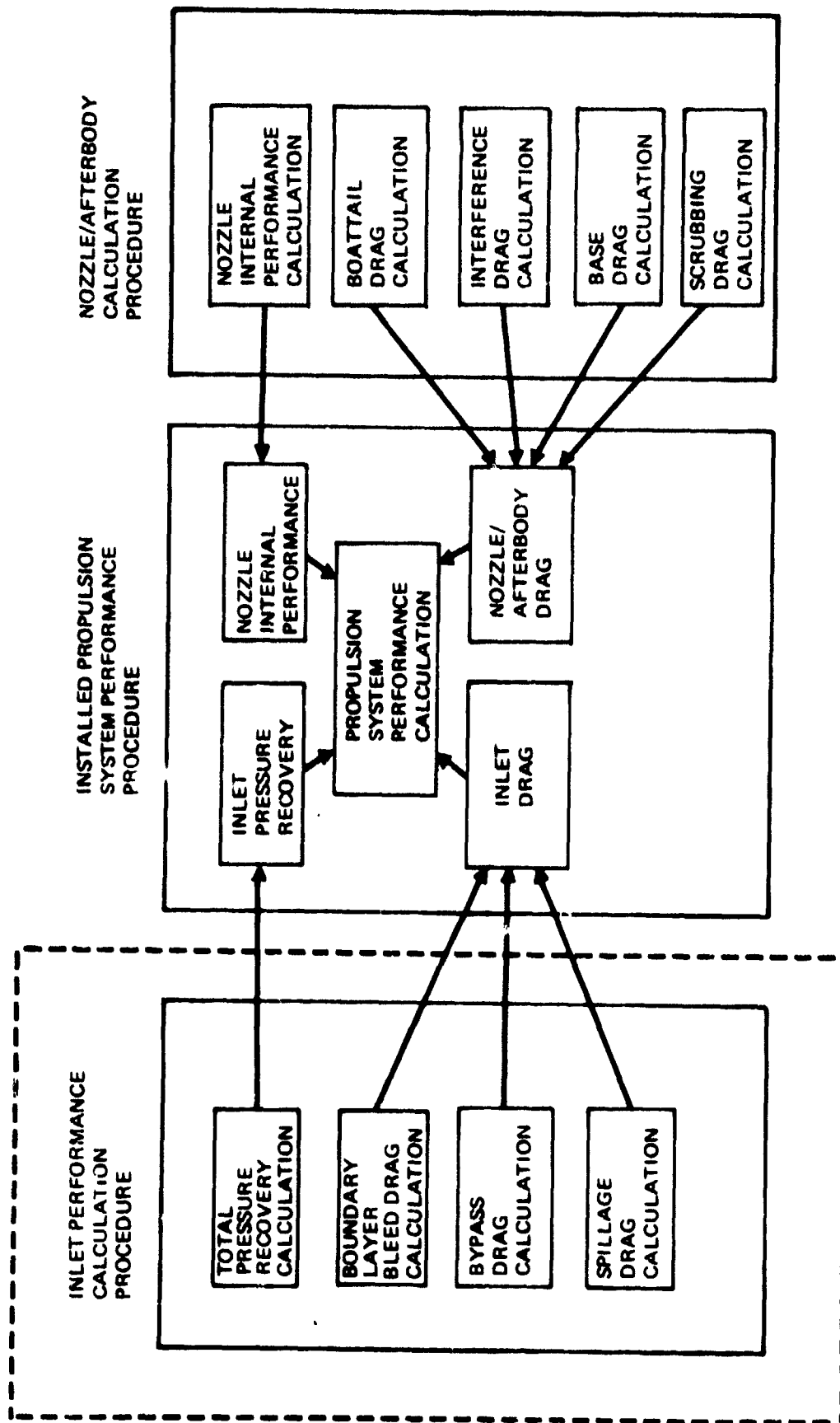


Figure 6: INLET PERFORMANCE PROCEDURE

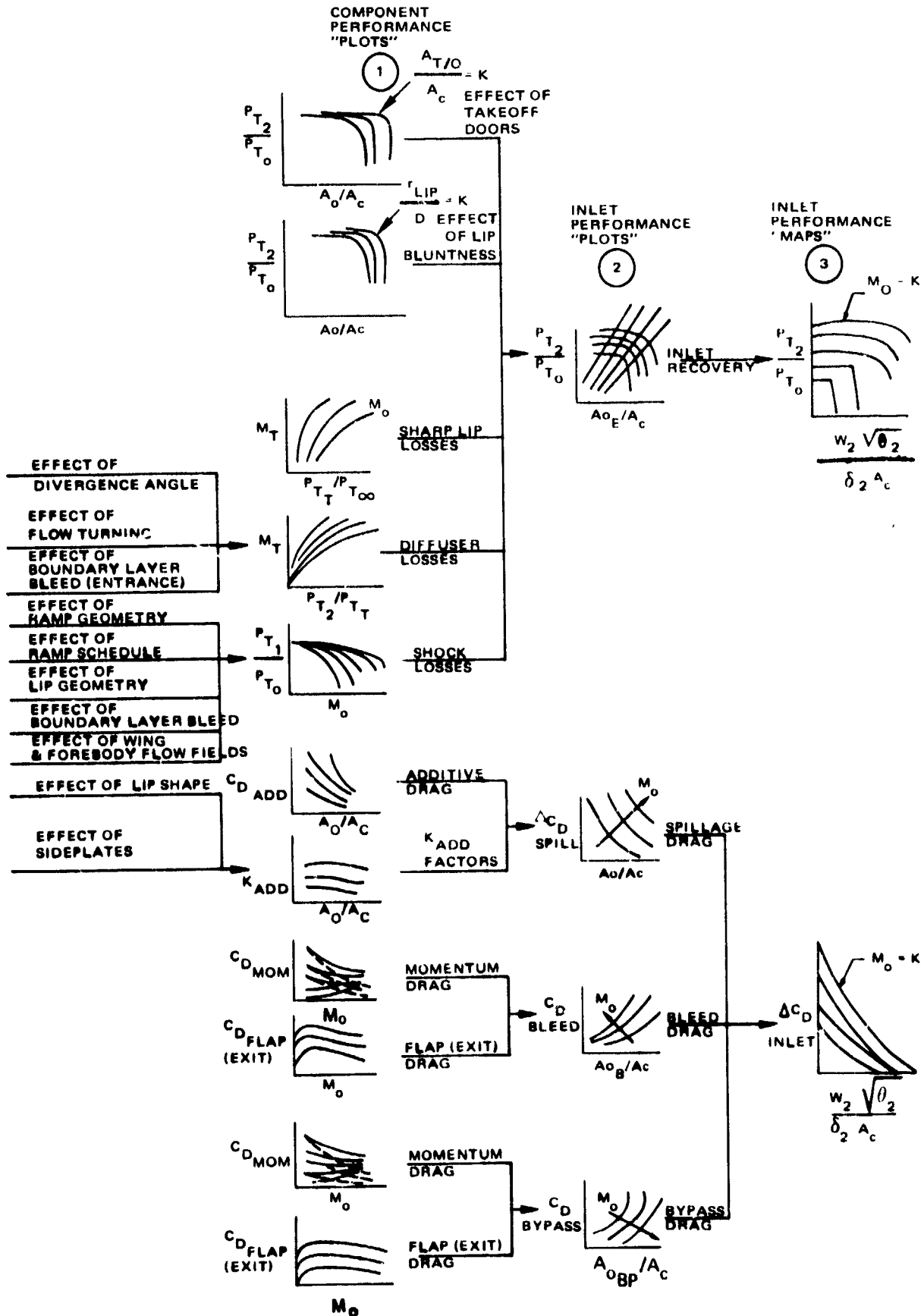


Figure 7: INLET PERFORMANCE ELEMENTS

The inlet performance calculations are performed by the inlet subprogram, Figure 8.

Inlet performance maps are input data to the inlet subprogram. This subprogram sizes the inlet capture area (if it is not specified) and converts the inlet performance maps into total pressure recovery and inlet drags that are matched to the corrected airflow demand of the engine.

The connecting link between the engine data and the inlet subprogram is engine-plus-secondary corrected airflow. The sizing routine permits the inlet to be sized for operation at a desired inlet mass flow ratio, consistent with a recovery associated with the design engine corrected airflow demand. A specified capture area size can also be input if desired, instead of requiring the program to calculate the size.

The inlet input requires twelve tables of input data which describe the performance characteristics of the inlet. Engineering data obtained from wind tunnel tests and theoretical calculations are used to obtain the inlet performance characteristics. The format for the inlet data is shown in Figures 9 and 10. Data taken from these engineering plots are punched on cards for input into the inlet subprogram.

The inlet subroutine recognizes three modes of inlet operation: low-speed, external compression, and mixed compression. The low-speed mode is used only at very low Mach numbers, e.g., take-off conditions, when only high engine power settings are likely to be of interest and inlet drag is negligible. The external-compression mode is used over the remaining Mach number regime for external-compression inlets. It is also used for the remaining subsonic regime and supersonic Mach numbers up to the starting Mach number for mixed-compression inlets. The mixed-compression mode is used at or above the starting Mach number for mixed-compression inlets.

- a) External-Compression Inlets. The calculation of recovery and drag for an external-compression inlet is illustrated in Figure 9. The required performance maps are input as tables, as indicated. Table 1 is used to represent the effect of the airplane flow field on the local Mach number seen by the inlet. Table 2A gives the basic recovery/mass-flow-ratio characteristics of the inlet. The minimum Mach number for which data is input in Table 2A is taken by the program to be  $M_{O \min}$ , below which only the low-speed mode is used.

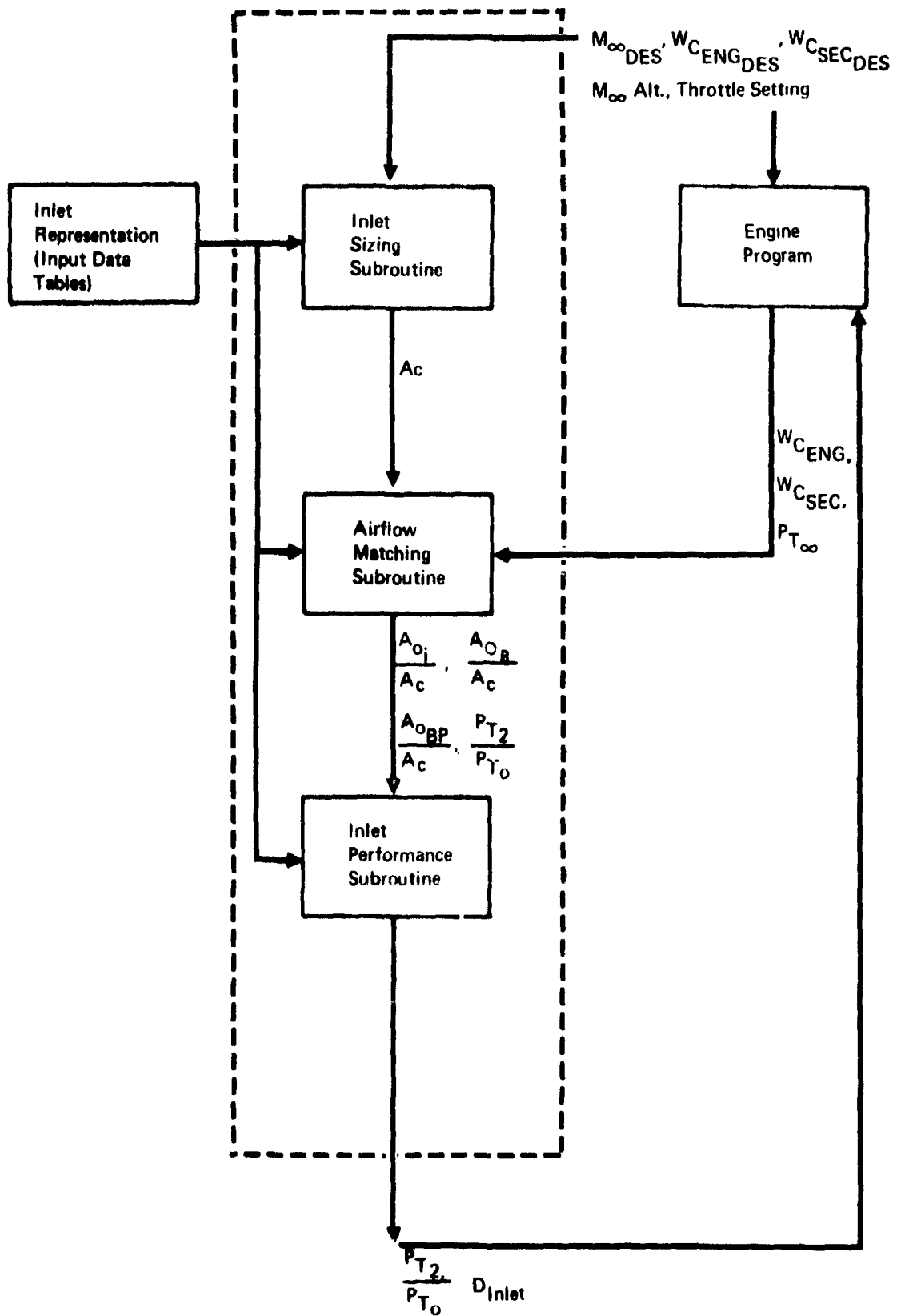


Figure 8: INLET SUBPROGRAM

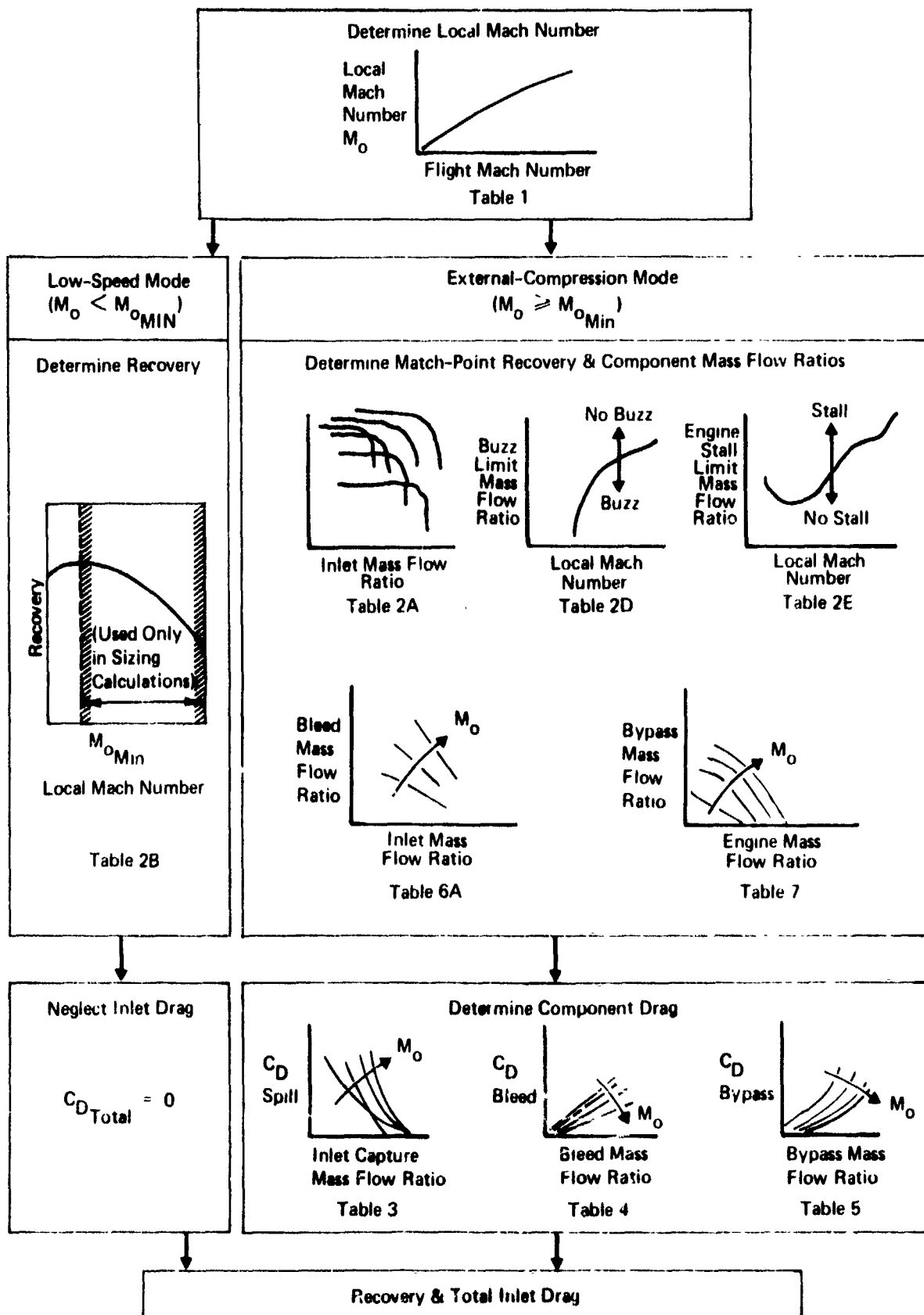


Figure 9: PERFORMANCE CALCULATION FOR AN EXTERNAL-COMPRESSION INLET

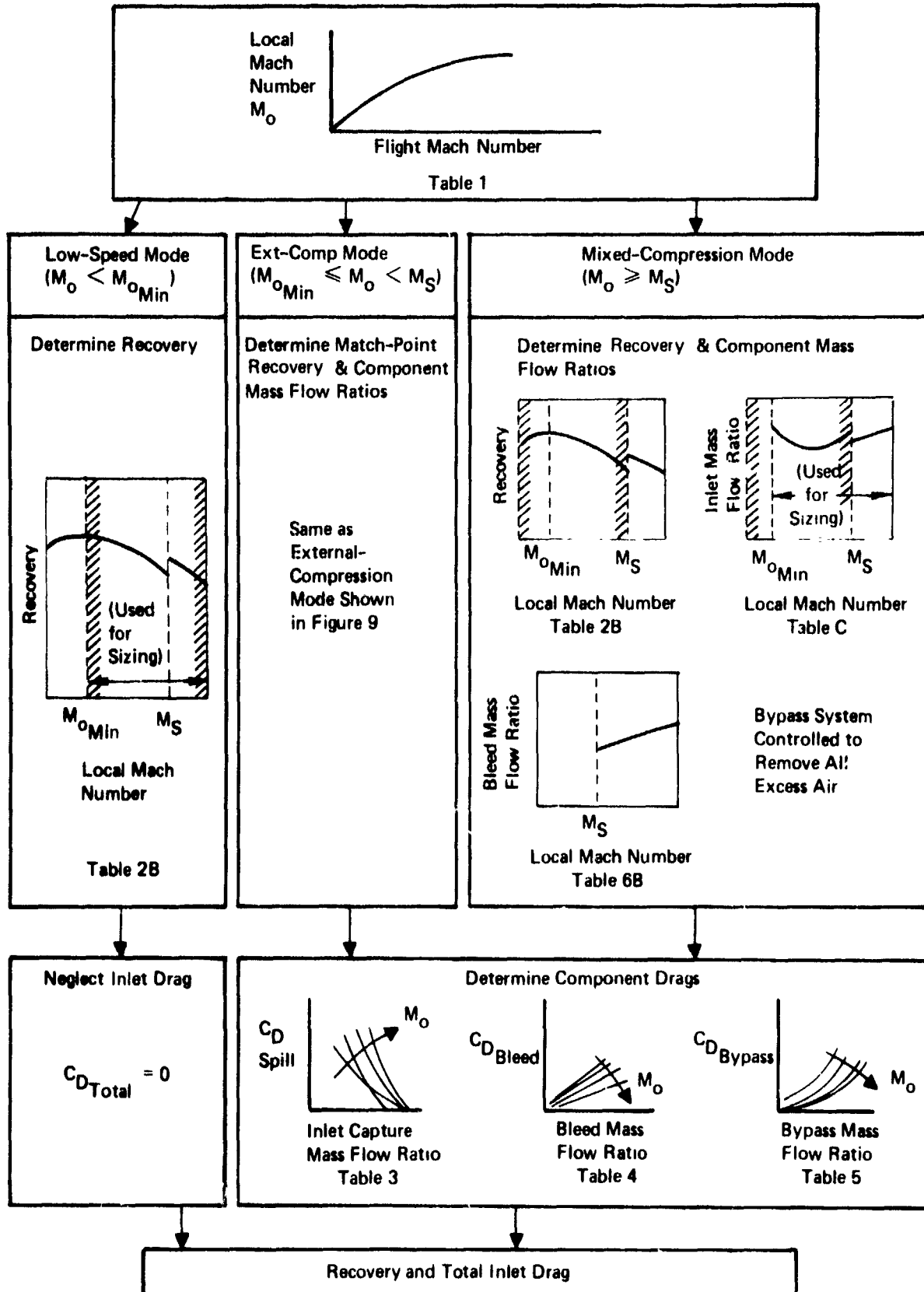


Figure 10: PERFORMANCE CALCULATION FOR A MIXED-COMPRESSION INLET

In the low-speed mode, recovery is read directly out of Table 2B as a function of local Mach number only, and inlet drag is neglected. If the Local Mach number exceeds  $M_0$ , the recovery and mass flow ratio are determined using Table 2A, Table 7 (which gives the scheduled bypass flow, if any, as a function of engine mass flow ratio), and engine corrected airflow demand. An iteration is performed to solve simultaneously for the match-point recovery and inlet mass flow ratio, as well as the engine mass flow ratio and scheduled bypass flow. If the indicated buzz (Table 2D) or distortion (Table 2E) limits are exceeded, an appropriate warning message will appear, but no fatal error will result. The bleed mass flow associated with the calculated inlet mass flow ratio is determined from Table 6A.

After the required mass flow ratios are determined, spillage, bleed, and bypass drags are found from Tables 3, 4, and 5, respectively. Spillage drag is the incremental change in additive drag and pressure drag on the airplane due to inlet operations at mass flow ratios less than a reference mass flow ratio. The bleed and bypass drags include door drags as well as momentum losses of the airflow.

- b) Mixed-Compression Inlets. The performance calculation for a mixed-compression inlet is illustrated in Figure 10. Below the starting Mach number  $M_S$ , the low speed mode and external-compression mode are used in the same way as in the case of an external-compression inlet. The mixed-compression mode, used at or above  $M_S$ , is based on the assumption that a closed-loop bypass system is available to remove all excess air. Thus, except for the case of excessive engine airflow demand, the inlet mass flow ratio, bleed flow, and recovery may all be scheduled as a function of local Mach number only; the bypass system compensates for changes in engine airflow demand.

If the corrected airflow delivered by the inlet is inadequate to meet the engine demand at the scheduled recovery, the program will permit the inlet to operate at an excessive supercritical margin. The recovery will be lowered sufficiently to match the engine corrected airflow demand, and an appropriate message will warn the user of an undersized inlet.

Inlet spillage, bleed, and bypass drag are found using Tables 3, 4 and 5 as in the external-compression mode. The data in these tables for Mach number equal to or greater than  $M_S$  apply only for started inlet operation.

#### 4.2 TOTAL PRESSURE RECOVERY

Three separate procedures are used to calculate inlet total pressure recovery, depending on the flight speed of the airplane.

##### 4.2.1 Low Speed

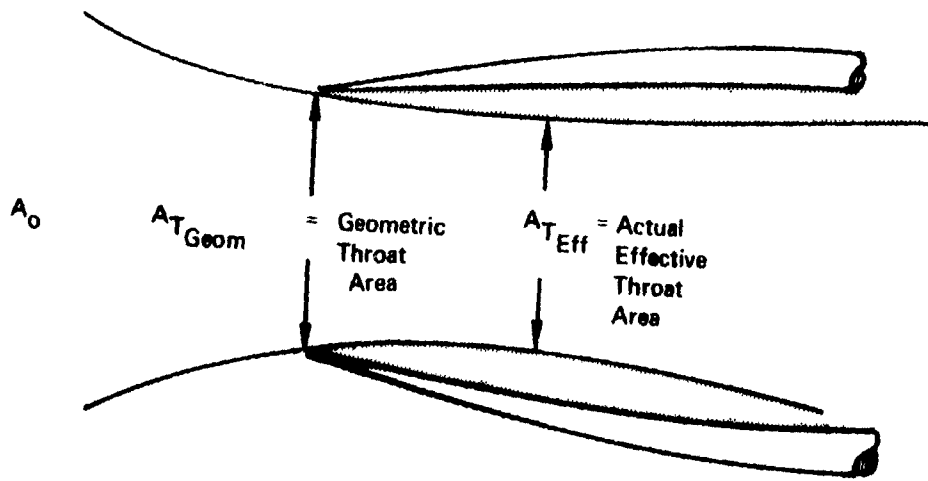
At takeoff and low speeds ( $0 \leq M \leq .40$ ), the primary total pressure loss generating mechanisms are sharp lip losses and subsonic diffuser losses. The methods used to calculate sharp lip losses accounts for lip bluntness, effect of takeoff door area, and inlet flow velocity. The subsonic diffuser losses are calculated by using an input variation of duct loss coefficient,  $\epsilon = \Delta P_T/q_1$ , as a function of inlet throat Mach number. The duct loss variation is obtained from a catalog of data provided (in Volume IV) for a range of configuration variables.

The sharp lip losses are combined with the subsonic diffuser losses as shown in the flow chart of Figure 60 to obtain the overall inlet total pressure recovery.

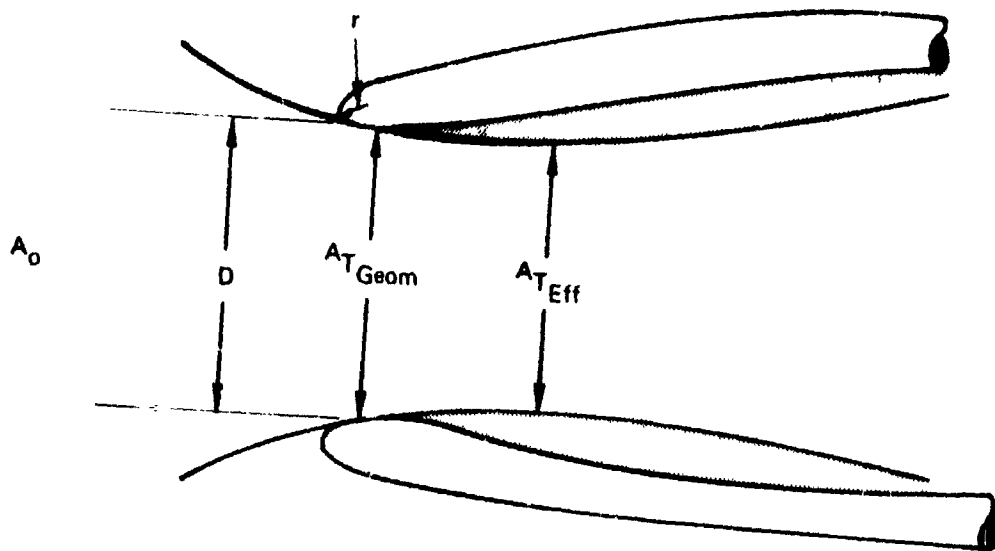
The nomenclature used to calculate the lip losses for low speed inlet operation is shown in Figure 11.

The required input quantities for the low speed calculation are:

$\frac{r}{D}$	~	lip bluntness parameter, ratio of lip radius to inlet lip hydraulic diameter, dimensionless.
$\frac{W \sqrt{\theta_2}}{\delta_2}$	~	engine corrected airflow, lb/sec.
$A_C$	~	inlet capture area, in. <sup>2</sup>
$M_O$	~	local inlet Mach number, dimensionless
$A_T$	~	inlet throat area, in. <sup>2</sup>



(a) SHARP LIP



(b) BLUNT LIP

Figure 11: NOMENCLATURE FOR LOW-SPEED INLET LIP LOSSES

- $A_{T.O.}$  ~ Takeoff door throat area, in.<sup>2</sup>
- $\epsilon$  ~ subsonic diffuser duct loss coefficient,  
 $\epsilon = \frac{\Delta P_T}{q_1}$ , dimensionless.

The basic calculation procedure is the same, regardless of the local Mach number; however, below  $M_0 = .20$ , inlet throat Mach number is based on the calculated throat corrected airflow parameter,

$$\frac{W_T \sqrt{\theta_T}}{\delta_{T_T} A_{T_{GEOM}}}$$

This parameter is calculated by the following equation:

$$\frac{W \sqrt{\theta}}{\delta A_{T_{GEOM}}} = \left( \frac{W_2 \sqrt{\theta_2}}{\delta_2 A_{T_{GEOM}}} \right) \left( \frac{P_{T_2}}{P_{T_0}} \right); A_{T_{GEOM}} = \text{Inlet throat geometric area, in.}^2 \quad (1)$$

After the throat corrected airflow parameter,  $\frac{W \sqrt{\theta}}{\delta A_{T_{GEOM}}}$ , is calculated, throat Mach number based on geometric throat area,  $M_{T_{GEOM}}$ , is obtained from.

$$\frac{W \sqrt{\theta}}{\delta A} = .592 \left[ \frac{M}{(1 + .2M^2)^3} \right]; \gamma = 1.40$$

This equation can be solved by computer or the input data curve can be programmed for a table look-up procedure. This curve is plotted in Figure 12.

Above  $M_0 = .20$ , the throat Mach number based on geometric area,  $M_{T_{GEOM}}$ , is obtained by calculating the throat sonic area ratio,  $(A/A^*)_{T_{GEOM}}$ . To accomplish this calculation, the inlet mass flow ratio is first calculated:

$$\frac{A_O}{A_C} = \frac{W_2 \sqrt{\theta_2}}{\delta_2 A_C} \times \left( \frac{A}{A^*} \right)_O \times \frac{P_{T_2}}{P_{T_0}} \quad (2)$$

.342

$W = \text{Lb/Sec}$   
 $A = \text{In}^2$   
 $\theta = T_T / T_{Std}$   
 $\delta = P_T / P_{Std}$

$$\frac{W \sqrt{\theta}}{A \delta} = .592 \left[ \frac{M}{(1 + .2 M^2)^3} \right]$$

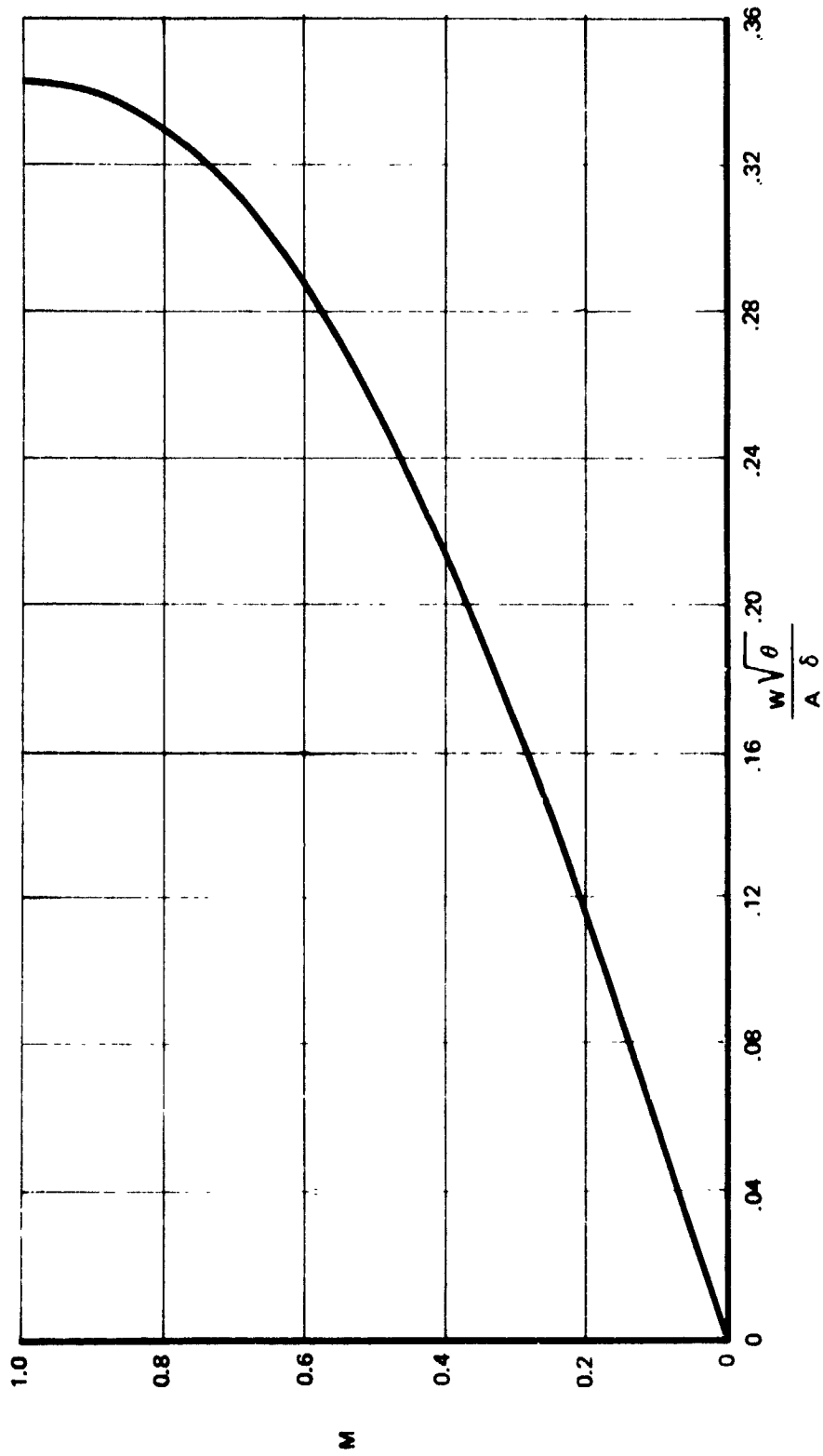


Figure 12: CORRECTED AIRFLOW PARAMETER

Next,  $(\frac{A}{A^*})_{T_{GEOM}}$  is calculated as follows:

$$\left(\frac{A}{A^*}\right)_{T_{GEOM}} = \left(\frac{A_T}{A_C}\right) \left(\frac{A_C}{A_O}\right) \left(\frac{A}{A^*}\right)_O \quad (3)$$

$M_{T_{GEOM}}$  is then obtained from the relation:

$$\frac{A}{A^*} = \frac{(1 + .2M^2)^3}{1.728M} \quad \gamma = 1.40 \quad (4)$$

This relation is plotted in Figure 13, for convenient use in performing hand calculations, if desired.

The effect of adding flow area by takeoff doors is accounted for by adding the takeoff door geometric throat area to the inlet geometric throat area and then calculating the throat Mach number the same way as before.

After calculating the throat Mach number based on geometric area,  $M_{T_{GEOM}}$ , the effective throat Mach number,  $M_{T_{EFF}}$ , is obtained from plotted data (or table-look-up, in case of the computer program) showing the variation of  $M_{T_{EFF}}$  as a function of  $M_{T_{GEOM}}$  and lip bluntness parameter,  $r/D$ . An example of this plotted data is shown in Figure 14.

The ratio of effective throat area to geometric throat area,  $\frac{A_{T_{EFF}}}{A_{T_{GEOM}}}$ , is next obtained from the following equation:

$$\frac{A_{T_{EFF}}}{A_{T_{GEOM}}} = \frac{(\frac{A}{A^*})_{EFF}}{(\frac{A}{A^*})_{GEOM}} = f(M_{T_{EFF}}, M_{T_{GEOM}}) \quad (5)$$

The simplifying assumption is made that  $\frac{A_{T_{EFF}}}{A_{T_{GEOM}}} = \frac{P_{T_2}}{P_{T_1}}$ .

This assumption is based on the following rationale:

If  $A_1 = A_2$  but there is a loss in total pressure between point 1 and 2, then the Mach number at point 2 will be higher than that at point 1, because of the effective

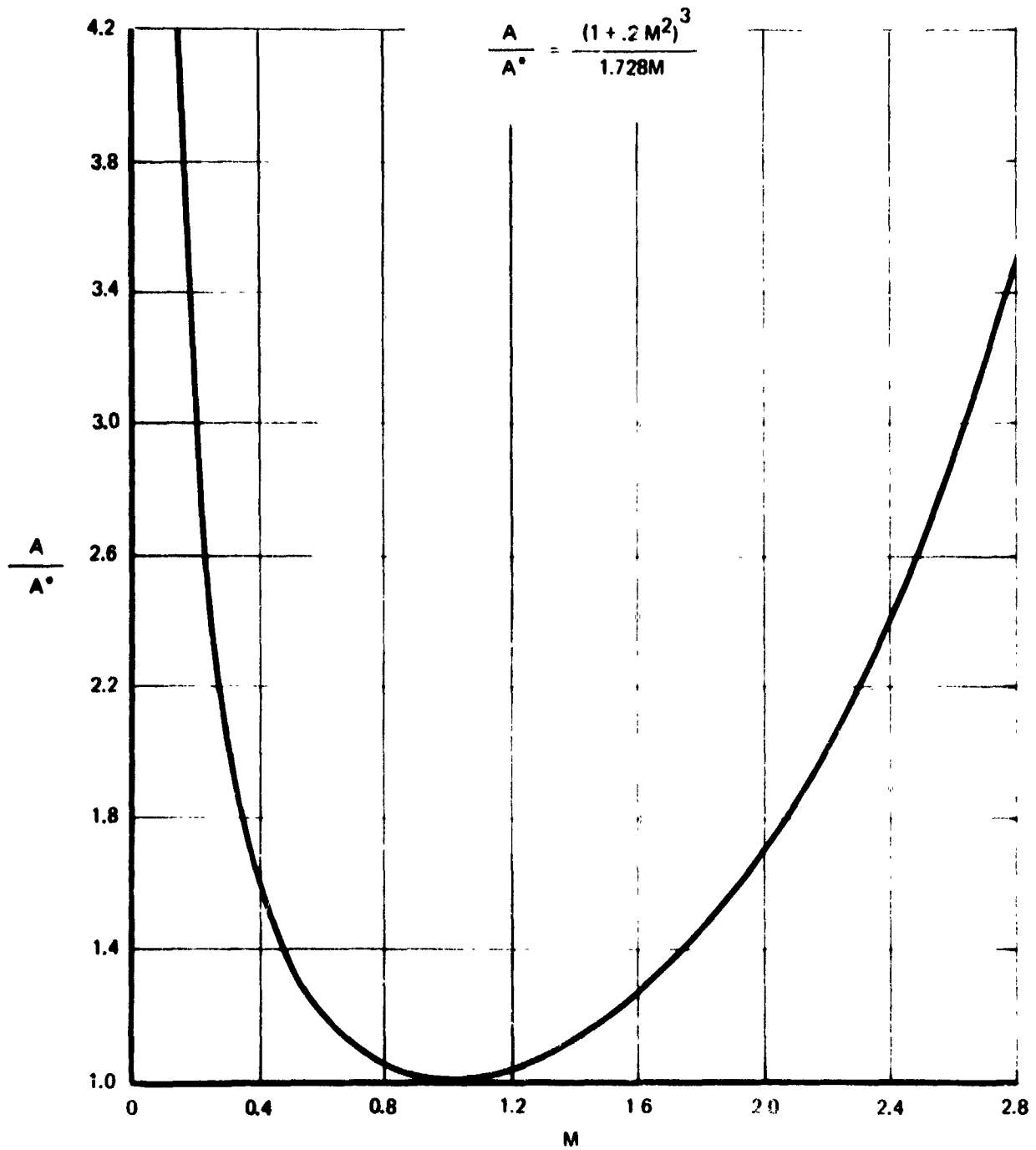


Figure 13: ISENTROPIC AREA RATIO

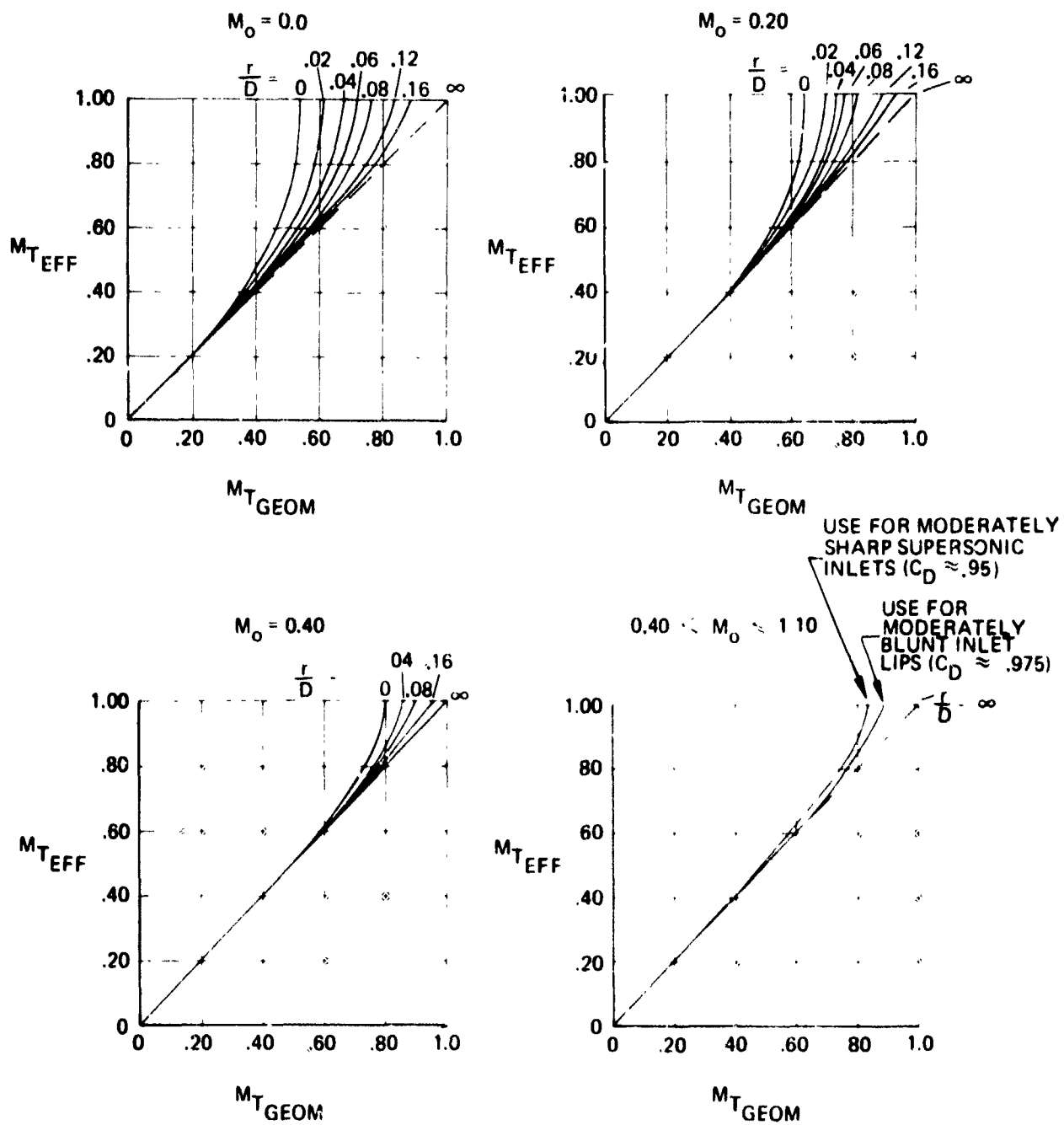


Figure 14: EFFECTIVE INLET THROAT MACH NUMBER

reduction in area ratio,  $(A/A^*)_2$ , since  $(A^*)_2$  has increased. The present method assumes that the reduction in  $(A/A^*)_2$  is equivalent to that obtained by reducing  $A_2$  and keeping  $A^*$  constant between points 1 and 2. Thus, there is a direct relationship between  $A_{2\text{EFF}}$  and  $A_1$  which is related to the lip loss. This relationship can be expressed as:

$$\frac{P_{T_T}}{P_{T_1}} = \frac{A_{2\text{EFF}}}{A_2}$$

and since  $A_2 = A_1$ , and  $A_2 = A_T$

$$\frac{P_{T_T}}{P_{T_1}} = \frac{A_{T\text{EFF}}}{A_{T\text{GEOM}}}$$

Thus, the  $\frac{A_{T\text{EFF}}}{A_{T\text{GEOM}}}$  can be substituted for  $\frac{I_{T_T}}{P_{T_1}}$ .

After throat effective Mach number,  $M_{T\text{EFF}}$ , is obtained, the subsonic diffuser duct loss coefficient,  $\epsilon = \Delta P_T / q_{E_1}$ , is obtained from input data showing the variation of  $\epsilon$  versus  $M_{T\text{EFF}}$ .

$\epsilon$  is then used in the following equation to calculate the total pressure recovery of the subsonic diffuser:

$$\frac{P_{T_2}}{P_{T_T}} = 1 - \epsilon \left[ 1 - \frac{1}{(1 + .2M_{T\text{EFF}}^2)^{3.5}} \right] \quad (6)$$

For convenience in performing hand calculations this relation is shown plotted in Figure 15.

Overall total pressure is next computed from the product of throat recovery and diffuser recovery:

$$\frac{P_{T_2}}{P_{T_0}} = \left( \frac{P_{T_T}}{P_{T_0}} \right) \left( \frac{P_{T_2}}{P_{T_T}} \right) \quad (7)$$

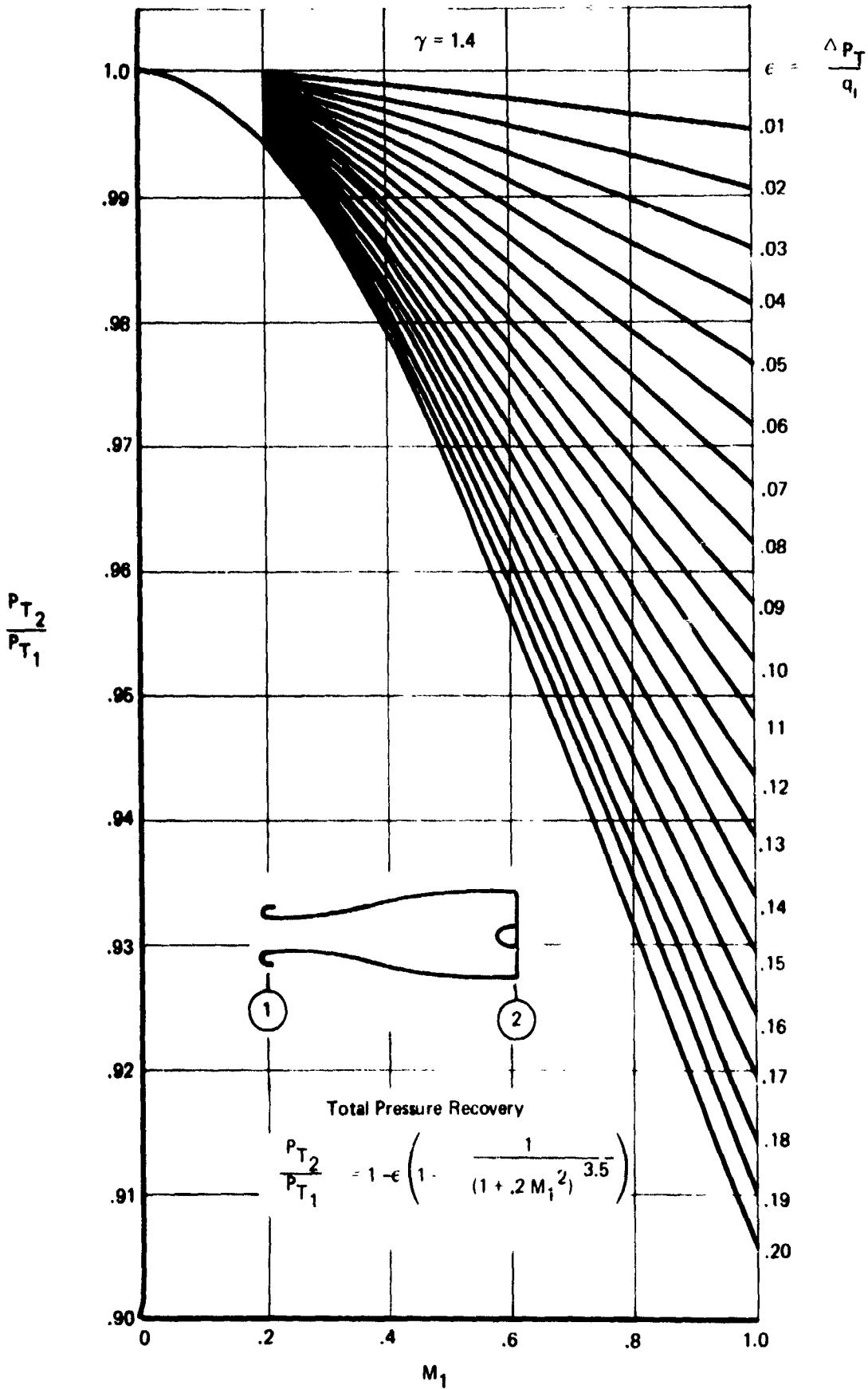


Figure 15: SUBSONIC DIFFUSER LOSS FACTORS

An assumption of  $P_{T_2}/P_{T_0} = .95$  is used for this purpose. The procedure operates by assuming a value of recovery, calculating throat Mach number, calculating sharp lip losses, calculating subsonic diffuser losses, sums the losses to obtain overall total pressure recovery and compares the calculated value with the assumed value. If the calculated and assumed values differ by more than .001, a new value of  $P_{T_2}/P_{T_0}$  is assumed that is equal to the average of the calculated and assumed recoveries and the calculation procedure is repeated.

#### 4.2.2 Subsonic and Transonic

In this speed range ( $.4 \leq M \leq 1.10$ ) the inlet total pressure recovery is determined almost entirely by the efficiency of the subsonic diffuser. Boundary layer bleed flow is usually not required. If excess air is taken into the inlet, it is discharged through a bypass system. At Mach numbers below 1.10, spillage is usually a better way to get rid of excess inlet airflow because it has a lower drag penalty than bypassing at these Mach numbers.

The total pressure recovery calculation procedure is shown in the flow chart of Figure 61.

The procedure involves an iterative solution for the diffuser losses that matches the airflow through the inlet. Initially, a recovery value of  $P_{T_2}/P_{T_0} = .95$  is assumed to begin the calculation. Using the assumed recovery, inlet mass flow ratio (assuming no bypass or internal bleed is used) is calculated by the following equation:

$$\frac{A_O}{A_C} = \frac{\left( \frac{W \sqrt{\theta}}{\delta} \right) \left( \frac{A}{A^*} \right)_O \left( \frac{P_{T_2}}{P_{T_0}} \right)}{(A_C) \cdot .343}$$

Next, the throat area ratio based on geometric throat flow area,  $\left( \frac{A}{A^*} \right)_{T_{\text{GEOM}}}$  is calculated from the following equation:

$$\left( \frac{A}{A^*} \right)_{T_{\text{GEOM}}} = \left( \frac{A_T}{A_C} \right) \frac{1}{(A_O/A_C)} \left( \frac{A}{A^*} \right)_O$$

From this area ratio, the throat Mach number,  $M_{T_{\text{GEOM}}}$ , is obtained from the relation:

$$\frac{A}{A^*} = \frac{(1 + .2M^2)^3}{1.728M} \quad (\text{This relation is illustrated in Figure 13})$$

A correction is then applied to account for the fact that the effective throat area is smaller than the geometric throat area. This correction is presented in the form shown in Figure 14. The correction is based on correlations of experimental data with theory used as a guide in fairing the curves where data points are not available. If the  $M_{T_{\text{EFF}}}$  is 1.00, then the assumed recovery is reduced by .05 and the process is reiterated, beginning with the calculation of  $A_0/A_C$  until a value of  $M_{T_{\text{EFF}}}$  is obtained which is just at or below  $M_{T_{\text{EFF}}} = 1.0$ .

The diffuser loss coefficient is then obtained from input data tables as a function of  $M_{T_{\text{EFF}}}$ . An example of this input data is presented in Figure 16.

Using the diffuser loss coefficient obtained above, the diffuser total pressure loss is calculated from:

$$\frac{P_{T_2}}{P_{T_T}} = 1 - \epsilon \left[ 1 - \frac{1}{(1 + .2 M_{T_{\text{EFF}}}^2)^{3.5}} \right]; \quad \gamma = 1.4$$

If there is also a loss in total pressure from free-stream to inlet location, the two losses are combined to yield the final total pressure recovery:

$$\frac{P_{T_2}}{P_{T_0}} = \left( \frac{P_{T_2}}{P_{T_T}} \right) \left( \frac{P_{T_T}}{P_{T_0}} \right)$$

If the calculated recovery differs by more than .001 from the assumed value, then the process is reiterated using a new value of recovery which is the average of the calculated and assumed values.

#### 4.2.3 Supersonic

The major causes of inlet total pressure losses in the supersonic speed regime ( $1.20 \leq M \leq 4.5$ ) are shock losses and subsonic diffuser losses. Shock-boundary layer interactions and the amount and distribution of boundary layer control

- (1) Ref: PG 117  
NA 68-655  
Vol X
- (2) Subsonic Entrance  
Profile
- (3) Diffuser  $L/h_t = 9$
- (4) Thin Boundary Layer

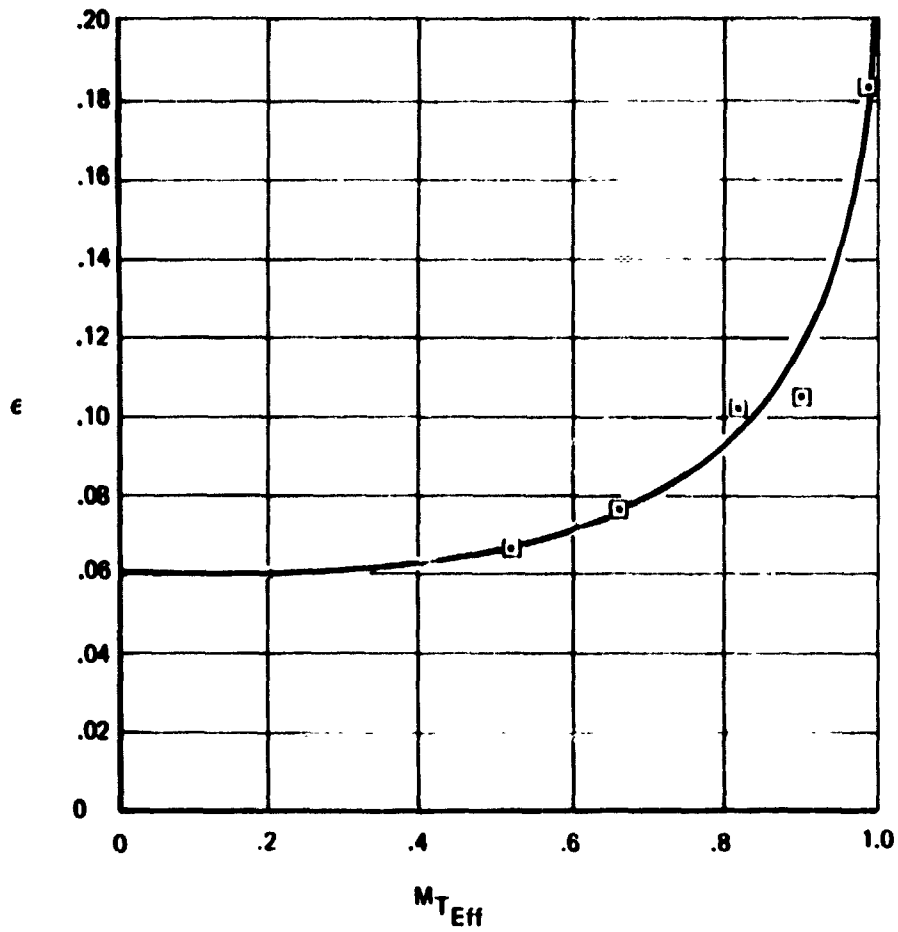


Figure 16: DIFFUSER LOSS COEFFICIENT

bleed airflow also affect both shock losses and subsonic diffuser efficiency. However, it is difficult to separate out the contribution of boundary layer effects on either shock losses or diffuser efficiency without extensive use of experimental data, which in many cases does not exist. The calculation method in the PITAP procedure uses estimated inviscid shock losses and subsonic diffuser losses based as much as possible on the results of experimental work. The effects of boundary layer on shock losses are accounted for by correcting the ideal shock losses to make them agree closer with experimental results. The effect of boundary layer on subsonic diffuser losses is accounted for by using realistic diffuser duct loss coefficients obtained from experimental data.

#### 4.2.3.1 Two-Dimensional Inlets

Inviscid total pressure recovery of an inlet supersonic diffuser depends on the number and strength of shocks used to decelerate the flow from supersonic to subsonic Mach numbers. Figure 17 shows the trends in total pressure recovery as a function of free-stream Mach number and the number of shocks, including all oblique shocks and the normal shock. Also shown in Figure 17 is a dashed line representing the approximate maximum obtainable recovery based on experimental data. When an inlet is operating at a free-stream Mach number which is at or below its design Mach number, and has variable ramps that can be positioned to provide nearly optimum ramp geometry, the total pressure recovery can be obtained from the curves of Figure 17. The maximum practical recovery (shown as a dashed line in Figure 17) is used as an upper bound. For the case where an inlet is operating above its maximum design Mach number (except for a normal shock inlet,  $N = 1$ ), flow stability problems are commonly encountered due to shock waves entering the inlet. Therefore, this condition is not of much practical interest for most preliminary design studies.

The ramp geometry required to provide the estimated total pressure recovery can be obtained from Figure 18, which shows the total deflection for optimum shock systems having various numbers of oblique shocks as a function of free-stream Mach number. If all the compression were accomplished externally, the summation of the deflection angles would be equal to the last ramp angle. If only a portion of the compression is done externally, the last external ramp angle is correspondingly less. In this way, depending on the specified external/internal compression split, the last external ramp angle can be calculated from the equation:

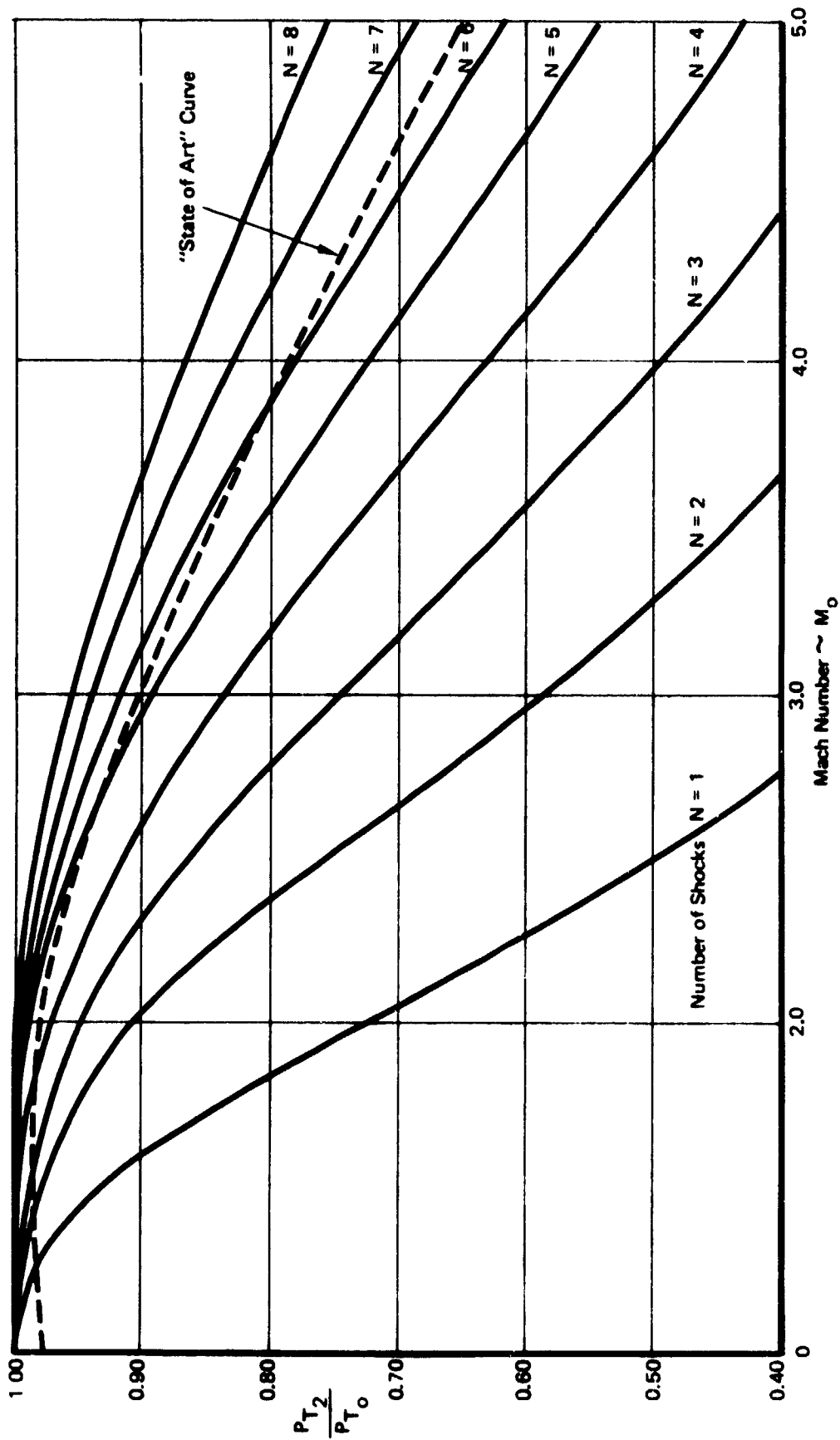


Figure 17: SHOCK LOSS DATA

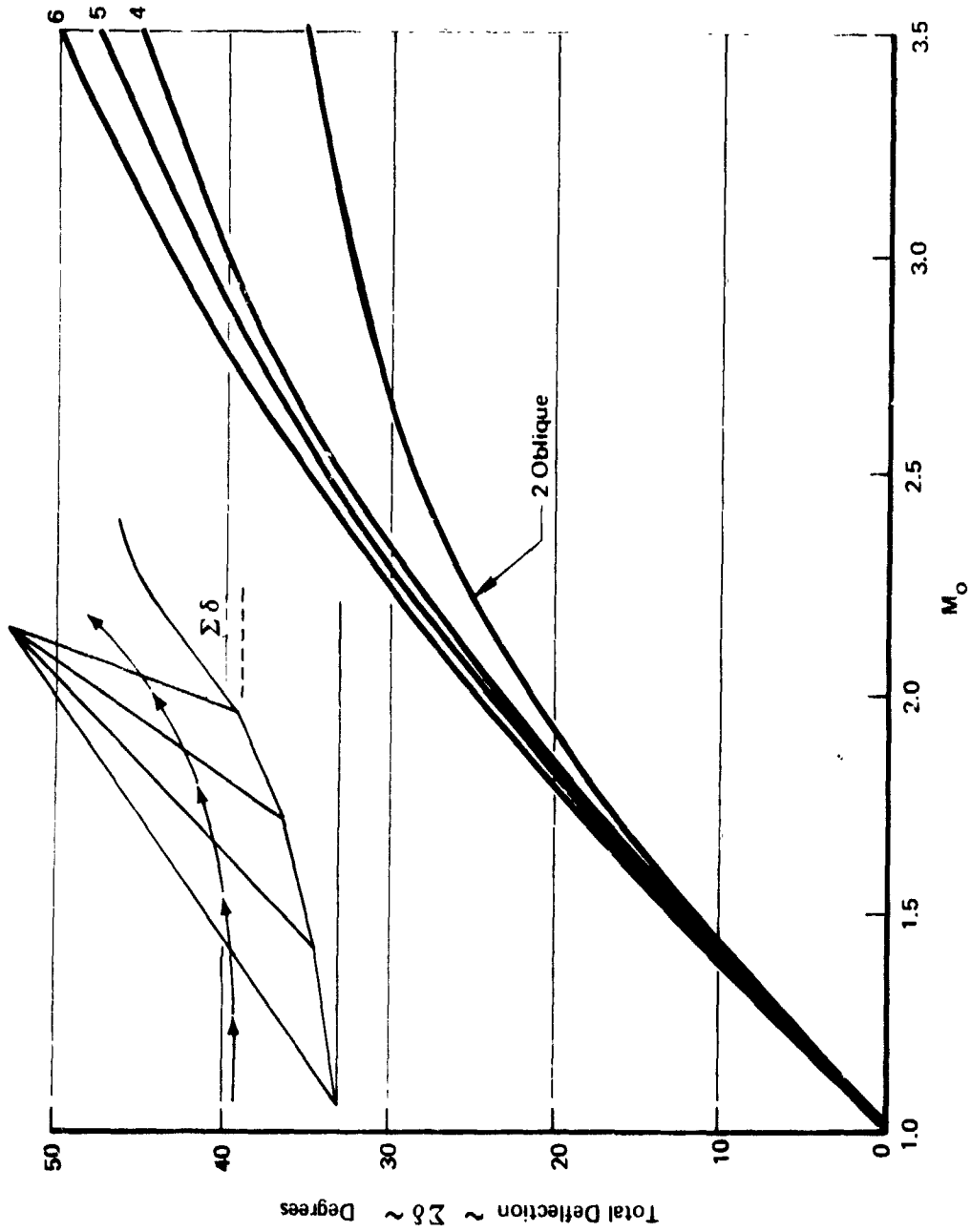


Figure 18: Shock Flow Deflections

$$\Sigma \delta_{EXT} = \left( \frac{\Sigma \delta_{EXT}}{\Sigma \delta} \right) (\Sigma \delta) \quad (8)$$

where  $\left( \frac{\Sigma \delta_{EXT}}{\Sigma \delta} \right)$  is the specified external/total compression split.

The inlet throat size is calculated from the following equation:

$$\frac{(A_T/A_C)}{(A_O/A_C)} = \left( \frac{A}{A^*} \right)_T \left( \frac{A^*_T}{A^*_O} \right) \left( \frac{A^*}{A_O} \right) \quad (9)$$

where  $A_T$  = throat area, in.<sup>2</sup>  
 $A_C$  = inlet capture area, in.<sup>2</sup>  
 $A_O/A_C$  = inlet mass flow ratio passing through the throat  
 $A/A^*_T = \frac{(1 + .2M_T^2)^3}{1.728 M_T}$   
 $A^*_T/A^*_O = \frac{1}{P_T/P_{T_O}}$

A flow chart showing the steps involved in the calculation procedure is presented in Figure 62.

#### 4.2.3.2 Axisymmetric Inlets

The total pressure recovery of an axisymmetric inlet can be obtained from the plotted data of Figures 19 and 20 in a similar manner to that used for two-dimensional inlets. Figure 19 presents recovery plots for external compression inlets and Figure 20 presents plots for inlets with external and internal compression.

#### 4.3 BOUNDARY LAYER BLEED DRAG

To calculate the drag of boundary layer bleed air, it is necessary to know the geometry and location of the bleed exit nozzle, the amount of bleed airflow, and the total pressure recovery of the bleed air at the nozzle exit. Methods for estimating the last two parameters and calculating the drag are described in this section.

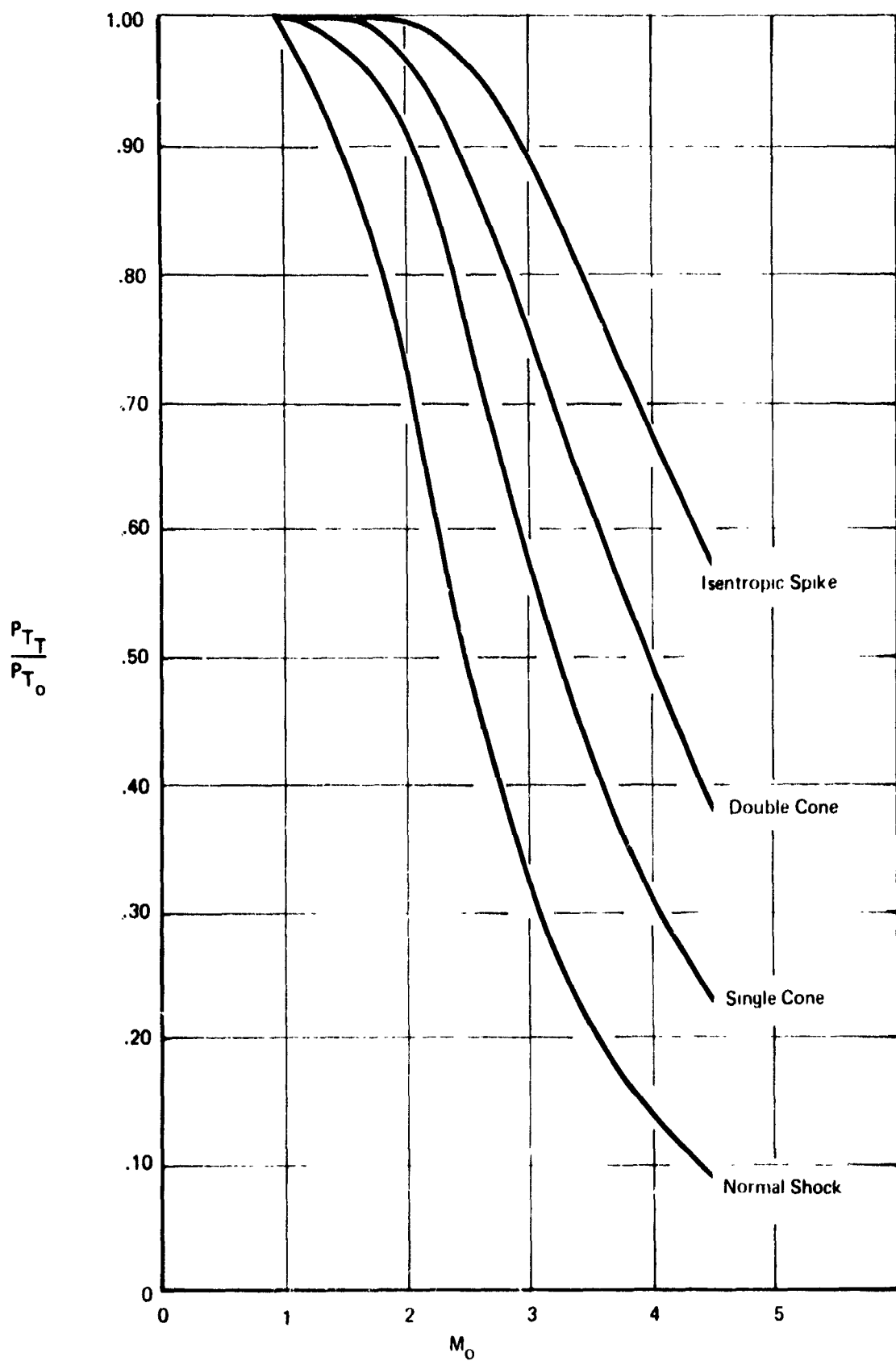


Figure 19: MAXIMUM INVISCID TOTAL PRESSURE RECOVERY FOR AXISYMMETRIC INLETS (EXTERNAL COMPRESSION)

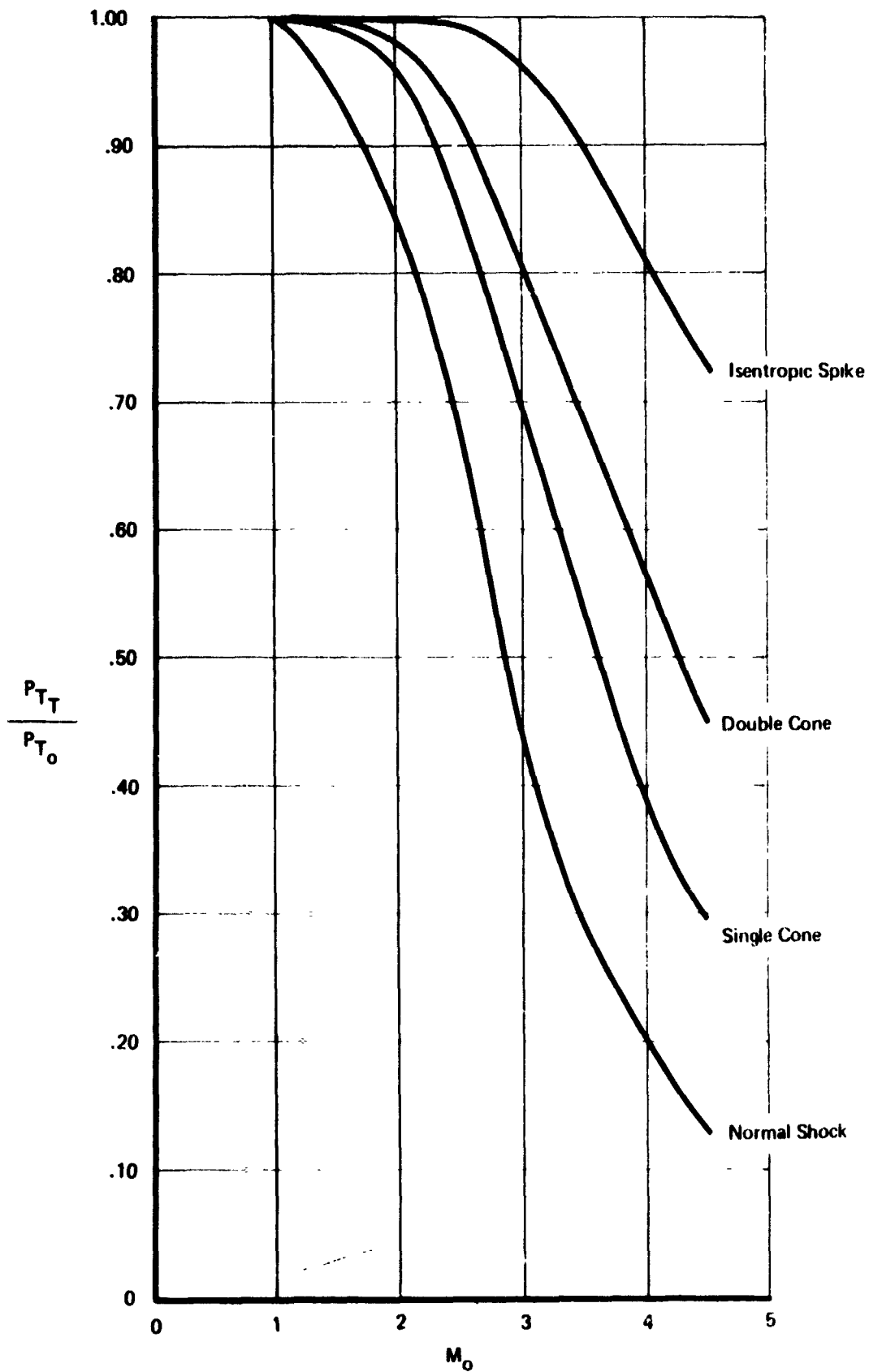


Figure 20: MAXIMUM INVISCID TOTAL PRESSURE RECOVERY FOR AXISYMMETRIC INLETS (EXTERNAL AND INTERNAL COMPRESSION)

#### 4.3.1 Airflow

The amount of bleed air required is obtained from Figure 21. These data were obtained from experimental data (References 2 through 6), and represent a nearly optimum bleed configuration.

#### 4.3.2 Recovery

The bleed plenum total pressure recovery is obtained from Figure 22. These pressure recoveries represent average values obtained from experimental data (References 3 through 5).

A flow chart showing the steps in the procedure required to obtain bleed airflow and total pressure recovery is presented in Figure 63.

#### 4.3.3 Drag

The output of the boundary layer bleed subroutine is used as input to the momentum and flap drag subroutines which are used for both bleed drag and bypass drag calculations. The only difference is that the bleed air,  $A_{O_{BLC}}/A_C$ , is used in

bleed calculations and bypass air is used in bypass drag calculations.

Bleed (and bypass) drag is composed of two parts: momentum drag and flap (or exit) drag. Momentum drag depends on the exit angle of the discharged air, total pressure recovery of the discharged air, type of nozzle through which the air is exited, and free-stream Mach number. Flap drag depends on door angle, door aspect ratio, and free-stream Mach number.

##### 4.3.3.1 Momentum Drag

The procedure for calculating momentum drag is presented in the flow chart of Figure 64. The input quantities required for the calculation are:

$M_O$	~	local Mach number, dimensionless.
$\theta$	~	exit angle of air relative to free-stream, degrees.
$\frac{P_{TE}}{P_{TO}}$	~	total pressure recovery of bypassed airflow, dimensionless.
$\frac{A_{O_{BLC}}}{A_C}$	~	boundary layer bleed mass flow ratio, dimensionless.

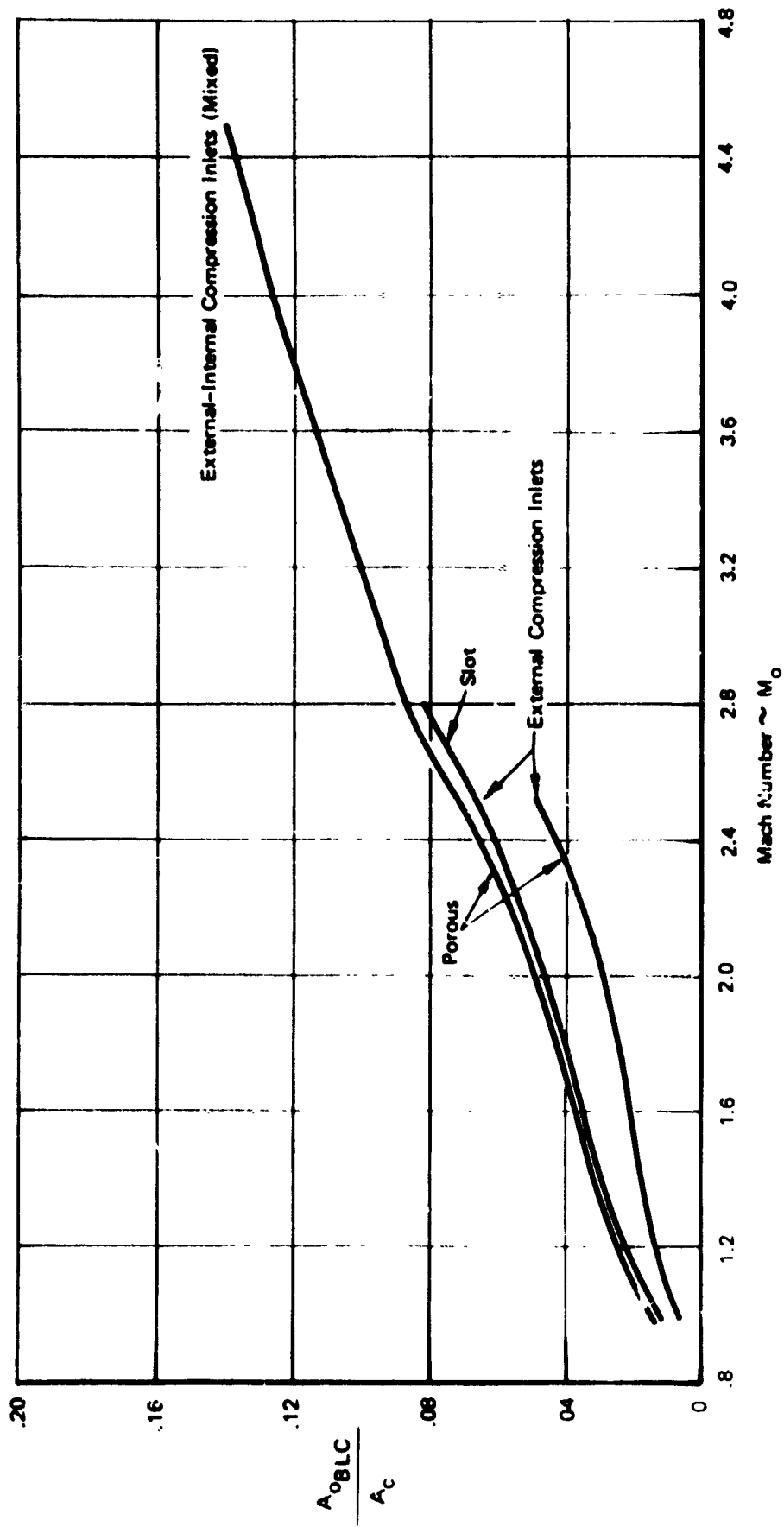


Figure 21. BOUNDARY LAYER BLEED

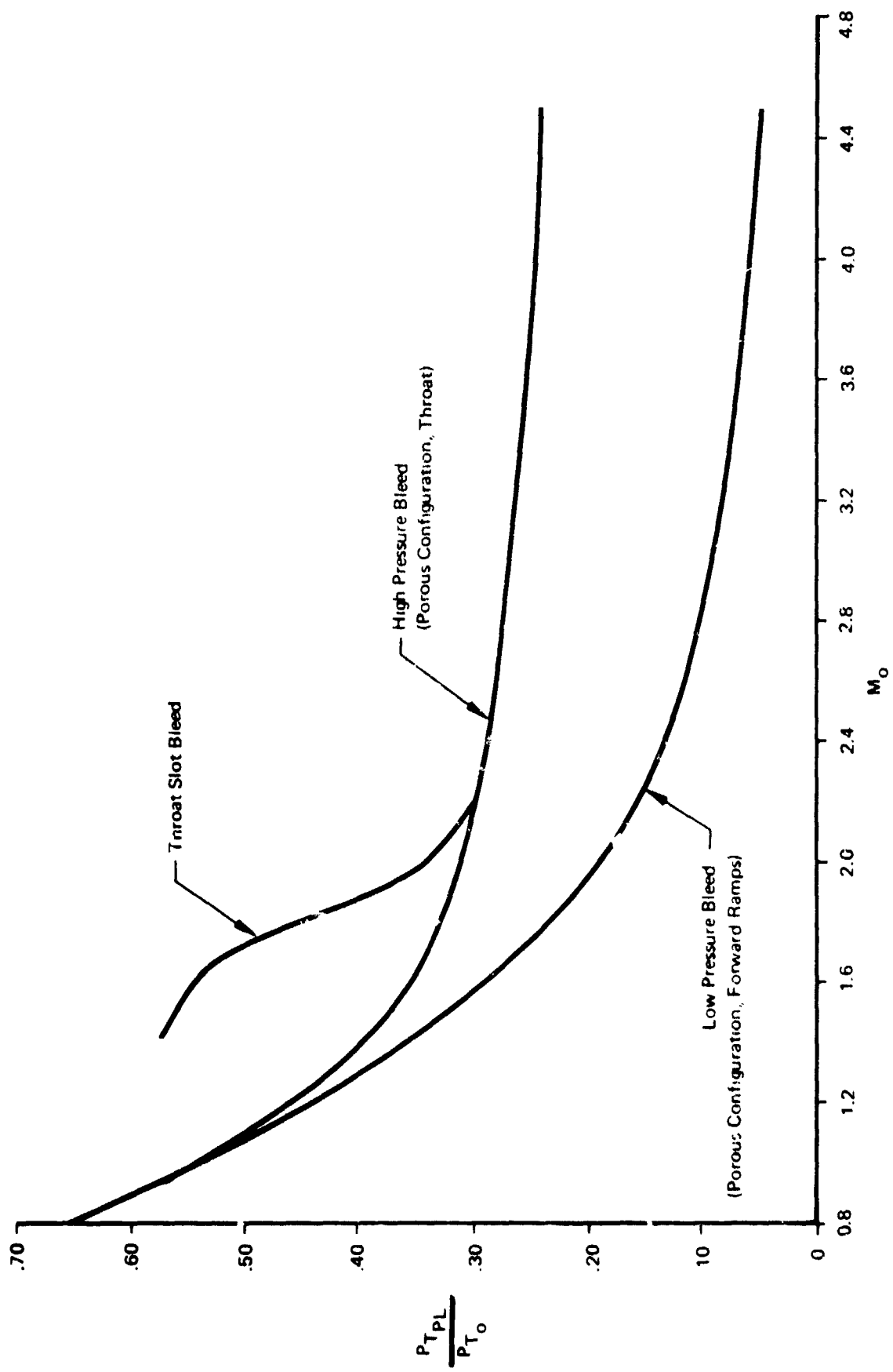


Figure 22: PLENUM TOTAL PRESSURE RECOVERY

$\frac{A_{O_{BP}}}{A_C}$  ~ bypass mass flow ratio, dimensionless.

$A_C$  ~ inlet capture area, in.<sup>2</sup>

Nozzle type must be specified as one of the following types:

- (a) ~ Convergent nozzle
- (b) ~ Convergent-divergent nozzle, fully expanded
- (c) ~ Convergent-divergent nozzle with a specified area ratio,  $A_E/A_T$ , dimensionless

$A_E$  = nozzle exit area, in.<sup>2</sup>

$A_T$  = nozzle throat area, in.<sup>2</sup>

(a) Convergent Exit

The first step in the calculation of momentum drag for the convergent nozzle is a test to determine if the nozzle is choked. This is accomplished by calculating  $M_{O_{min}}$  according to the following equation:

$$M_{O_{min}} = \sqrt{\frac{6}{\left(\frac{P_{TE}}{P_{TO}}\right)^{.286}} - 5} \quad (10)$$

$M_{O_{min}}$  represents the lowest free-stream Mach number at which the available pressure ratio will be sufficient to choke the nozzle throat. If  $M_O < M_{O_{min}}$ , the nozzle throat is assumed choked,  $M_E = 1.0$ , and  $P_E/P_O = 1.0$ .

Next, the nozzle throat area is calculated by the equation:

$$A_T, \text{ in.}^2 = \frac{\left(\frac{A_{O_{BLC}}}{A_C}\right) A_C}{\left(\frac{A}{A^*}\right)_O \left(\frac{P_{TE}}{P_{TO}}\right)} \quad (11)$$

Drag, as a fraction of the free-stream momentum of the bypassed airflow,  $\frac{D}{\frac{(W_a V_O)}{g}}$ , is calculated by the following equation:

$$\frac{D}{\frac{(W_a V_O)}{g}} = 1 - \frac{\cos \theta}{M_O} \sqrt{\frac{2 + .4 M_O^2}{2.4}} \left\{ 1.715 - \left[ \frac{.715}{\left( \frac{P_{T_E}}{P_{T_O}} \right) \left[ \frac{2 + .4 M_O^2}{2.4} \right]^{3.5}} \right] \right\} \quad (12)$$

Converting the above drag to  $C_D$ :

$$C_D = 2 \left( \frac{A_{O_{BLC}}}{A_C} \right) \left[ \frac{D}{\frac{(W_a V_O)}{g}} \right] \quad (13)$$

If exit area,  $A_E$ , and  $P_{T_E}/P_{T_O}$  are specified instead of  $A_{O_{BLC}}/A_C$  and  $P_{T_E}/P_{T_O}$ , (as above) the following calculation procedure is used to determine bleed drag:

The bleed airflow,  $A_{O_{BLC}}/A_C$ , is first computed (if it is not specified) by the following equation:

$$\frac{A_{O_{BLC}}}{A_C} = \frac{(A_T)}{(A_C)} \left( \frac{A}{A^*} \right)_O \left( \frac{P_{T_E}}{P_{T_O}} \right)$$

After  $A_{O_{BLC}}/A_C$  is calculated, the drag calculation proceeds in the same way as before, using Equation (12).

For an unchoked convergent nozzle, ( $M_O = M_{O_{min}}$ ), the exit static-to-total pressure ratio,  $P_E/P_{T_E}$ , is calculated by the following steps:

$$\frac{P_O}{P_{T_O}} = \frac{1}{(1 + .2 M_O^2)^{3.5}} \quad (14)$$

Next, the exit static-to-total pressure ratio is calculated:

$$\frac{P_E}{P_{T_E}} = \frac{\left(\frac{P_O}{P_{T_O}}\right)}{\left(\frac{P_{T_E}}{P_{T_O}}\right)} \quad (15)$$

Next,  $M_E$  is obtained from  $\frac{P_E}{P_{T_E}}$  using Equation (14).

Then  $\left(\frac{A}{A^*}\right)_E$  is obtained using  $M_E$  and the following equation:

$$\left(\frac{A}{A^*}\right)_E = \frac{(1 + .2 M_E^2)^3}{1.728 M_E}$$

The throat area is then calculated by:

$$A_T = \frac{\left(\frac{A_{O_{BLC}}}{A_C}\right) A_C \left(\frac{A}{A^*}\right)_E}{\left(\frac{A}{A^*}\right)_O \left(\frac{P_{T_E}}{P_{T_O}}\right)} \quad (16)$$

Drag, as a fraction of free-stream momentum, is calculated by:

$$\frac{D}{\frac{W a V_O}{g}} = 1 - \cos \theta \sqrt{\left[\frac{2}{.4 M_O^2} + 1\right] \left[1 - \frac{1}{(1 + .2 M_O^2) \frac{P_{T_E}}{P_{T_O}} .286}\right]} \quad (17)$$

$C_D$  is then calculated as before:

$$C_D = 2 \left(\frac{A_{O_{BLC}}}{A_C}\right) \left(\frac{D}{\frac{W a V_O}{g}}\right)$$

(b) Convergent-Divergent Exit

A test is first performed to determine whether the nozzle throat is choked.  $M_{O_{min}}$  is calculated and compared with  $M_O$

as in the case of the convergent nozzle calculation. If the calculation shows that the nozzle throat is not choked, the C-D nozzle is not a good choice and the configuration should be re-examined, since excessive drag would result from the use of this configuration. If this happens, the computer program terminates the case and goes to the next case.

If the test shows that the throat is choked, two calculation procedures can be followed.

(c) C-D Exit Fully Expanded

If it is specified in the input data that the C-D nozzle is to be fully expanded, the exit static pressure,  $P_E$ , is assumed to be equal to ambient pressure,  $P_O$ , and the nozzle exit static-to-total pressure ratio  $P_E/P_{T_E}$  is calculated from the following equation:

$$\frac{P_E}{P_{T_E}} = \frac{\left(\frac{P_O}{P_{T_O}}\right)}{\left(\frac{P_{T_E}}{P_{T_O}}\right)}$$

Using the above ratio, exit Mach number is obtained from the relation:

$$\frac{P_E}{P_{T_E}} = \frac{1}{(1 + .2M_E^2)^{3.5}}$$

Next, the free-stream static-to-total pressure ratio is calculated:

$$\frac{P_O}{P_{T_O}} = \frac{1}{(1 + .2 M_O^2)^{3.5}}$$

Then  $\frac{P_E}{P_O}$  is calculated from the relation:

$$\frac{P_E}{P_O} = \frac{\left(\frac{P_E}{P_{T_E}}\right) \left(\frac{P_{T_E}}{P_{T_O}}\right)}{\left(\frac{P_O}{P_{T_O}}\right)} \quad (18)$$

Nozzle area ratio is calculated by:

$$\frac{A_E}{A_T} = \frac{(1 + .2 M_E^2)^3}{1.728 M_E} \quad (19)$$

Nozzle throat area size is calculated by:

$$A_T, \text{ in}^2 = \frac{\left(\frac{A_{O_{BLC}}}{A_C}\right) (A_C)}{\left(\frac{A}{A^*}\right)_O \left(\frac{P_{T_E}}{P_{T_O}}\right)} \quad (20)$$

Nozzle exit area is calculated from:

$$A_E, \text{ in}^2 = \left(\frac{A_E}{A_T}\right) (A_T) \quad (21)$$

Drag is then computed from the following relation:

$$\frac{D}{\left(\frac{W}{g}\right) \left(\frac{V}{a_O}\right)} = 1 - \cos \theta \sqrt{\left[\frac{2}{.4 M_O^2} + 1\right] \left[1 - \frac{1}{(1 + .2 M_O^2) \left(\frac{P_{T_E}}{P_{T_O}}\right)^{.286}}\right]}$$

Converting to  $C_D$ :

$$C_D = 2 \left( \frac{A_{O_{BLC}}}{A_C} \right) \left( \frac{D}{\frac{W_a V_O}{g}} \right)$$

(d) Convergent-Divergent Exit with Specified Area Ratio

If the throat of the nozzle is choked, as will have been determined from the test that was made using  $M_O \geq M_{O_{min}}$ , the calculation proceeds as described below.

The nozzle area  $A_E/A^*$  is set equal to the specified nozzle area ratio  $A_E/A_T$ . Then the free-stream  $(A/A^*)_O$  is obtained from Figure 13. These data provide the necessary items to calculate nozzle throat area according to the following equation:

$$A_T = \frac{\left( \frac{A_{O_{BLC}}}{A_C} \right) (A_C)}{\left( \frac{A}{A^*} \right)_O \left( \frac{P_{T_E}}{P_{T_O}} \right)}$$

Then nozzle exit area is computed from:

$$A_E = \left( \frac{A_E}{A_T} \right) (A_T)$$

The nozzle exit Mach number,  $M_E$ , is obtained from Figure 13 as a function of the nozzle  $A_E/A^*$  ratio. Then the exit pressure ratio,  $P_E/P_{T_E}$ , is calculated from the equation:

$$\frac{P_E}{P_{T_E}} = \frac{1}{\left( 1 + .2 M_E^2 \right)^{3.5}}$$

Also, the free-stream pressure ratio is calculated from the same equation.

Next, the exit pressure ratio,  $\frac{P_E}{P_O}$ , is calculated from :

$$\frac{P_E}{P_O} = \frac{\left(\frac{P_E}{P_{T_E}}\right) \left(\frac{P_{T_E}}{P_{T_O}}\right)}{\frac{P_O}{P_{T_O}}}$$

Drag is then computed from:

$$\left(\frac{D}{\frac{W a V_O}{g}}\right) = 1 - \frac{\cos \theta}{M_O} \left\{ M_E \left[ \frac{1+.2M_O^2}{1+.2M_E^2} \right]^{1/2} - \frac{\left[ \left(\frac{P_{T_E}/P_{T_O}}\right) - \frac{[1+.2M_O^2]}{[1+.2M_E^2]} \right]^{3.5}}{\left(\frac{A_T}{A_E}\right) (.808) [1+.2M_O^2]^3} \right\} \quad (22)$$

This is converted to drag coefficient by:

$$C_D = 2 \left(\frac{A_{O_{BLC}}}{A_C}\right) \frac{D}{\left(\frac{W a V_O}{g}\right)}$$

All the equations for bypass momentum drag and flap drag are the same as those used for boundary layer control bleed airflow drag calculations.

#### 4.3.3.2 Flap Drag

Flap drag is calculated by integrating the predicted pressure coefficients acting on the exit doors in the flight direction. To accomplish this, tables of average pressure coefficients for doors of various aspect ratios (W/h) from .75 to 4.0 are used as input data to obtain the pressure coefficients.

A correction is also applied to account for the fact that the doors are usually operating in a region of turbulent boundary layer. The detailed steps used in the calculation procedure are shown in Figure 64 and described in the sections which follow.

- W ~ door width, inches
- h ~ length of door, inches
- n ~ number of doors, dimensionless
- $A_{O_{BLC}}/A_C$  ~ Bleed mass flow ratio
- $A_C$  ~ capture area size, in<sup>2</sup>
- $M_O$  ~ free-stream Mach number, dimensionless
- $\frac{P_{T_E}}{P_{T_O}}$  ~ total pressure recovery of the airflow, dimensionless
- $C_p$  vs  $M_O$ ,
- $R$  &  $\theta$  EFF ~ tables of average pressure coefficient vs free-stream Mach number, door aspect ratio, and door angle.

Door aspect ratio is computed from the input door dimensions:

$$R = W/h \quad (23)$$

The next step in the calculation procedure is to compute the ratio of door exit area to capture area,  $A_E/A_C$ . Two possibilities exist: convergent nozzle and convergent-divergent nozzle.

For a convergent exit, the exit area is calculated by the following equation:

(where  $A_E/A^*_E = 1.0$  for a choked convergent nozzle)

$$\frac{A_E}{A_C} = \frac{\left(\frac{A_{O_{BLC}}}{A_C}\right) \left(\frac{A_E}{A^*_E}\right)}{\left(\frac{A}{A^*}\right)_O \left(\frac{P_{T_E}}{P_{T_O}}\right) (.95)} \quad (24)$$

(0.95 is the assumed flow coefficient)

This equation assumes that the exit consists of  $n$  doors of equal size.

The door flap angle is calculated from:

$$(\theta_{FLAP})_{ACTUAL} = \tan^{-1} \left[ \frac{\left(\frac{A_E}{A_C}\right)}{\left(\frac{A_{FLAP}}{A_C}\right)} \right] \quad (25)$$

$$\text{Where } \frac{A_{FLAP}}{A_C} = \frac{Wh}{A_C} \quad (26)$$

Using  $(\theta_{FLAP})_{ACTUAL}$  and free-stream Mach number,  $M_O$ , the effective door angle is obtained from the plotted data of Figure 23, which shows the effect that turbulent boundary layer has on reducing flap angle. From the plotted data,  $(\theta_{FLAP})_{EFF}$ , the effective door flap angle, is obtained as a function of actual door angle and free-stream Mach number, assuming average turbulent boundary layer conditions.

The average pressure coefficient over the surface of the door is obtained from the data of Figure 24 as a function of  $(\theta_{FLAP})_{EFF}$ ,  $M_O$ , and  $R$ .

Using the pressure coefficients, the flap drag coefficient is calculated from the following equation:

$$(C_{D_{FLAP}})_{TOTAL} = \left\{ C_P \left[ \sin (\theta_{FLAP})_{ACTUAL} \right] \left( \frac{A_{FLAP}}{A_C} \right) n \right\} \quad (27)$$

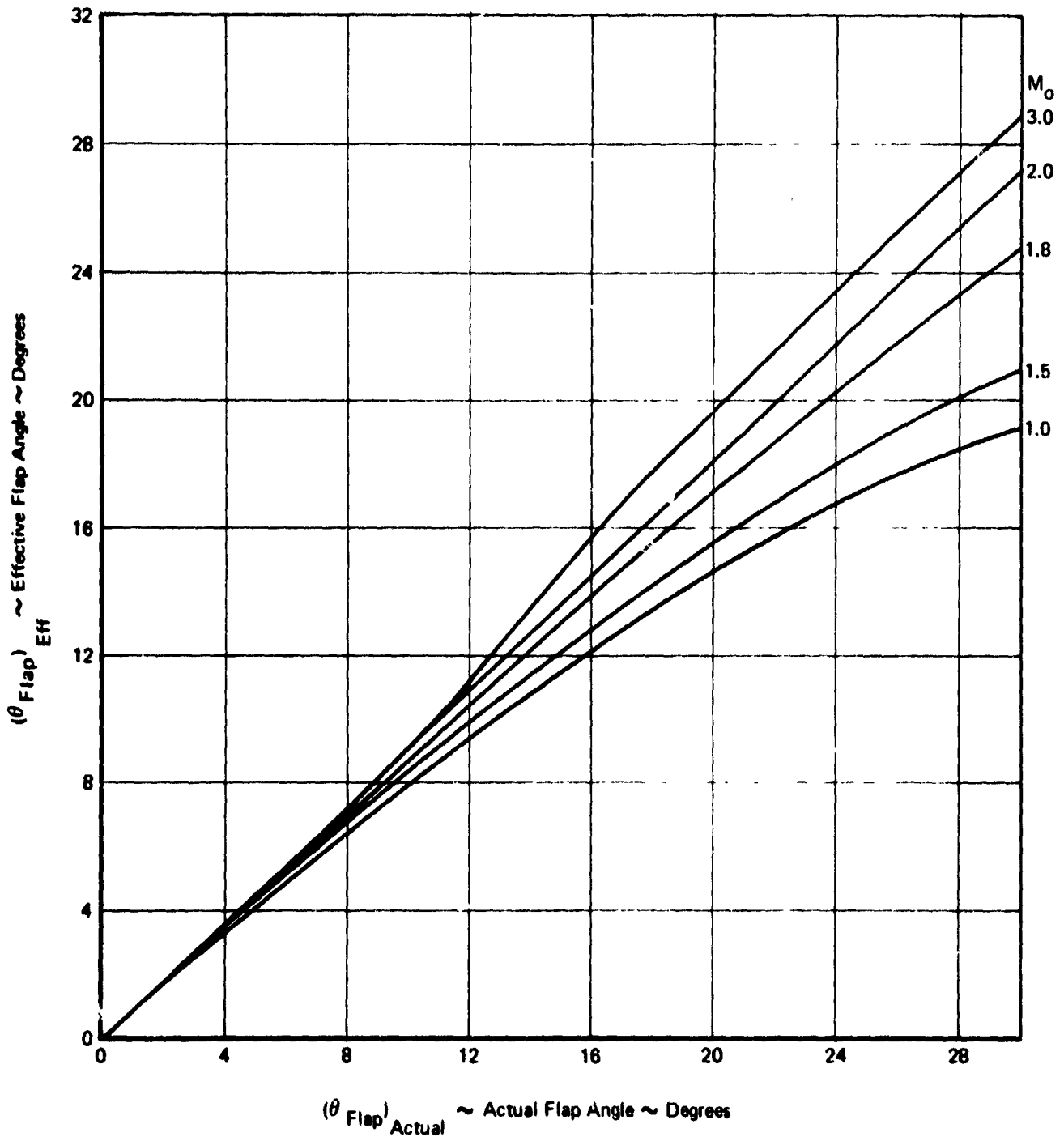


Figure 23: EFFECT OF TURBULENT BOUNDARY LAYER ON BYPASS FLAP ANGLE

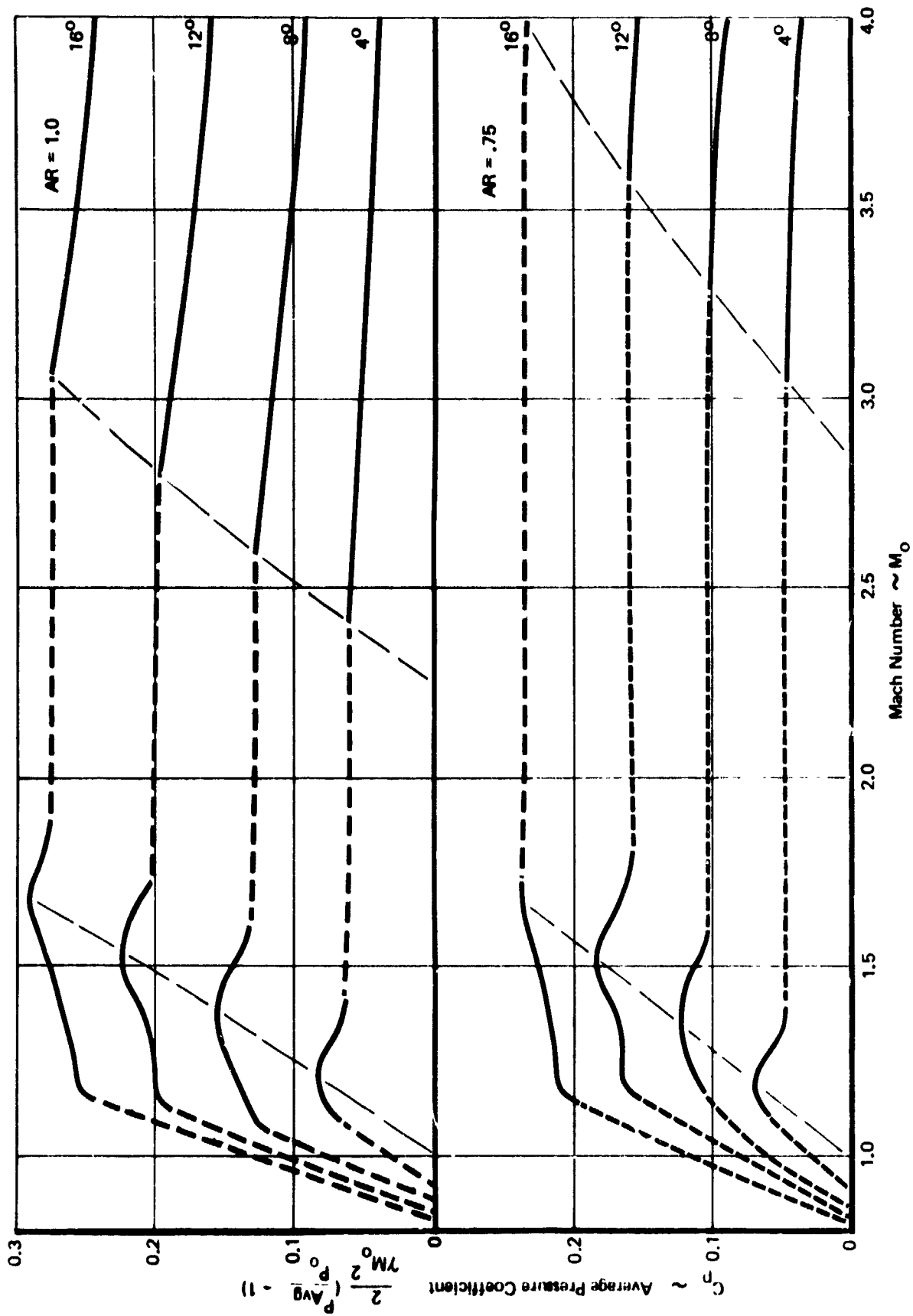


Figure 24: BYPASS DOOR PRESSURE COEFFICIENTS

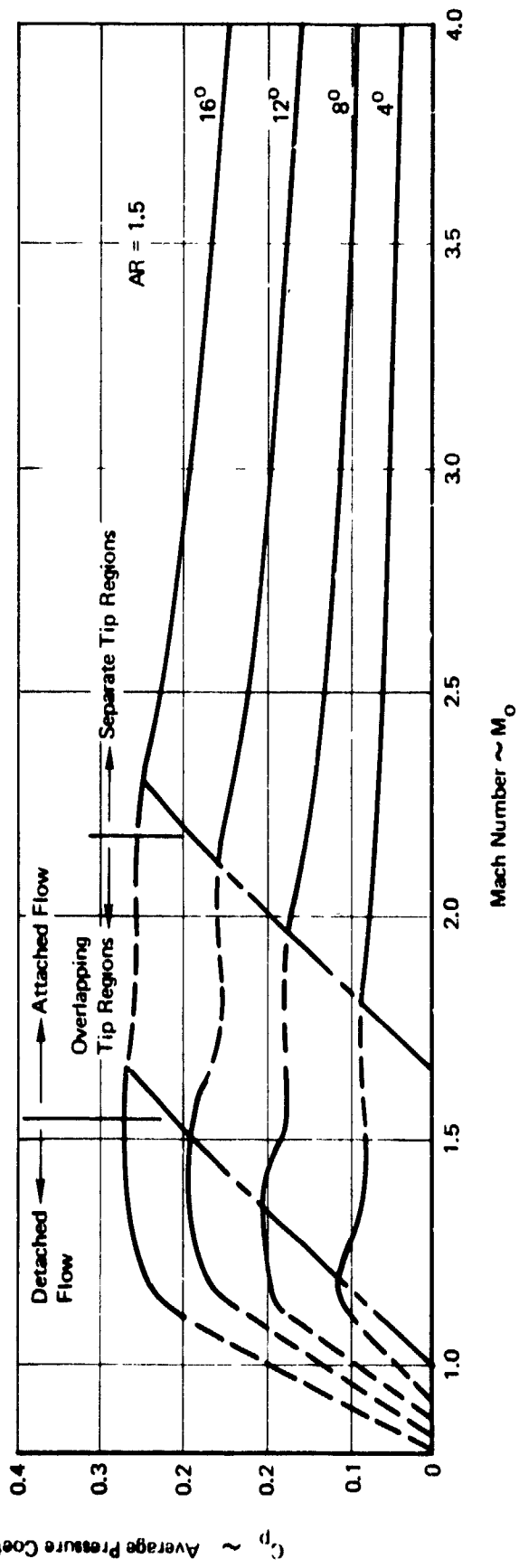
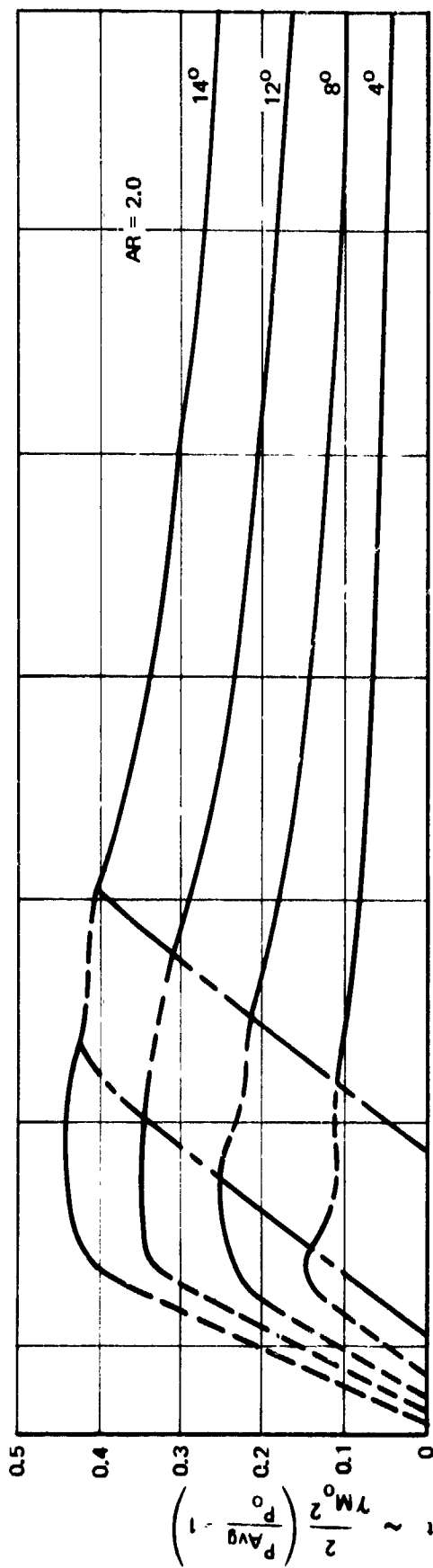


Figure 24. BYPASS DOOR PRESSURE COEFFICIENTS (Cont)

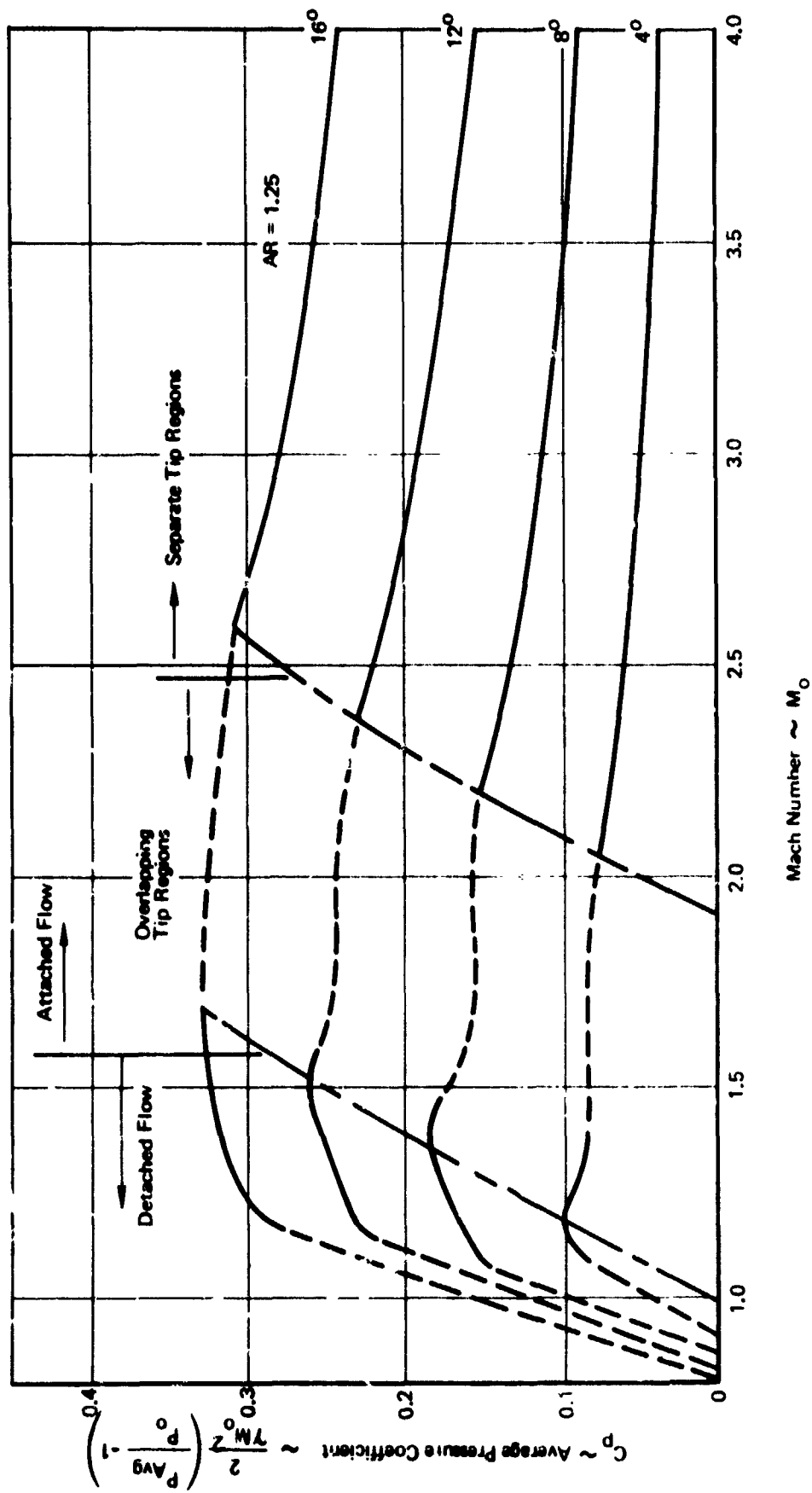
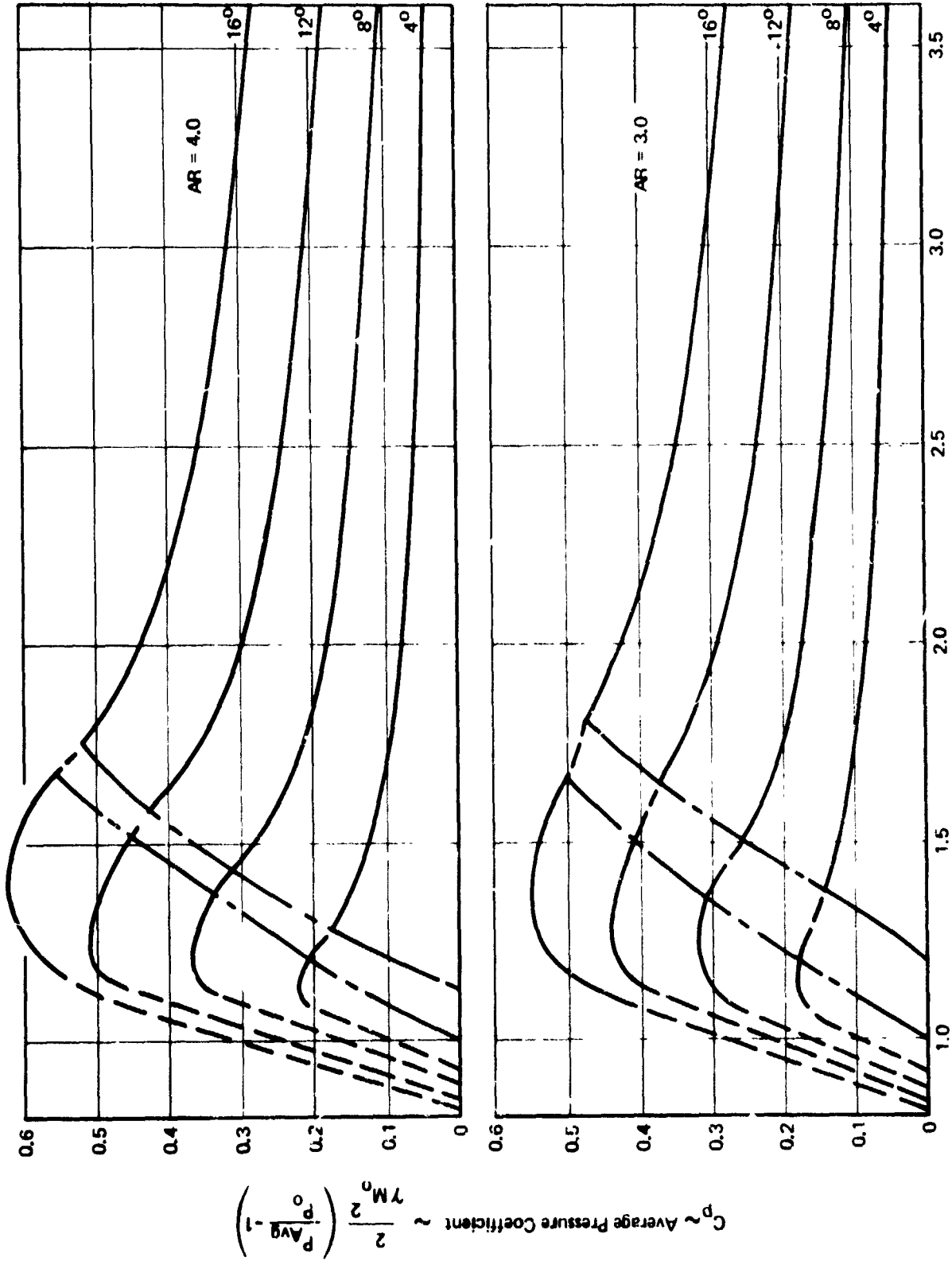


Figure 24. BYPASS DOOR PRESSURE COEFFICIENTS (Cont)



$$C_p \sim \text{Average Pressure Coefficient} \sim \frac{2}{\gamma M_0^2} \left( \frac{P}{P_{\text{AVG}}} - 1 \right)$$

Mach Number ~ M<sub>0</sub>  
 Figure 24. BYPASS DOOR PRESSURE COEFFICIENTS (Concluded)

If a convergent-divergent exit nozzle is used, the nozzle throat area is first calculated by:

$$\frac{A_T}{A_C} = \frac{\left(\frac{A_{O_{BLC}}}{A_C}\right) \left(\frac{A}{A^*}\right)_T}{(n) \left(\frac{A}{A^*}\right) C \left(\frac{P_{T_E}}{P_{T_O}}\right)^{(.95)}} \quad \begin{array}{l} \text{(Assumes } (A/A^*)_T = 1.0 \\ \text{for a choked throat)} \end{array} \quad (28)$$

The nozzle exit area is then obtained from input curves of  $\frac{A_E}{A_T}$  vs  $A_T$  which represent the geometric characteristics of the doors.

Exit area is then calculated from the relation:

$$\frac{A_E}{A_C} = \left(\frac{A_T}{A_C}\right) \left(\frac{A_E}{A_T}\right) \quad (29)$$

The calculation then proceeds the same way as for a convergent nozzle.

#### 4.4 BYPASS DRAG

The calculation procedure for computing bypass drag is the same as that for boundary layer bleed drag except that bypass total pressure recovery is different (usually higher) than that of the boundary layer bleed air. The recovery of the bypass air may be assumed to be  $.85 \times (P_{T_2}/P_{T_O})$  for preliminary

studies. If a more refined calculation is required, the bypass recovery may be varied linearly from a value of  $1.00 \times (P_{T_2}/P_{T_O})$

with the bypass doors closed to a value of  $.70 \times (P_{T_2}/P_{T_O})$  with

the doors full open (which usually bypasses around fifty per cent of captured inlet airflow). The recommended bypass recovery factors are illustrated in Figure 25.

The method described in previous sections for calculating exit drag for bypass and boundary layer bleed air has covered only the specific case where flap-type doors are used for exits. The same methods can also be used for other types of exits by use of the engineering assumptions shown in Table III.

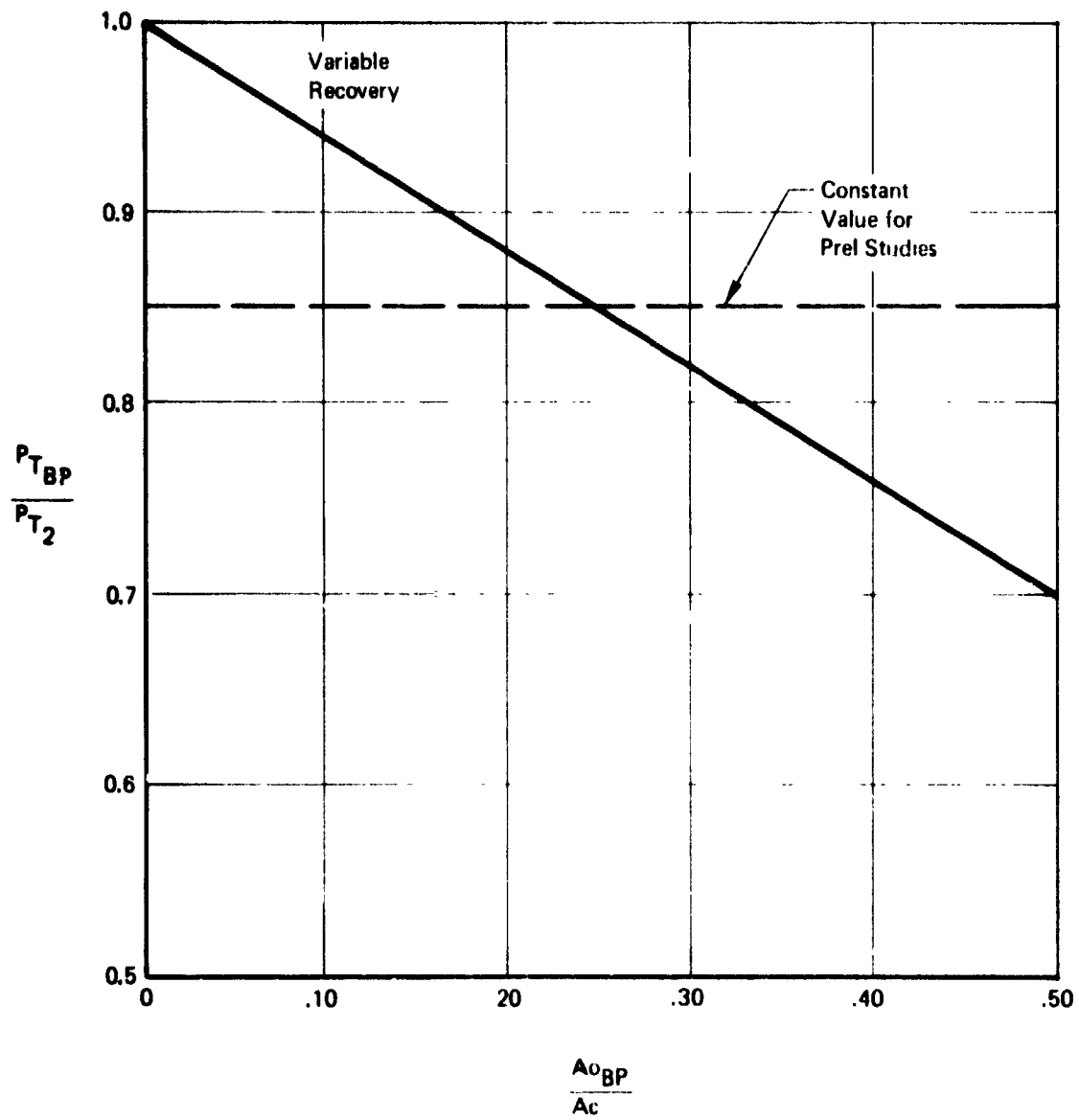
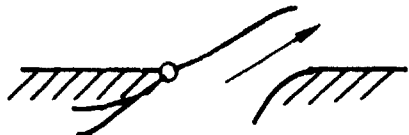
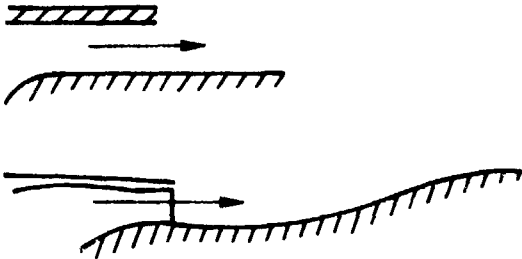


Figure 25: BYPASS AIRFLOW TOTAL PRESSURE RECOVERY

**Table III. ENGINEERING ASSUMPTIONS FOR BOUNDARY LAYER BLEED AND BYPASS EXITS**

Type of Exit	Assumption
<p data-bbox="467 648 642 681">Flap-Type Door</p> 	<p data-bbox="1052 648 1180 724">Use Method Described in Volume I</p>
<p data-bbox="467 957 642 989">Slot-Type Exits</p> 	<p data-bbox="1052 957 1240 1215">Assume Exit Drag is Same as for Flap at <math>Q_{Air} = Q_{Flap}</math> Because External Pressure Field Will be Created Just as if a Door Were Present</p>
<p data-bbox="467 1302 659 1334">Flush-Type Exits</p> 	<p data-bbox="1065 1403 1180 1457">Omit Flap Drag Term</p>

#### 4.5 SPILLAGE DRAG

Spillage drag is calculated from the following equation:

$$C_{D_{SPILL}} = K_{ADD} C_{D_{ADD}}$$

It is defined as the incremental change in total airplane drag due to spilling excess air ahead of the inlet. However, it is usually measured as an increment ( $\Delta C_{D_{SPILL}}$ ) from the

drag level obtained for the full airplane configuration with the inlet operating at a baseline mass flow ratio. When the inlet is operating at this baseline mass flow ratio, the  $\Delta C_{D_{SPILL}}$  is zero. The spillage drag at the baseline mass

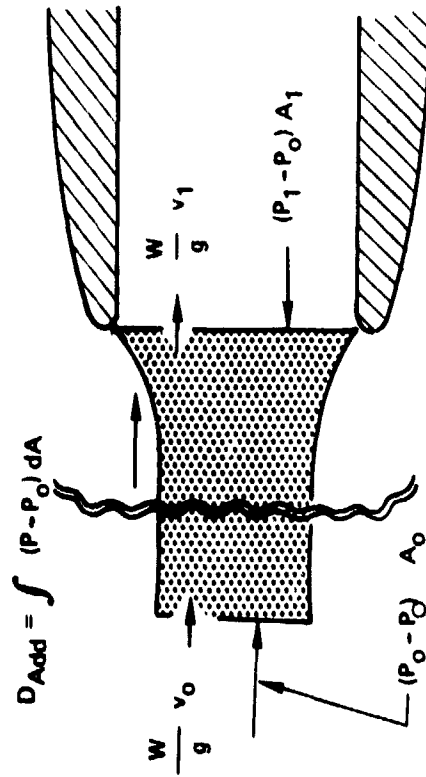
flow ratio is included in the airplane aerodynamic drag. The baseline mass flow ratio is specified for each inlet configuration as a function of free-stream Mach number. It is normally selected at mass flow ratios where spillage effects will be a minimum, for realistic operating airflow conditions. This baseline mass flow is normally taken to be the critical mass flow ratio. At supersonic speeds, with the shock wave attached to the first ramp, critical inlet operation means that the normal shock is at or inside the cowl lip. For subsonic and detached shock wave conditions, it means that inlet captured free-stream tube area,  $A_0$ , is equal to the physical flow area at the cowl. The establishment of the baseline mass flow ratio as described provides a basis for accounting of aero and propulsion forces. The throttle-dependent drag is thus included in the spillage drag (which is accounted for in installed net thrust) and the drags that are independent of throttle setting are included in the aerodynamic drag of the airplane.

##### 4.5.1 Theoretical Additive Drag

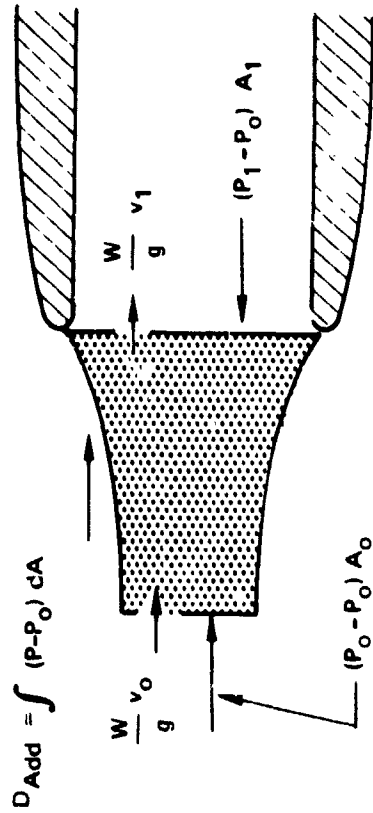
$C_{D_{ADD}}$  is the theoretical additive drag of the inlet. It is computed by several different methods, depending on the configuration of the inlet, free-stream Mach number, and shock geometry. This section describes the methods which are used for each particular situation.

The additive drag of an open-nose inlet is calculated as shown in Figure 26. This equation can be used for both subsonic Mach numbers and supersonic Mach numbers where a normal shock is standing ahead of the inlet.

For two-dimensional inlets at subsonic Mach numbers and for supersonic Mach numbers with the terminal shock at or inside the inlet lip, the method shown in Figure 27, is used.



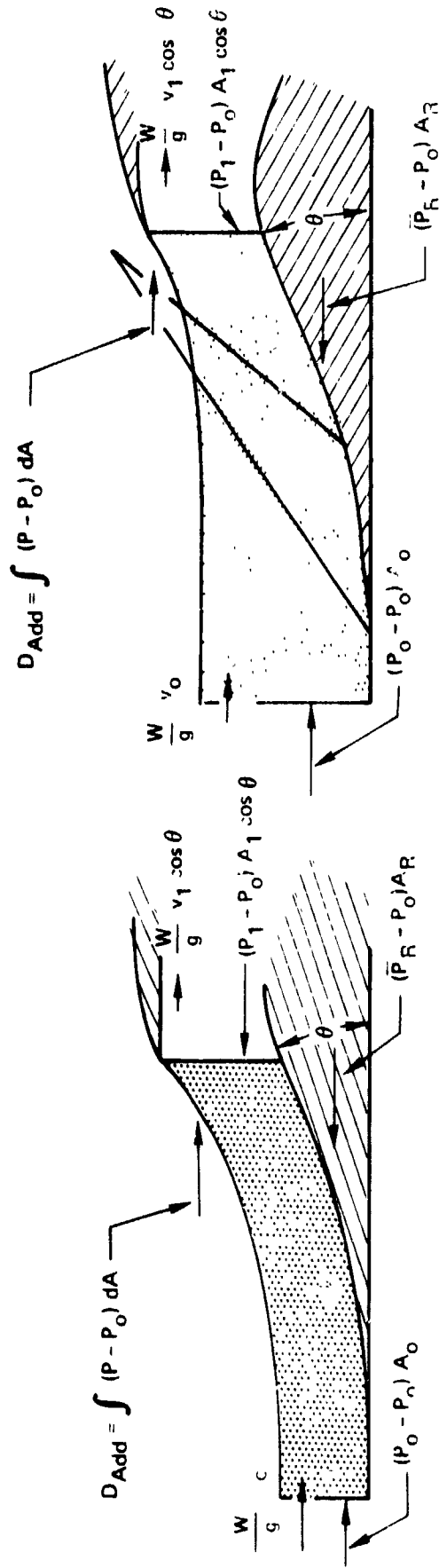
(B) Supersonic



(A) Subsonic

$$D_{Add} = \int (P - P_0) dA = \frac{W}{g} v_1 + (P_1 - P_0) A_1 - \frac{W}{g} v_0$$

Figure 26. ADDITIVE DRAG OF A PITOT INLET



(A) Subsonic

(B) Supersonic, Terminal Shock

$$D_{\text{Add}} = \int (P - P_0) dA = \left[ \frac{W}{g} v_1 + (P_1 - P_0) A_1 \right] \cos \epsilon - \frac{W}{g} v_0 + (P_R - P_0) A_R$$

Figure 2. ADDITIVE DRAG OF A TWO-DIMENSIONAL INLET

The last term on the right hand side of the equation (ramp drag) represents the incremental change in ramp drag due to reducing the mass flow ratio below the reference value. This incremental drag is obtained by calculating the pressure drag on the ramp, using the average pressure on the ramp,  $(P_0 + P_1)/2$  and the projected ramp area,  $A_R$ . The reference ramp drag is obtained from the plotted data of Figure 28, as a function of ramp thickness ratio,  $t/c$ , and free-stream Mach number.

For two-dimensional inlets operating at supersonic Mach numbers with the normal shock outside the inlet lip (subcritical), the additive drag calculation method of Reference 7 is used.

This method has been programmed for the CDC 6600 computer as a separate program and is not included in this report.

Theoretical additive drag for an axisymmetric inlet at subsonic Mach numbers and for supersonic Mach number conditions where the normal shock is at or inside the inlet lip, the method shown in Figure 29 is used.

Incremental spike drag is calculated in much the same way as ramp drag for the two-dimensional inlet. The average spike pressure and projected spike area are used to calculate the incremental drag. The spike reference drag is obtained from pressure drag data on cones (Figure 30).

For axisymmetric inlets operating with the terminal shock ahead of the inlet lip, the method documented in Reference 8 is used. This method has been programmed for the CDC 6600 computer as a separate program and is not documented in this report.

#### 4.5.2 $K_{ADD}$ Factors

The theoretical additive drag is multiplied by a correction factor,  $K_{ADD}$ , based on experimental data, to account for the configuration effects. These effects include the effect of cowl lip shape, bluntness, and sideplate cutback. The  $K_{ADD}$  factors are obtained by comparing experimentally measured drag variation as a function of inlet mass flow ratio with the theoretically calculated drag variation. A catalog of  $K_{ADD}$  factors to be used is presented in Volume IV.

#### 4.6 ANGLE-OF-ATTACK EFFECTS

Correction procedures are discussed here for the three most frequently encountered types of inlet installations: free-

Note:  $A_R$  Used in the Reduced Drag Coefficient is Planform Area of the Wedge or Ramp

$$\frac{\text{Reduced Drag Coefficient}}{(\gamma + 1)^{1/3} (t/c)^{5/3}} \quad (D_R / q_\infty A_R)$$

Data from Ref. 7

Config.	$\alpha^\circ$	$\beta^\circ$
R1SP1C1	5	5
R1SP1C1	5	9
R1SP1C1	5	12
R1SP2C1	5	5
R1SP3C1	5	5
R2SP1C1	7	7
R3SP1C1	12	12
R4SP4C1	5	5
R4SP4C6	5	9
R4SP4C1	5	12

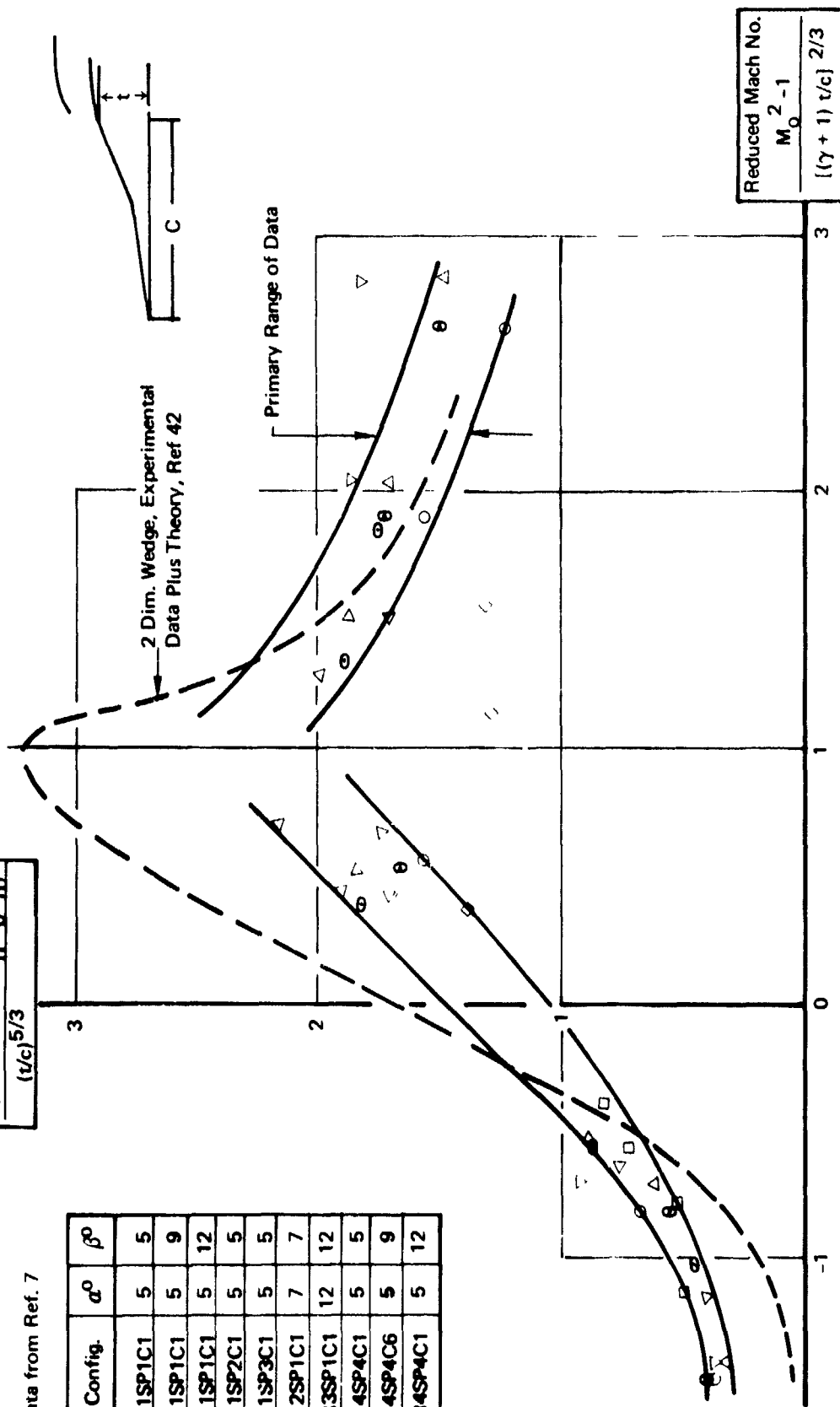
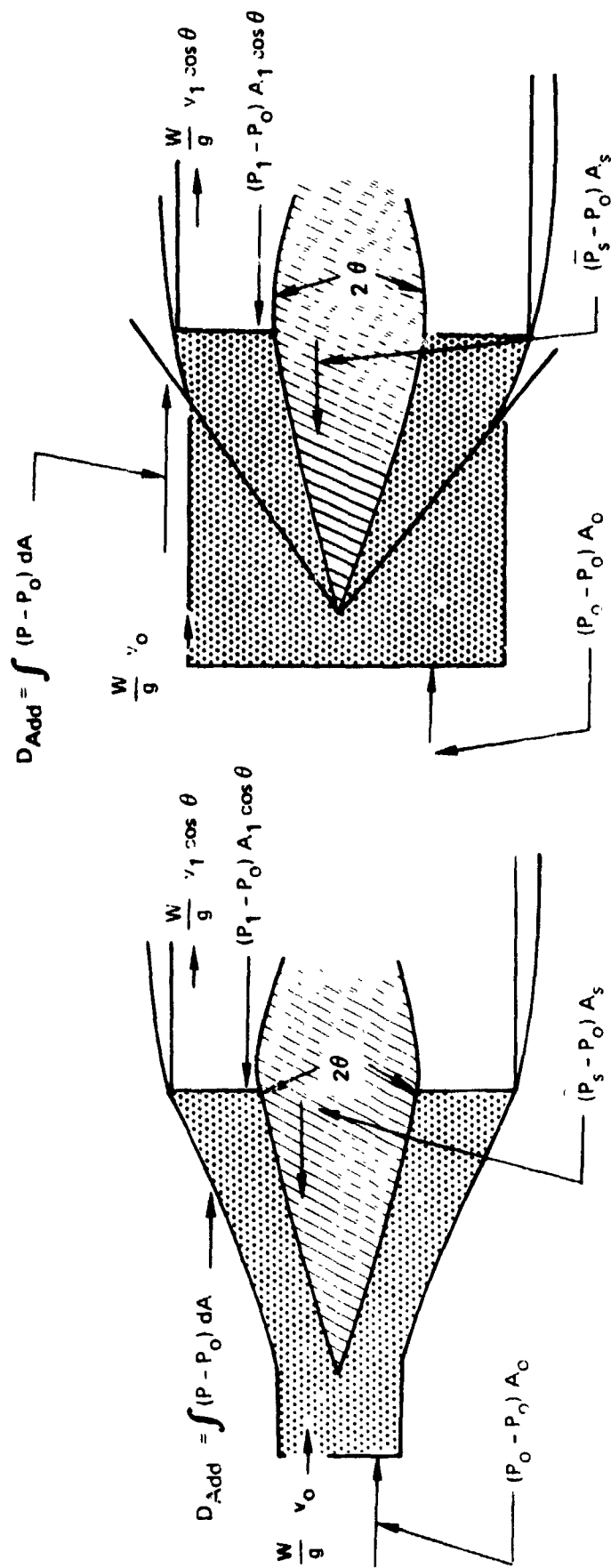


Figure 28 : REFERENCE RAMP DRAG



$$D_{Add} = \int (P - P_0) dA = \left[ \frac{W}{g} v_1 + (P_1 - P_0) A_1 \right] \cos \theta - \frac{W}{g} v_0 + \underbrace{(P_s - P_0) A_s}_{\substack{\text{Shock} \\ \text{Drag}}}$$

Figure 29. ADDITIVE DRAG OF AN AXISYMMETRIC INLET

$$C_{D_o} = \frac{L}{q S_{\text{Frontal}}}$$

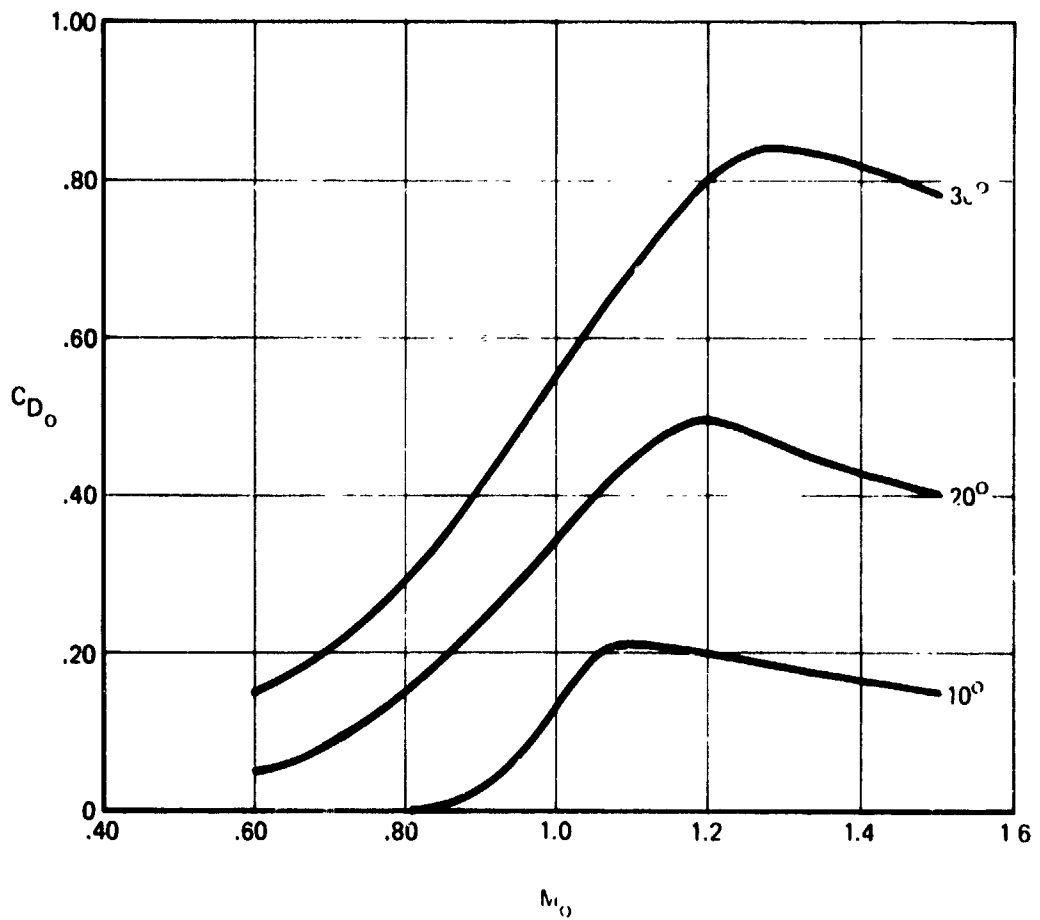
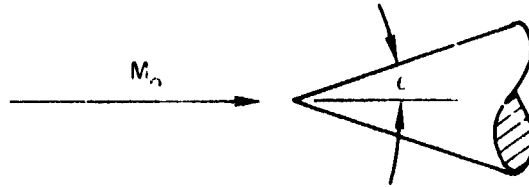


Figure 30: PRESSURE DRAG ON CONES IN TRANSONIC FLOW

stream, underwing and fuselage mounted.

For free-stream installations, each angle of attack position is calculated as a separate data point without applying a correction for the presence of the wing or the forebody.

For all types of installations, it is assumed that the basic inlet is installed in a location where it is free of adverse boundary layer effects.

For the underwing inlet location, it is assumed that the inlet is located within the flowfield of a two-dimensional wing. As angle-of-attack is increased, the wing compression field provides a local flowfield at the inlet that is different from free-stream according to the relations plotted in Figures 31 through 34.

Figure 31 presents a correction factor,  $K$ , used to compute the local Mach number behind a wing shock. It is derived from the linear portions of the  $M_0$  vs  $\alpha$  data shown in Figure 32.

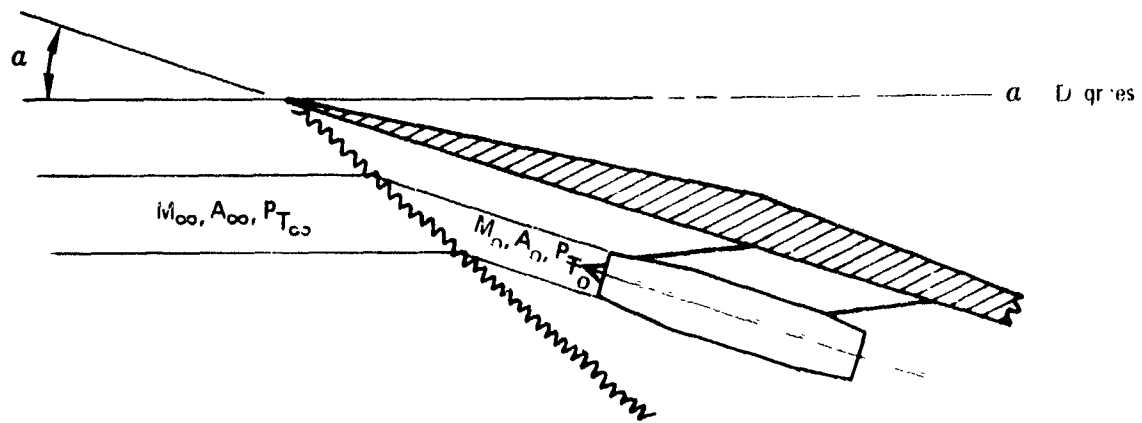
Figure 33 shows the effect of angle-of-attack on local stream tube area for supersonic Mach numbers.

For preliminary design purposes, the performance calculations for an inlet in the wing flow field are approximately equal to those for an inlet in free-stream except that the effect of wing compression on local inlet flowfield properties must be accounted for before the inlet performance calculations are made. Figures 31-34 are used for this purpose.

For side-mounted inlet installations, the available experimental data (Volume IV) indicates there is relatively little effect of angle-of-attack on local inlet Mach number and total pressure recovery up to 20 degrees angle-of-attack. Therefore, for preliminary studies, it is assumed that the inlet local flowfield properties are the same as free-stream.

For under-fuselage mounted inlets, the fuselage provides increasing compression as angle-of-attack increases. This compression field reduces the local Mach number ahead of the inlet and can also reduce the total pressure recovery ahead of the inlet.

Although this compression field is dependent on the shape of the forebody ahead of the inlet and the location of the inlet, aft of the forebody nose, the experimental data have prevailing trends that indicate the flowfield effects are generally somewhere between those produced by a conical forebody and a



$$iM_0 = M_{\infty} \cdot K \alpha$$

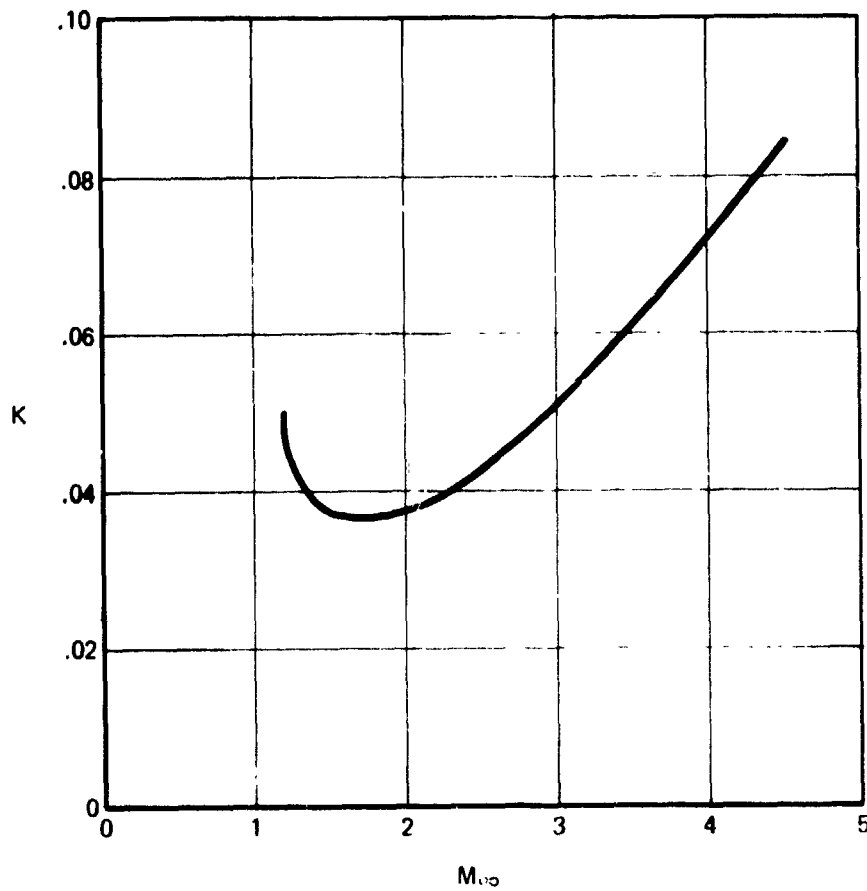


Figure 31: MACH NUMBER CORRECTION FACTOR FOR TWO-DIMENSIONAL WINGS

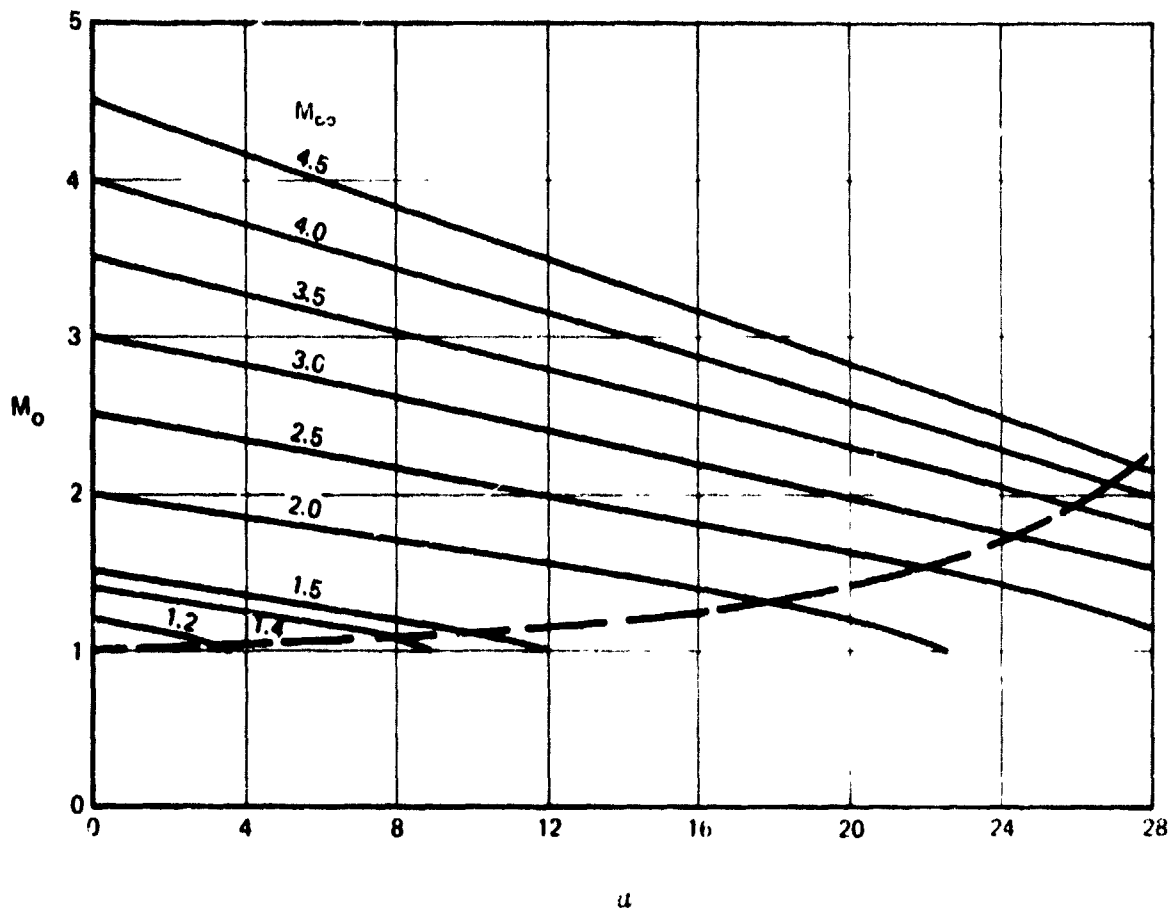


Figure 32: EFFECT OF ANGLE-OF-ATTACK ON INLET LOCAL MACH NUMBER (TWO-DIMENSIONAL WING)

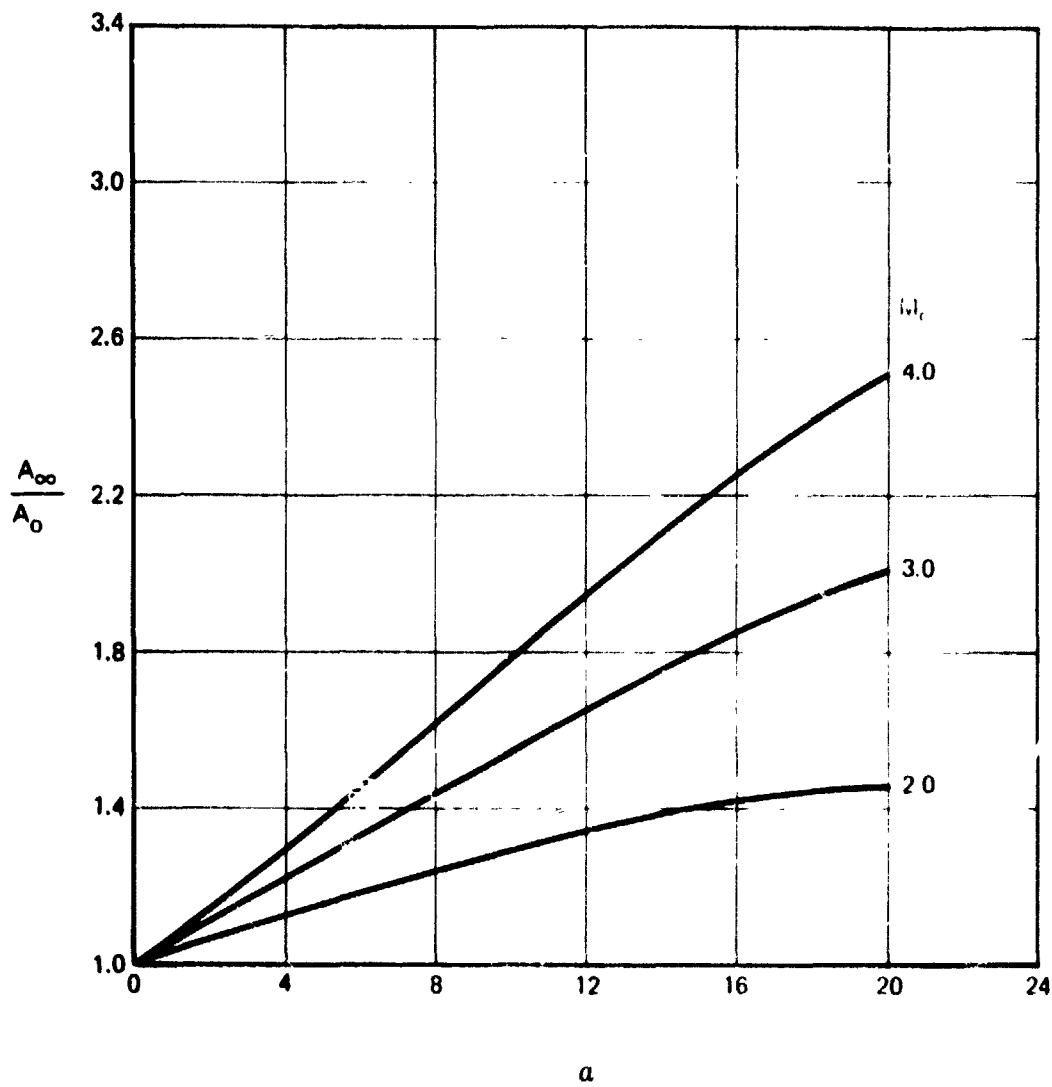


Figure 33: EFFECT OF ANGLE-OF-ATTACK ON STREAM TUBE AREA FOR A TWO-DIMENSIONAL WING

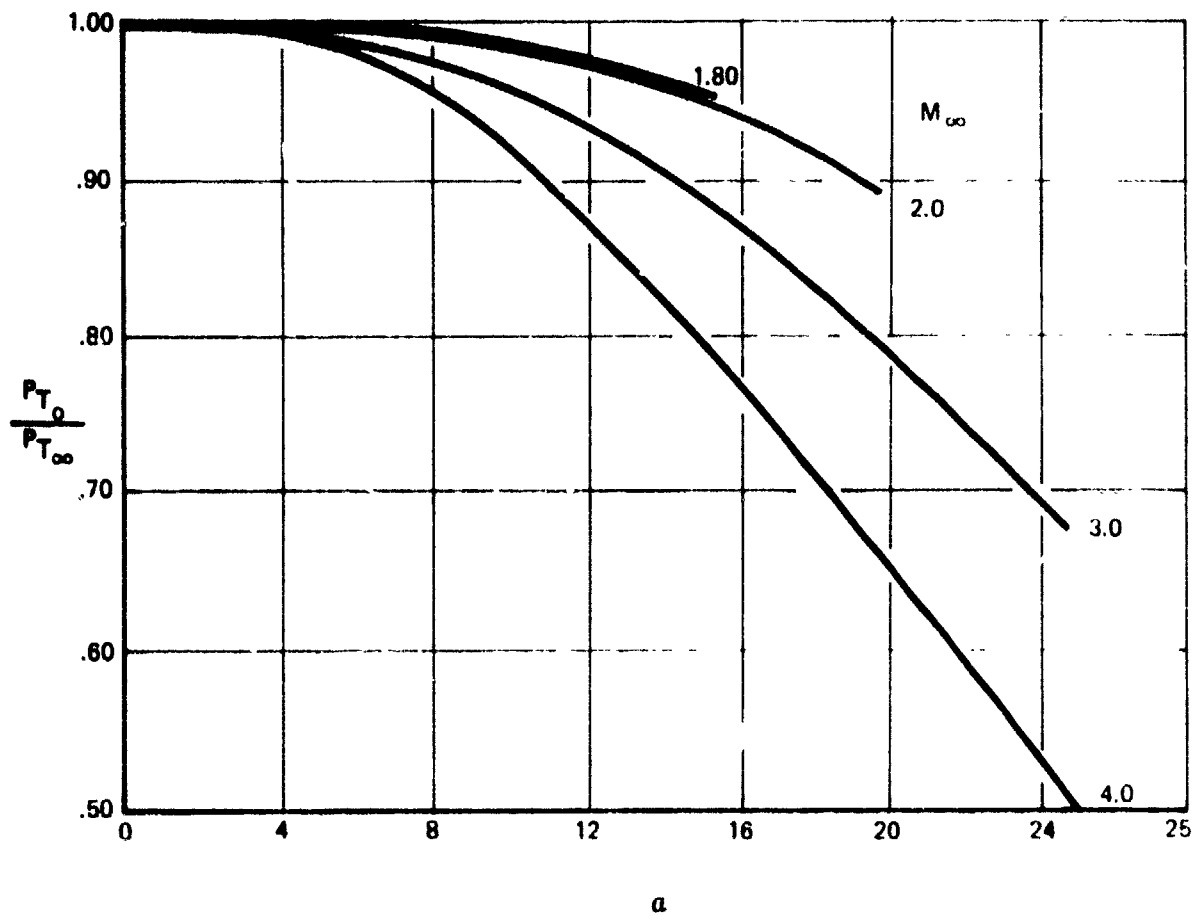


Figure 34: EFFECT OF ANGLE-OF-ATTACK ON TOTAL PRESSURE RECOVERY UNDER A TWO-DIMENSIONAL WING

two-dimensional surface. The correction curves to be used for the under-fuselage inlets are presented in Figures 35 and 36. They are based on experimental data from Reference 9.

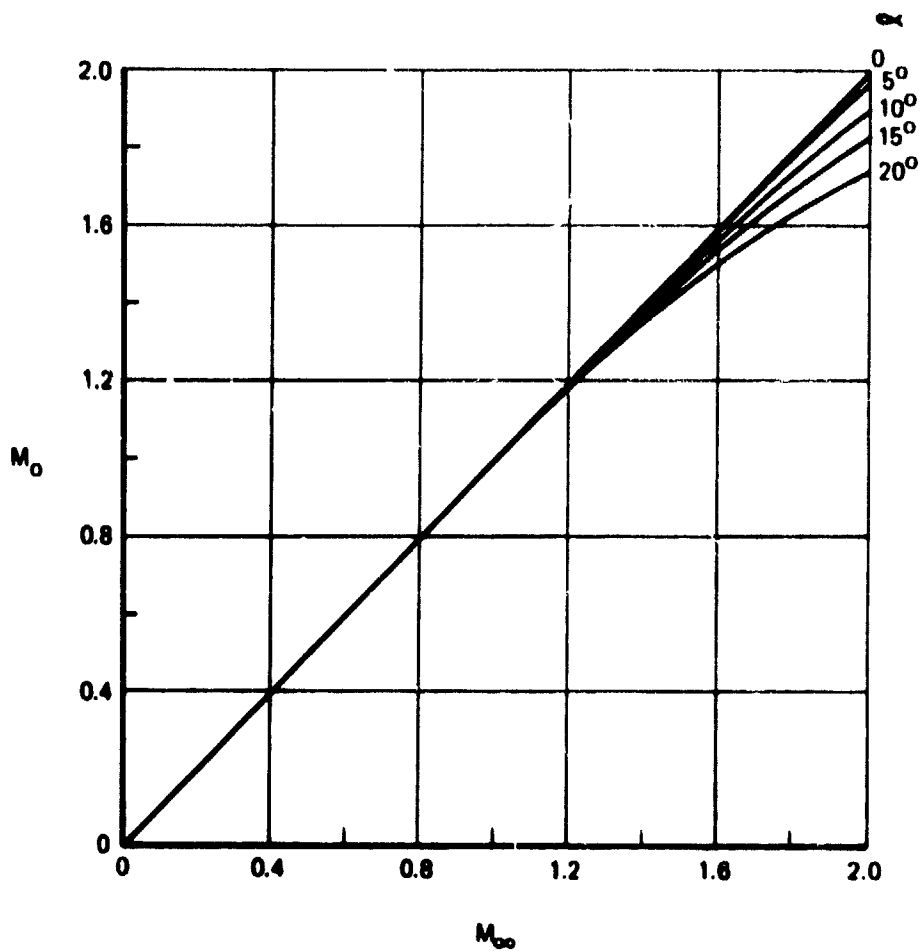
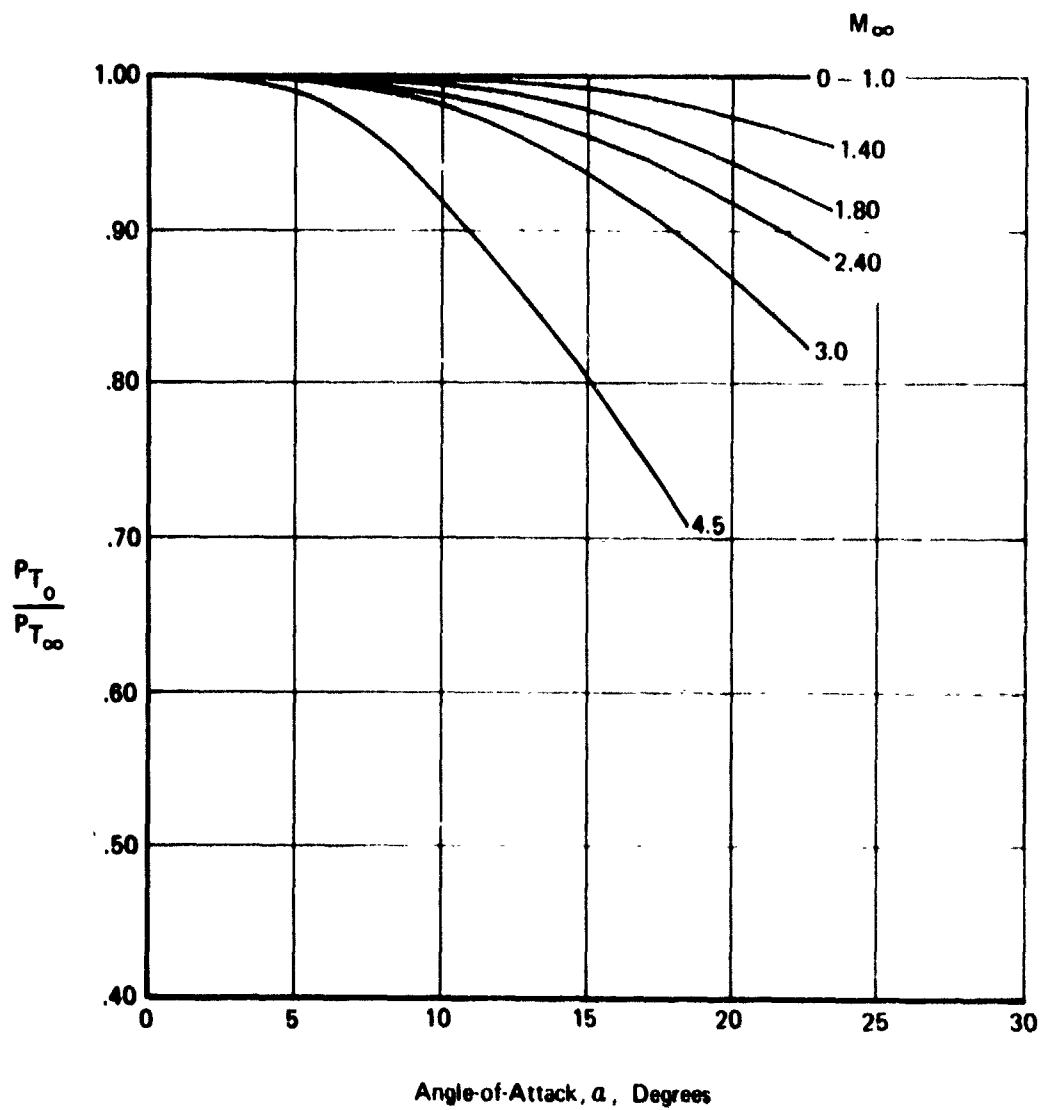


Figure 35: EFFECT OF ANGLE-OF-ATTACK ON LOCAL INLET MACH NUMBER FOR AN UNDER-FUSELAGE MOUNTED INLET



**Figure 36: EFFECT OF ANGLE-OF-ATTACK ON LOCAL INLET TOTAL PRESSURE RECOVERY FOR AN UNDER-FUSELAGE MOUNTED INLET**

## SECTION V

### NOZZLE/AFTERBODY PERFORMANCE

#### 5.1 NOZZLE INTERNAL PERFORMANCE

Figure 37 presents a diagram showing how the nozzle/afterbody calculation procedures relate to the installed propulsion system performance procedures. Each of the nozzle/afterbody procedures is discussed in detail in the following sections.

##### 5.1.1 Convergent

Test data are available in Volume IV, Section III that show the measured velocity coefficients ( $C_V$ ) for a series of convergent nozzles as a function of entrance to exit diameter ratio, pressure ratio, and nozzle convergence angle. The velocity coefficients are defined as follows:

$$C_V = \frac{(F_G)_{\text{MEASURED}}}{(\dot{m})_{\text{ACTUAL}} (V)_{\text{ISENTROPIC, FULLY EXPANDED}}}$$

These measured  $C_V$ s are used with the ideal, fully expanded gross thrust calculated by methods described in Section III to obtain the predicted nozzle gross thrust for a given mass flow. Convergent nozzle discharge coefficients were also measured during the tests. These coefficients, presented in Reference 29, are used to relate the effective to actual throat areas for purposes of sizing the nozzle throat to pass a given mass flow or, conversely, for determining the effective throat area for a given throat geometric area.

The experimental  $C_V$ s are accurate to within  $\pm .25\%$ , and should be adequate for most preliminary design purposes.

If it is desired to calculate the internal performance of a convergent nozzle by theoretical buildup, it is recommended that  $C_V$  be calculated as follows:

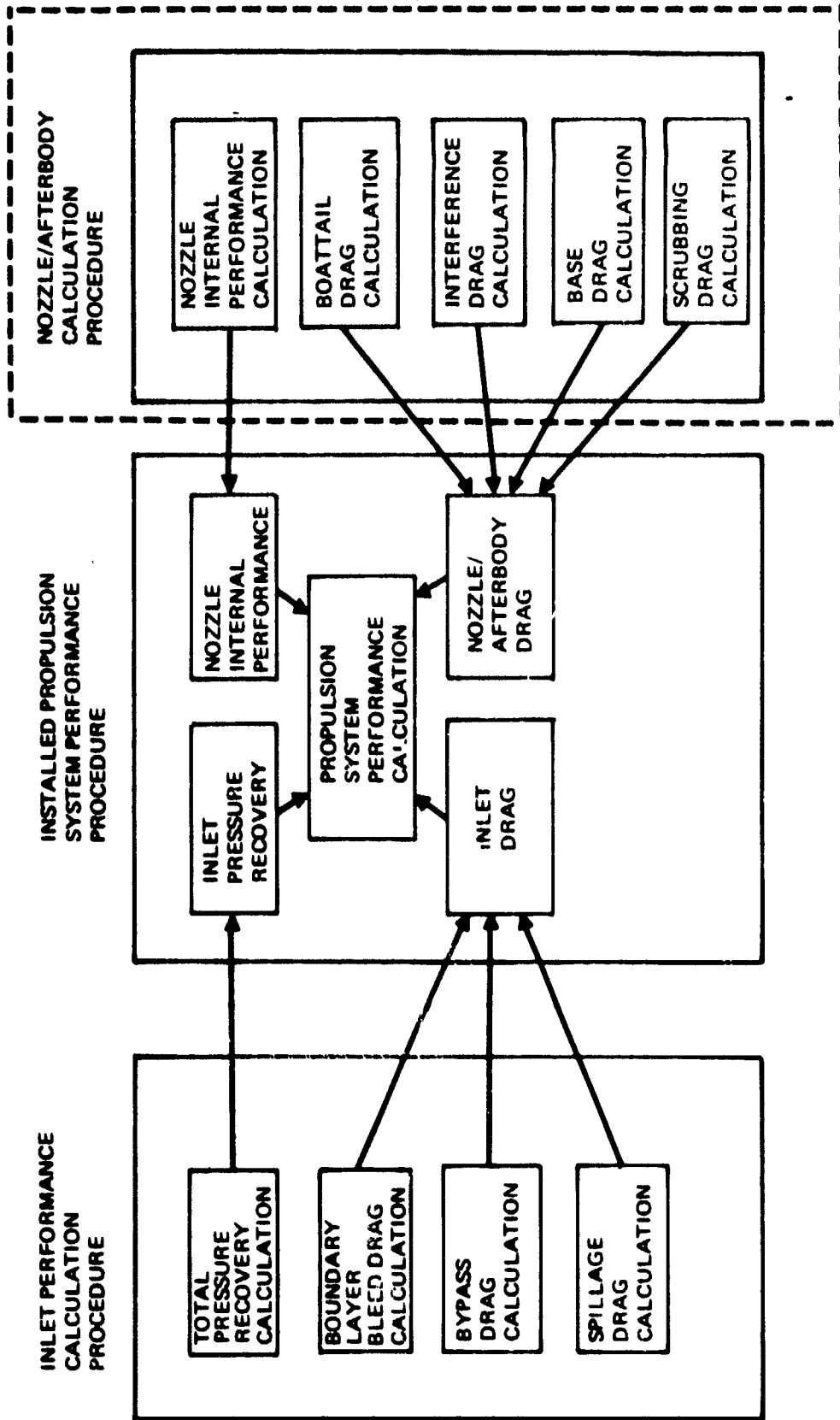


Figure 3-7: NOZZLE/AFTERBODY CALCULATION PROCEDURE

$$C_V = 1 - \Delta C_{VS} - \left( 1 - \frac{WV_8 + A_8 (P_8 - P_{amb})}{F_{g_i}} \right)$$

where  $A_8$  = actual throat area =  $A_8^*/C_D$  ;  $A_8^*$  = thermodynamic throat area, in.<sup>2</sup>,

$C_D$  = experimental throat discharge coefficient, dimensionless (Ref. 43)

$P_8$  = static pressure at the throat, lb/in.<sup>2</sup>

$V_8$  = jet velocity at the throat, ft/sec

$F_{g_i}$  = ideal gross thrust for fully expanded flow

$\Delta C_{VS}$  = internal loss due to skin friction (calculated by methods of Ref. 44)

Theoretical methods are also contained in Reference 44 for calculating the effect of boundary layer growth on nozzle discharge coefficient.

### 5.1.2 Convergent-Divergent

The performance of a convergent-divergent nozzle is determined from the stream thrust coefficient discussed in Volume IV, Section III.

The procedures for calculating the thrust of a convergent-divergent nozzle are given in Section III. By these procedures, the gross thrust is:

$$F_g = C_S \left( \frac{W}{g} V_9 + P_9 A_9 \right) - P_{amb} A_9$$

where  $C_S$  = stream thrust coefficient  $(1 - \Delta C_S) = f(A_8, A_9, \theta)$

from Figure 38. Dimensionless

$A_9$  = nozzle exit area, in.<sup>2</sup>

$\theta$  = nozzle divergence angle, degrees

### 5.1.3 Ejector

There is not sufficient test performance data in Volume IV, Section 5 to calculate ejector nozzle performance for all operating conditions. The discussion in Reference 10 indicates

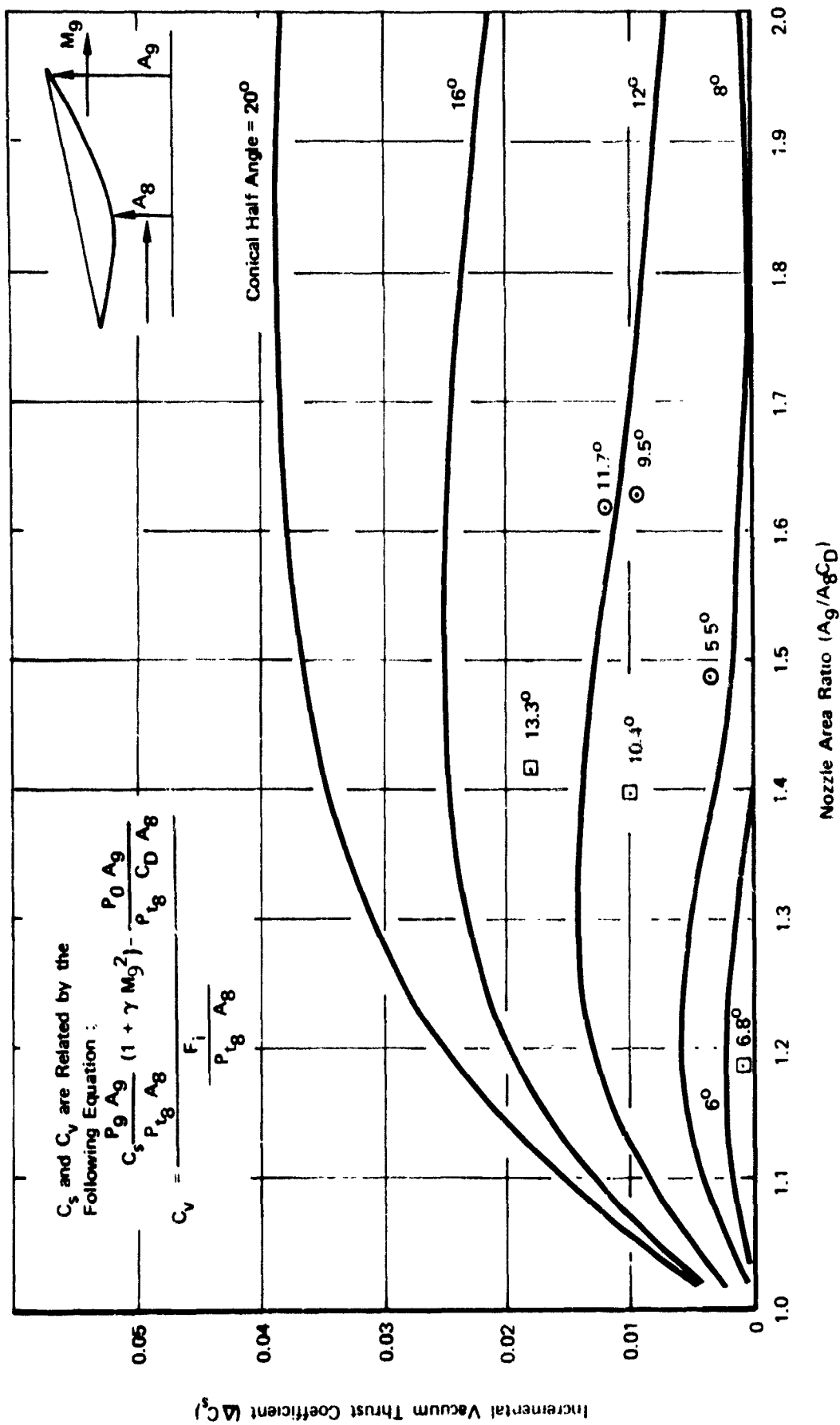


Figure 38: CONICAL CONVERGENT/DIVERGENT NOZZLE NON-ISENTROPIC EXPANSION LOSS

that for certain conditions ejector nozzle performance calculated by compound flow theory and experimental results show excellent agreement. Therefore, this method was selected for use in calculating ejector performance where no test data are available. Using this method, the nozzle thrust for an ejector nozzle with dual flow can be calculated as follows:

$$F_g = C_\theta \left( \frac{W_p V_{9p}}{g} + P_9 A_{9p} \right) + \frac{W_s V_{9s}}{g} + P_9 A_{9s} - P_{amb} A_g$$

where  $C_\theta$  = divergence loss coefficient =  $1/2 (1 + \cos \theta)$ , dimensionless

$W_s$  = secondary flow rate, lb/sec

$W_p$  = primary flow rate, lb/sec

$A_{9p}$  = nozzle exit area for the primary stream, in.<sup>2</sup>

$A_{9s}$  = nozzle exit area for secondary stream, in.<sup>2</sup>

$A_g$  = nozzle exit area, in.<sup>2</sup>

$V_{9s}$  = nozzle exit velocity of secondary airflow, ft/sec

$V_{9p}$  = nozzle exit velocity of primary airflow, ft/sec

The nozzle geometry and secondary inlet flow conditions must be specified to calculate the secondary flow ( $W_s$ ). If compound choking does not occur (see Reference 10) then the secondary flow is calculated at the exit plane by iterating until the static pressures of both streams are matched (See Section 3.2.3.3).

$$A_{W_s} = A_g - A_{9p}$$

$$W_s = \frac{A_{W_s} P_9 V_{9s}}{53.342 T_{9s}}$$

The same procedure is repeated for the nozzle throat and if the calculated secondary flow is less than the exit flow, it is assumed that this exit area can be reduced to match the flow.

An iteration on  $A_{WS}$  to obtain maximum secondary is required for the compound-choked flow condition.

#### 5.1.4 Plug

There is not sufficient test performance data in Volume IV, Section III to calculate plug nozzle performance for all operating conditions. A good estimate of plug nozzle performance can be made by subtracting the added skin friction drag due to the external plug surface from the calculated gross thrust of a concentric nozzle:

$$F_g = F_{g_i} (C_{V_{MAX}}) - D_{SKIN}$$

where

$$C_{V_{MAX}} = 1 - \left[ \frac{(0.014)}{\sqrt{D_{h_e}}} \right]$$

It is assumed the velocity at the end of the plug is equal to fully expanded isentropic flow. The average dynamic pressure,  $q$ , over the plug is used to calculate skin friction drag.

$$D_{SKIN} = C_F \frac{\gamma}{2} \frac{P_8 + P_{amb}}{2} \left( \frac{M_8 + M_9}{2} \right)^2 (S_{WET})$$

where  $C_F$  = average skin friction coefficient, dimensionless.

$D_{SKIN}$  = skin friction drag, lb

$$D_{h_e} = \frac{(4\pi A_8)^{1/2}}{\text{Perimeter}}, \text{ dimensionless}$$

$C_{V_{MAX}}$  = maximum thrust coefficient for a concentric nozzle (Reference 28) dimensionless

#### 5.2 NOZZLE/AFTERBODY DRAG

Nozzle/afterbody drag includes all drag elements associated with the exhaust system installation that are affected by the engine power setting. Drag associated with skin friction is included in the airplane drag polars. Drag elements identified as contributors to the nozzle/afterbody drag include:

1. Nozzle/afterbody boattail drag
2. Interference effects for multi engine installations
3. Afterbody base drag
4. Scrubbing drag

Nozzle/afterbody drag is computed using maps which represent the afterbody drag characteristics (Figure 39), external input geometric data, and fundamental engine data obtained internally from the engine subprogram. The external inputs are required constants that describe the nozzle and afterbody geometry: maximum nacelle diameter, boattail length, lateral nozzle spacing, base area, etc. Fundamental engine data obtained internally from the engine subprogram include nozzle thrust area, nozzle pressure ratio, free-stream conditions and ideal gross thrust. An essential geometry input is the nozzle exit area,  $A_9$ , which is required for boattail drag computation. This parameter is obtained in either of two ways:

1. From the engine subprogram when the existing nozzle data are used.
2. From a table of  $A_9/A_8$  that is developed when new nozzle data are used.

The logic used to connect the input drag data and the engine subprogram is illustrated in Figure 40.

The nozzle/afterbody subprogram requires much less external input data than the inlet subprogram. This is due to the fact that the maps used to obtain nozzle/afterbody drags have been generalized to cover a wide range of possible configurations, and are built into the program. Thus, it is necessary to supply as external input data only the geometric parameters used to specify the afterbody geometry.

#### 5.2.1 Boattail Drag

The generalized maps which are now in the program are shown in Figures 41, 42, 43 and 44. Figure 41 shows the variation of boattail drag as a function of boattail angle and Mach number for free-stream Mach numbers up to .95. From Mach 1.0 to 3.0, the equation shown in Figure 41 is used. These drag data are based on isolated wind tunnel data for circular arc boattails at nozzle pressure ratios,  $P_T/P_0$  of 2.5. For nozzle pressure ratios greater than 2.5, an additional correction is applied to the basic boattail drag coefficient obtained from Figure 42. This added correction shown in Figure 42 is a function of nozzle pressure ratio and boattail

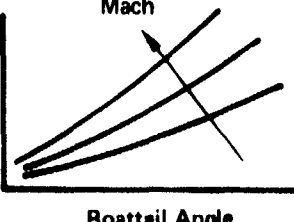
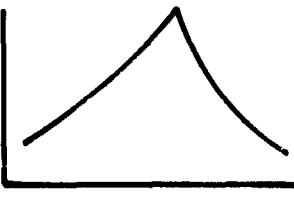
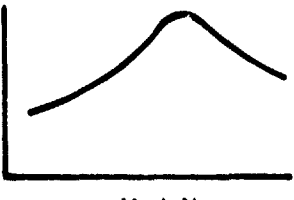
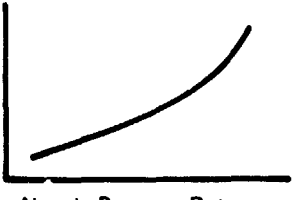
<b>Boattail Drag</b>	$C_{DA_{Max}}$ 	Derived from Isolated Nozzle Wind Tunnel Test Data
<b>Interference Effect</b>	$\frac{\Delta D_{Int}}{F_{ip}}$ 	Empirical Correlation of Lateral Spacing Effects on Nozzle/Afterbody Drag Using Wind Tunnel Data
<b>Base Drag</b>	$C_{D_{Base}}$ 	Derived from Test Data, Included When Base Areas are Present in the Afterbody that May Be Affected by Engine Power Setting
<b>Scrubbing Drag</b>	$C_{DS}$ 	Derived from Theory and Empirical Correlations Included When Nozzle Exhaust Flow Impinges on Aircraft or Nacelle Surfaces

Figure 39: NOZZLE/AFTERBODY DRAG REPRESENTATION

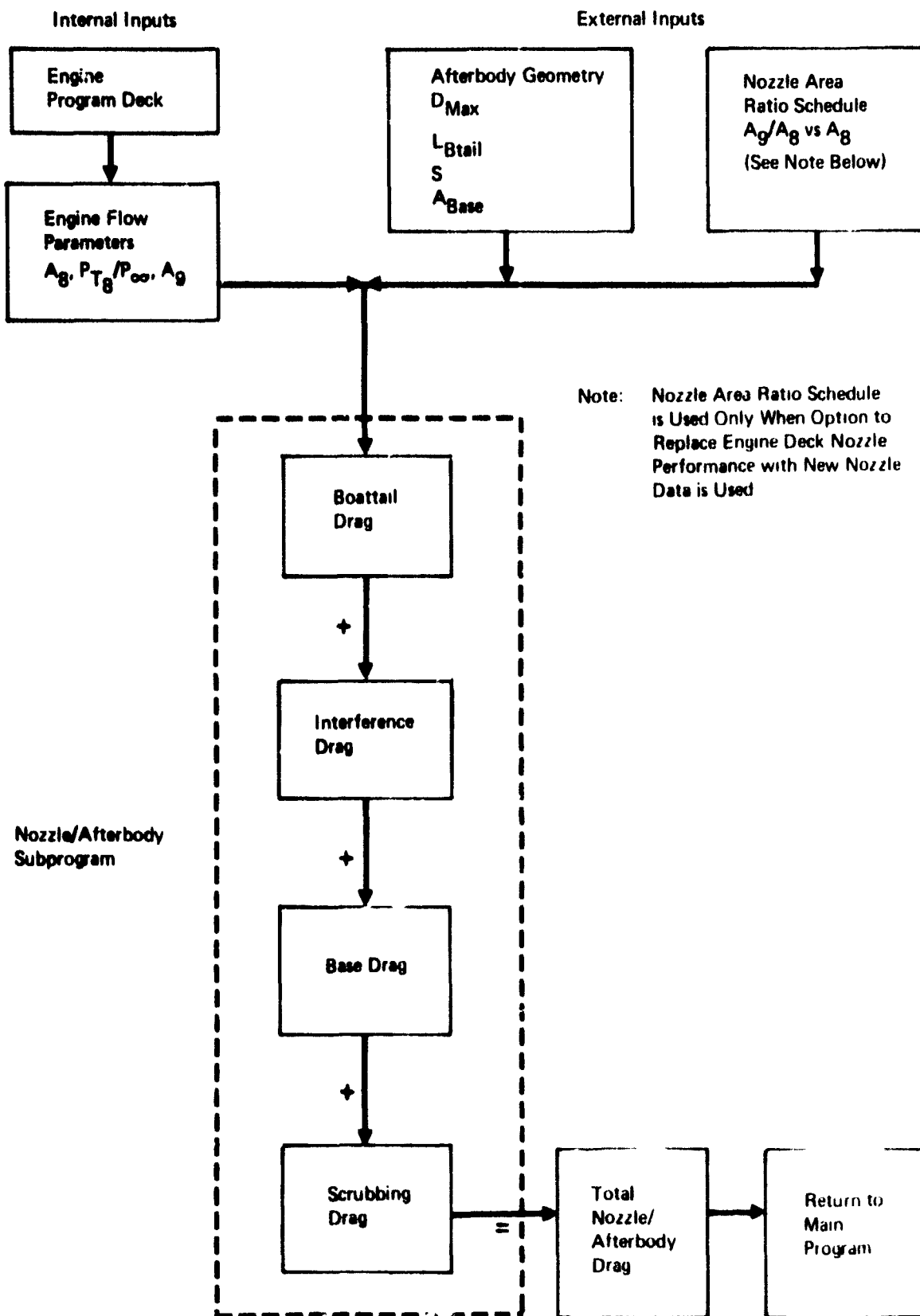


Figure 40: NOZZLE/AFTERBODY DRAG SUBPROGRAM

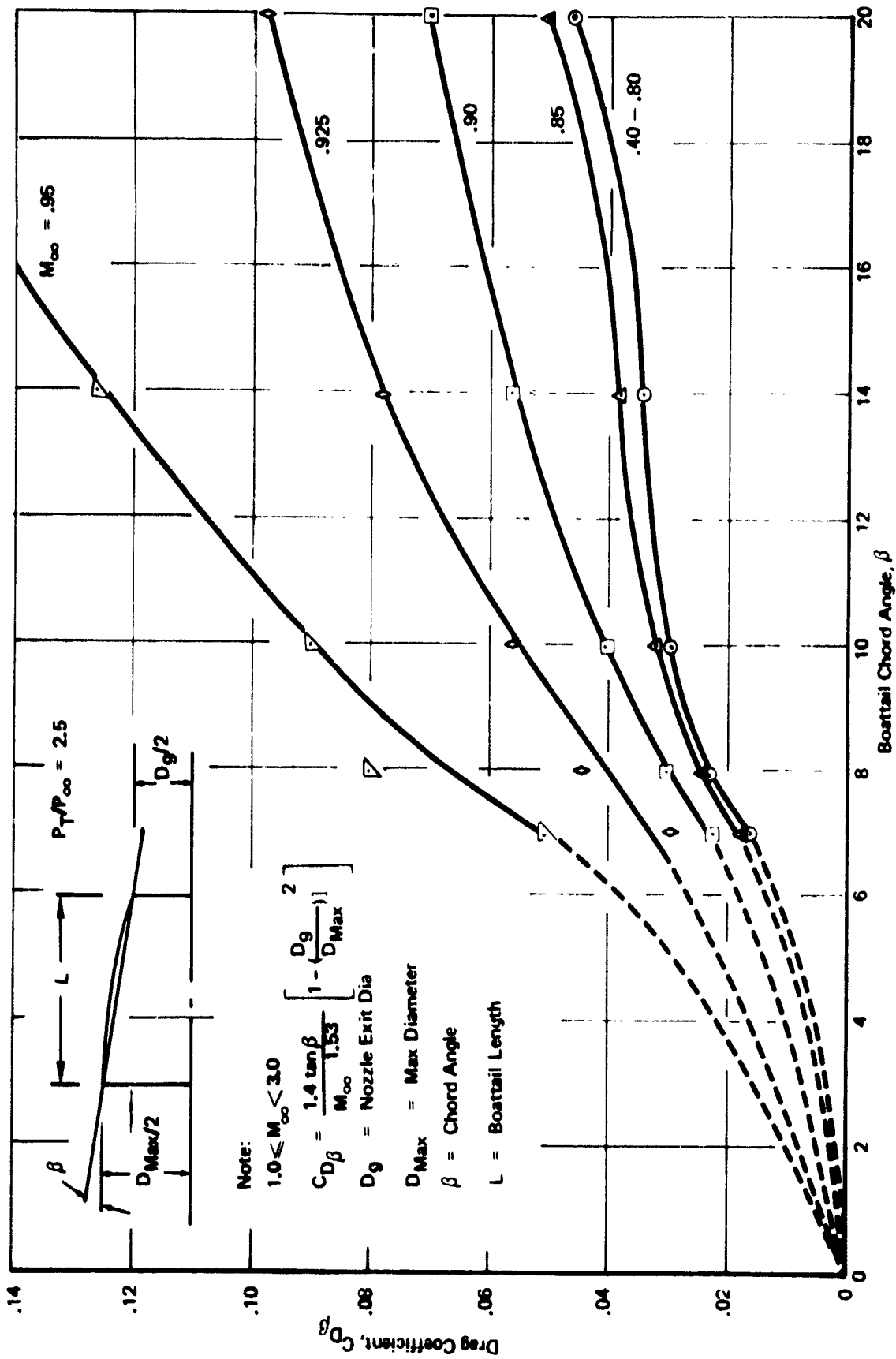


Figure 41: NOZZLE BOATTAIL PRESSURE DRAG COEFFICIENTS AS  $f(\beta)$

- Data Sources: 1. NASA TM X-1960  
 2. Boeing Test Data  
 3. Unpublished Boeing SST Data

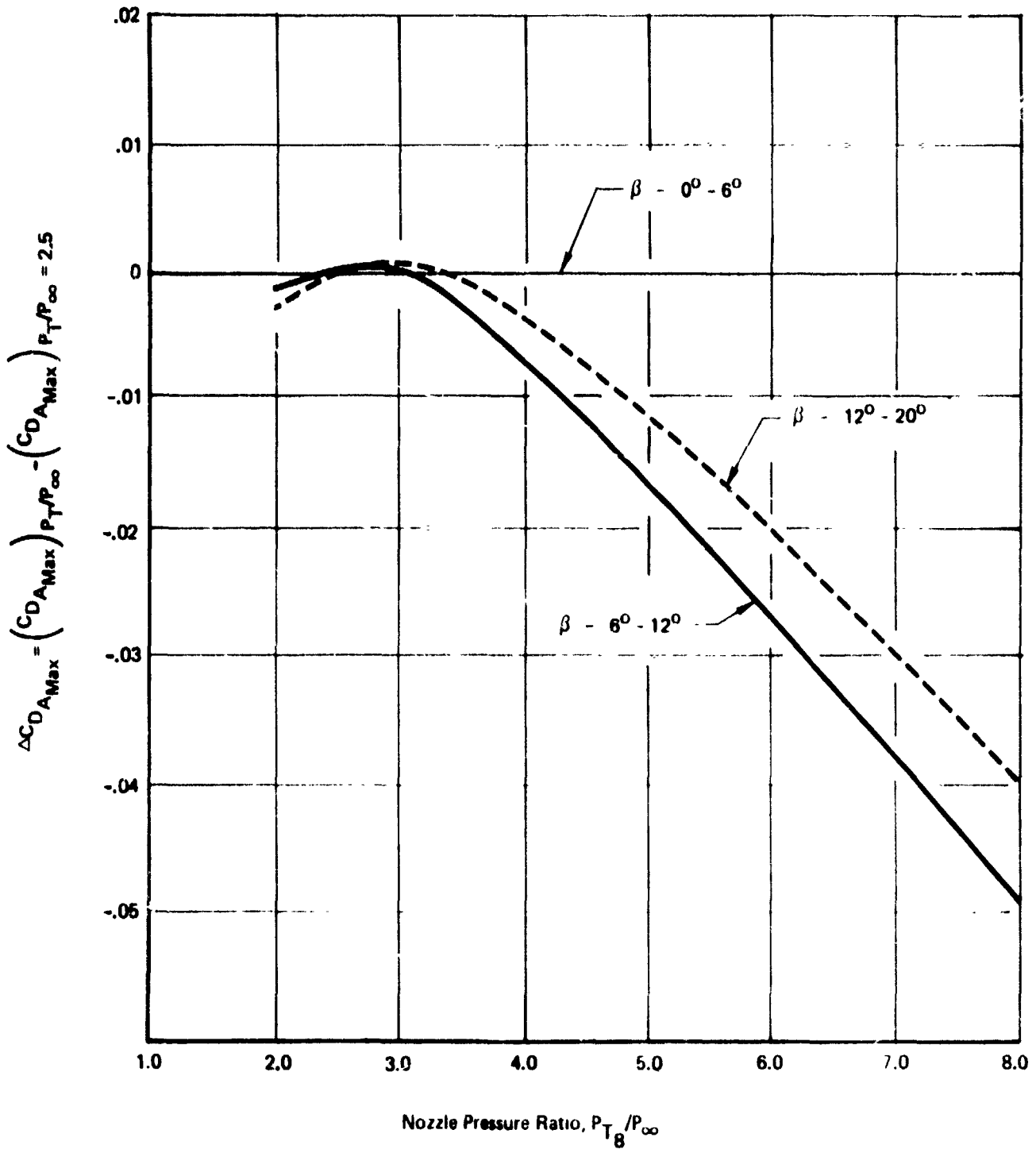


Figure 42: BOATTAIL DRAG CORRECTION FOR NOZZLE PRESSURE RATIOS GREATER THAN 2.5



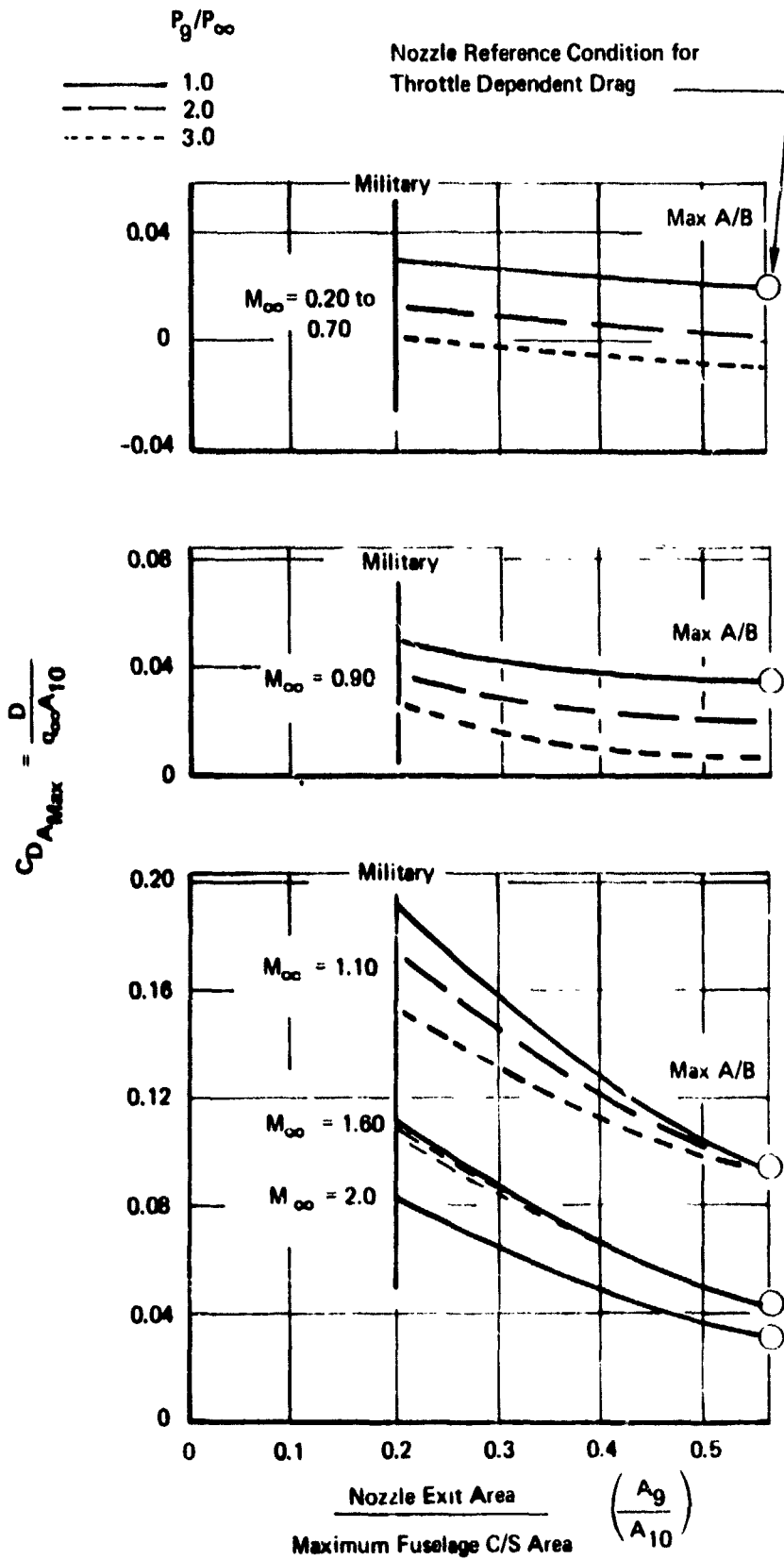


Figure 44: NOZZLE/AFTERBODY DRAG COEFFICIENTS AS  $f(A_g/A_{10})$

angle. This added correction procedure is included in existing nozzle/afterbody subprogram.

For supersonic Mach numbers greater than Mach 1.0, PITAP uses the expression given in Figure 41. This represents an empirical correlation of data from several sources, as shown on Figure 43. The correlation was biased at the lower Mach numbers toward data obtained with blown jet simulation. The form of the correlation was suggested by supersonic wave drag considerations (Reference 11) and, as shown in the Figure 43, it does a reasonably good job of collapsing the data.

The option is available in the computer program to calculate complete afterbody drag as a function of the ratio of nozzle exit area to maximum fuselage cross-sectional area,  $A_9/A_{10}$ . The drag maps built into the program for this calculation are shown in Figure 44.

The drag of a plug nozzle subjected to subsonic external flow may be estimated by considering the cowl and the external boundary of the jet to define an equivalent boattail as shown in Figure 45. The jet diameter at the end of the plug should be computed assuming full expansion to ambient static pressure. The drag of this equivalent boattail may then be estimated from the data of Figure 41. Reference 30 contains experimental data comparing measured plug nozzle drag with C-D nozzle drags. This data substantiates that the equivalent nozzle concept is suitably accurate for preliminary design analyses.

The drag of a plug nozzle at supersonic speeds and high nozzle pressure ratios is simply the drag of the solid boattail created by the nozzle shroud. This drag can be estimated from the data of Figure 41.

The installed thrust-minus-drag of a plug nozzle may be estimated by summing all the internal and external losses for the nozzle and subtracting these losses from one. Thus,

$$\begin{aligned} \frac{F - D}{F_i} &= 1 - \sum \frac{\Delta F}{F_i} - \frac{D}{F_i} \\ &= 1 - \sum \Delta C_V - \frac{C_{D_{MAX}} q_{\infty} A_{MAX}}{F_{IDEAL}} \end{aligned}$$

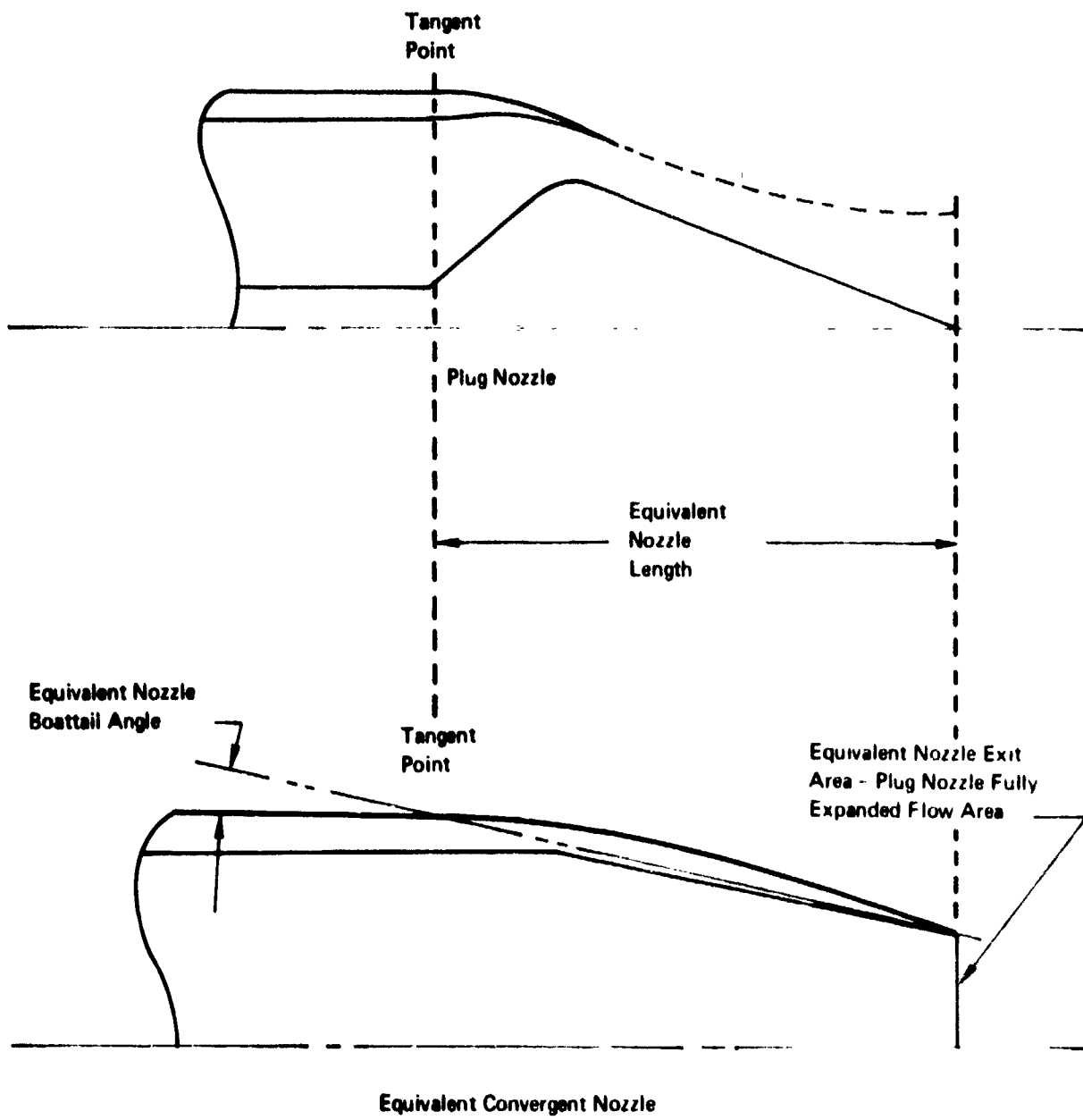


**Figure 45: DEFINITION OF AN EQUIVALENT NOZZLE**

The losses in internal thrust which are accounted for in the velocity coefficient term,  $\Sigma AC_V$ , include skin friction, non-ideal expansion, and convergence losses.  $C_{D_{A_{MAX}}}$  accounts for boattail drag.

### 5.2.2 Interference Drag

PITAP is programmed to accept an input drag increment table giving "interference" drag. Potentially this slot could be used to account for any discrepancies between the calculated isolated nacelle drag and the actual drag of the nacelle installed in an airplane configuration.

At the present time this table is being used solely to account for the twinning penalties associated with putting two nacelles side by side with a clean, sharp-edged interfairing in between. The independent variables are Mach number and spacing ratio, i.e., center line spacing over nozzle exit diameter. (The present version of PITAP, however, can handle any number of side-by-side nozzles in a row, adding  $n-1$  twinning penalties for  $n$  nozzles.)

The interference drag coefficients used in the table (Figure 46) at spacing ratios greater than those for which  $C_{D_I}$  is a maximum are based on data from References 12 and 13, which are in generally good agreement with recent data reported in Reference 14. At lower spacing ratios, the curves correspond to completely separated flow on the inside half of the nozzles and on the entire interfairing and base drag has been computed for this region.

Figure 46 has been shown to work quite well when applied to plug nozzles as well as convergent or convergent-divergent nozzles. In this case the equivalent nozzle concept is first used to estimate isolated nozzle drag, and then Figure 46 is used, with spacing ratio defined to be center-line spacing over fully expanded exit diameters. Figure 47 (from Reference 18) shows a comparison of twin-nacelle thrust-minus-drag predicted performance and measured performance for both plug and convergent-divergent nozzles. Although the agreement is better for the convergent-divergent nozzles, in both cases the prediction is within about one per cent of gross thrust.

For nozzle interfairings that differ from clean sharp-edged fairings, a considerable amount of data (References 12, 14, 15, 16 and 17) is available, but reliable correlations of the interference effects as such do not exist.

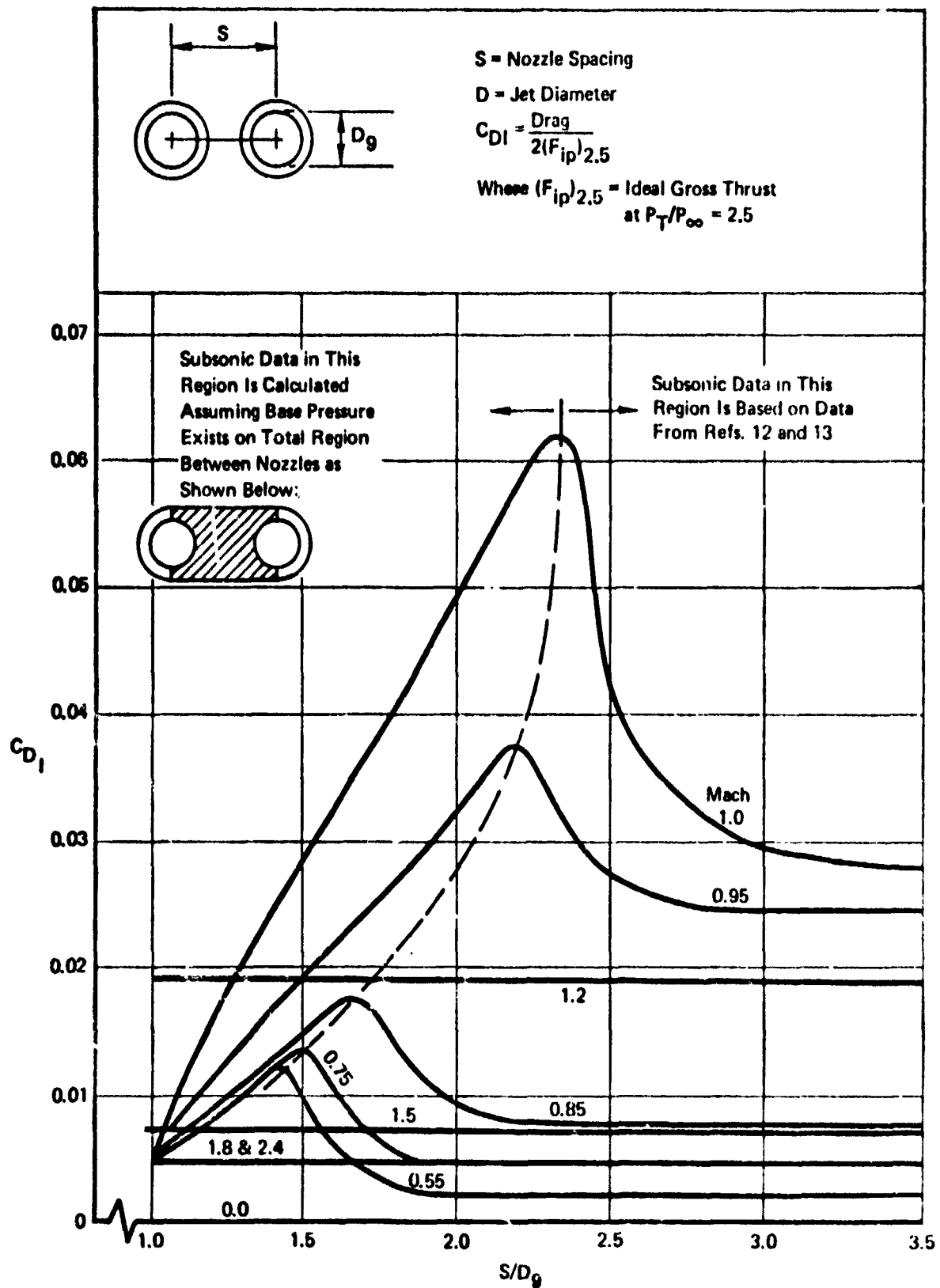


Figure 46: NOZZLE INTERFERENCE DRAG COEFFICIENT

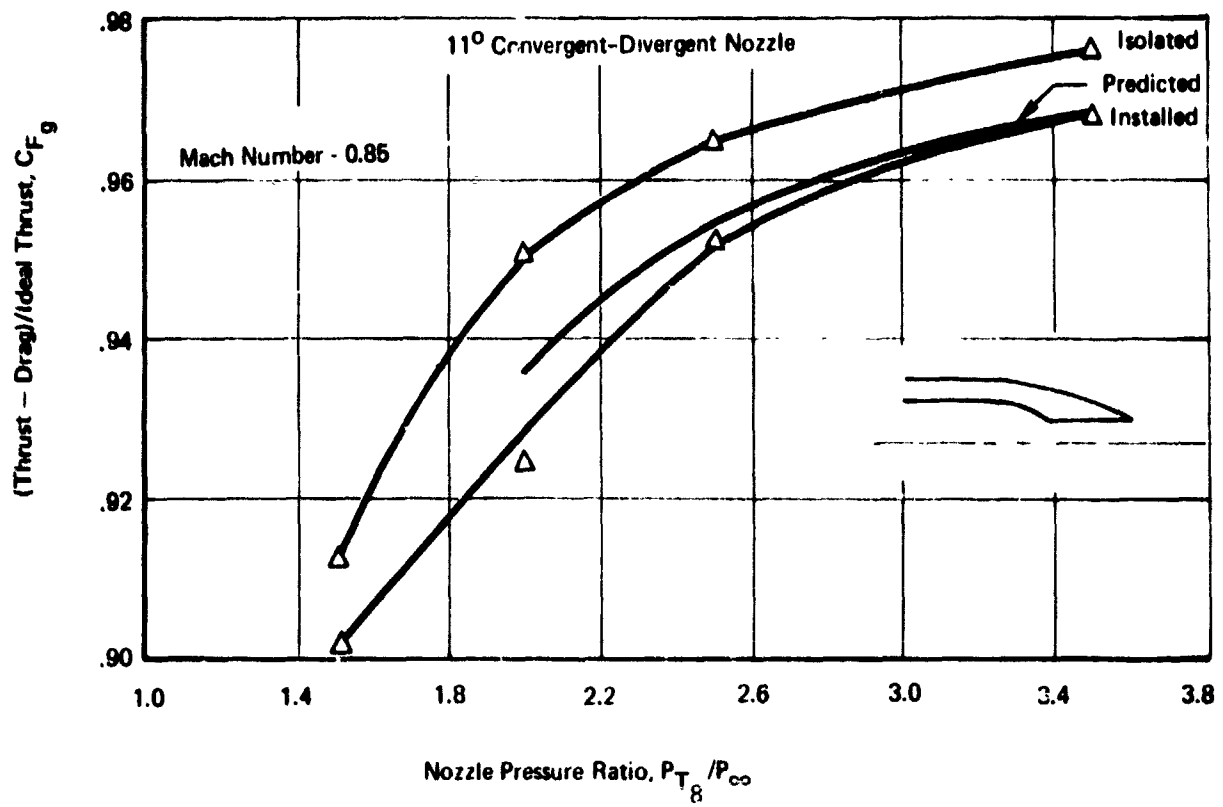
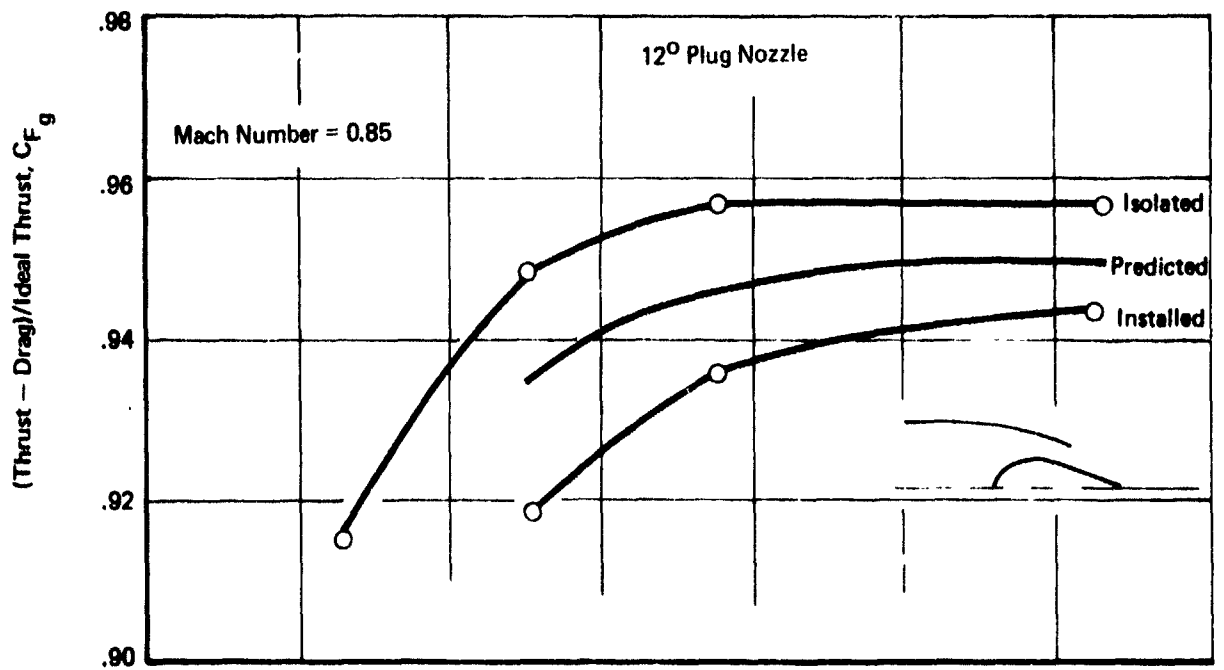


Figure 47: INSTALLATION EFFECTS FOR PLUG & CONVERGENT-DIVERGENT NOZZLES

In principle the interference table now in PITAP could be replaced by an additional table that would account for the interference between a strut-mounted engine and a wing, or perhaps an aft fuselage. A generalized table, however, applicable to a wide range of configurations would be extremely difficult to produce.

In a recent program at NASA Lewis (References 19, 20 and 21), interference effects between an underwing engine nacelle and an F106B wing were evaluated both in a wind tunnel test and in actual flight. A similar test with a simulated wing is also reported in Reference 22. These reports give pressure-integrated boattail drags, as well as some wing pressure data. Integrated forces on the wing must also be computed before total installation loss effects and interference effects can be extracted from the data. These tests also have limited applicability to the present program because the emphasis was on the interference effects for a limited range of nozzle geometric variations (e.g., only a 15 degree boattail angle was used) rather than the installation losses for a range of simulated power settings.

The pressure ratio correction used in PITAP is shown in Figure 42. The effect of increasing jet pressure ratio is two-fold. Increasing the size of the exhaust plume tends to force higher pressures on the nozzle surfaces, decreasing drag. Jet entrainment effects tend to pump down the pressure on nozzle surfaces, particularly where separated regions exist, increasing drag. Over a moderate range of pressure ratios these effects tend to cancel out. Reference 23 provides an example where these two opposing effects were isolated. Between jet-off conditions and a particular jet pressure ratio no net effect was observed. Using a solid plume simulator, thus eliminating entrainment effects, it was determined that the jet plume produced a favorable increase in isolated boattail drag coefficient of 0.02, while entrainment had accounted for -0.02.

The relative importance of entrainment and plume effects is a strong function of how much of the flow is separated or in a base region, and thus sensitive to entrainment effects. The Boeing data of Figure 48 clearly illustrates this phenomenon. The upper three bands of data represent twin nozzle configurations for which oil flow photographs revealed significant separated regions. Between a pressure ratio of two (barely more than ram pressure ratio) and four there is little apparent effect of pressure ratio on drag. The dashed line is a single nozzle reference configuration which had no separated flow. For this nozzle, plume effects cause a continuous reduction in drag with increasing pressure ratio.

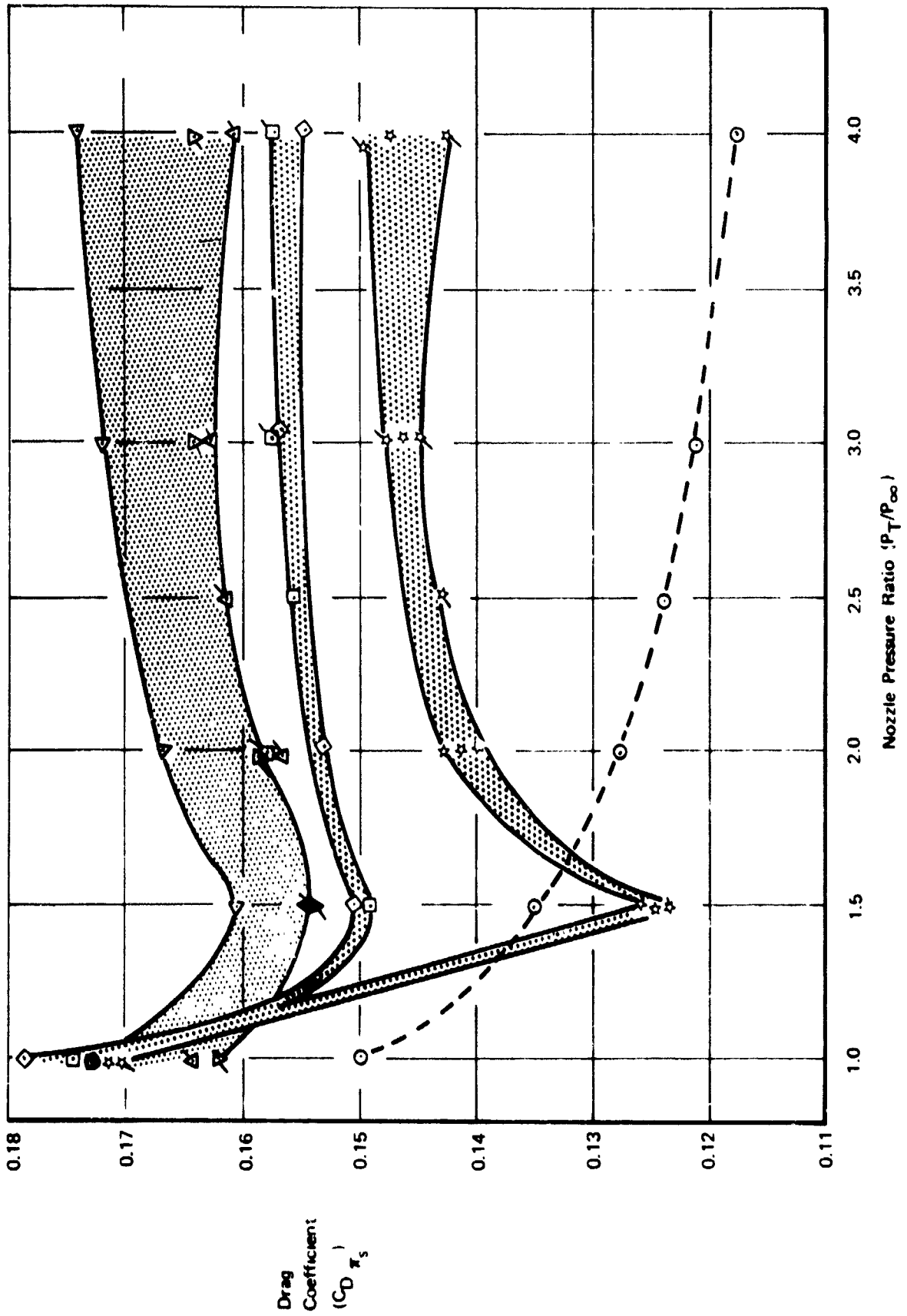


Figure 48: EFFECT OF NOZZLE PRESSURE RATIO ON AFT FUSELAGE DRAG - MACH 0.95

Similarly, in Figure 48, the highest angle nozzle does not benefit as much from high pressure ratio as the intermediate angle nozzles. (The low-angled nozzles are almost zero drag at the outset.)

Considerations such as these suggest that the pressure ratio effects might correlate well with the initial drag level at a reference pressure ratio. If the drag coefficient were normalized by the projected nozzle/afterbody external surface area, it represents a measure of how much separation existed at the reference nozzle pressure ratio.

### 5.2.3 Base Drag

The PITAP method is currently set up to receive an input table of base pressure coefficient versus Mach number for a specified afterbody geometry. It can use the base pressure coefficient from the input table and a specified base area to compute base drag as a function only of free-stream Mach number. However, to be throttle-sensitive, the base area must be located where it is also affected by the propulsive jet effects which vary with nozzle pressure ratio. In addition, the base pressure is known to be sensitive to approaching boundary layer conditions. Therefore, methods to account for these effects should be incorporated into the calculation procedure to obtain an improved base pressure prediction.

Subsonically, the effects of the propulsive jet may be accounted for by using correlations obtained by McDonald and Hughes (Reference 24).

The McDonald and Hughes correlation gives the increment in base pressure coefficient between a base with no jet effects and one with a jet of a given nozzle pressure ratio and a given temperature. The correlation is presented in Reference 24 for a free-stream Mach number of 0.9 and jet total pressure ratios of 2.0 and 3.0. The correlation is seen to work for approach boattail angles from 8 to 24 degrees, and specifically treats the case of an annular base around the jet. The key correlating parameter is the jet diameter squared divided by the product of the base diameter and the maximum diameter. Figure 49 presents this correlation for a jet pressure ratio of 2.0. The success of this parameter in correlating the data at Mach 0.9 suggests that it be tried at other subsonic Mach numbers. The method of McDonald and Hughes for Mach 0.90 is now programmed into PITAP.

For supersonic Mach numbers, from 1.0 to 2.2, an excellent base pressure correlation has been reported in Reference 25.

- $P_{TJ}$  = Propulsive Jet Total Pressure
- $P_{\infty}$  = Freestream Static Pressure
- $\Delta C_{pb}$  = Base Pressure Increment
- $D_j$  = Jet Diameter
- $D_b$  = Base Diameter
- $D_m$  = Body Maximum Diameter
- $\beta$  = Boattail Angle

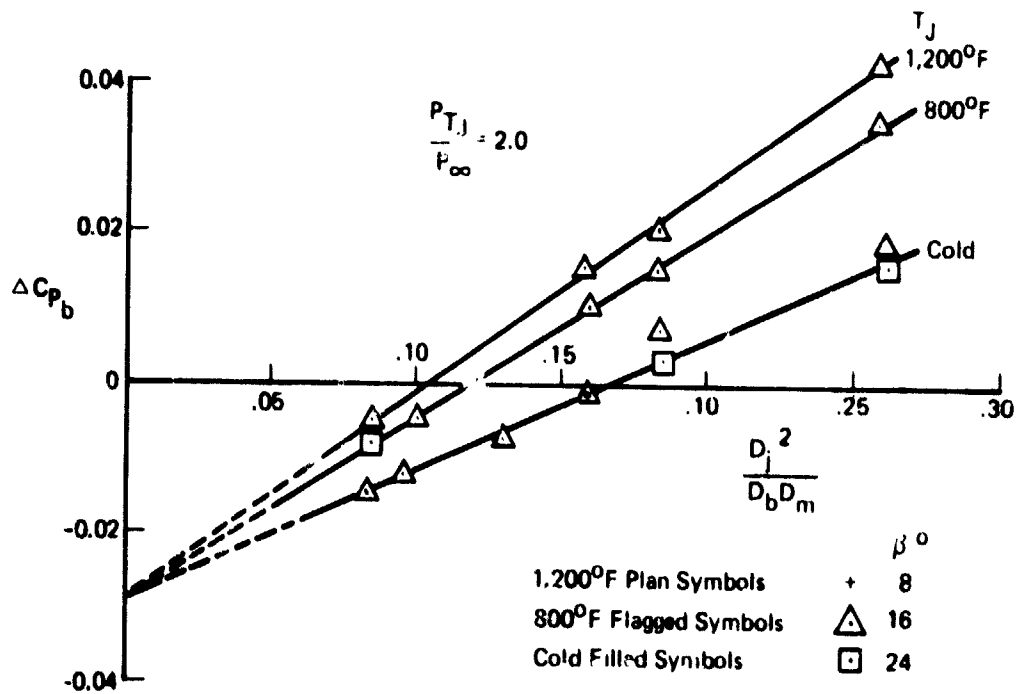
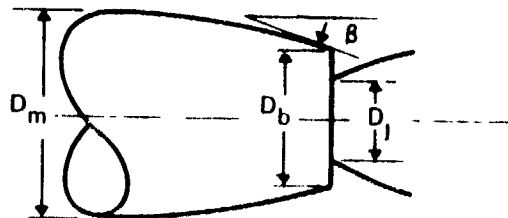


**Figure 49: CORRELATION OF INCREMENTAL BASE PRESSURE DUE TO PROPULSIVE JET AS A FUNCTION OF JET TO BASE-TO-MAXIMUM BODY DIAMETER FUNCTION**

Using correlation parameters called B and C which involve a reference base pressure level and known information about nozzle geometry and pressure ratio, a remarkable collapsing of the available data is obtained, as shown in Figure 50.

The parameters B and C are defined below:

$$B = M_\infty \ln^{-1} (.815 - 1.15 \ln K) \left(\frac{P_b}{P_\infty}\right)_M \left(\frac{P_b}{P_\infty}\right)_K$$

where  $\left(\frac{P_b}{P_\infty}\right)_M$  = model base pressure ratio

$\left(\frac{P_b}{P_\infty}\right)_K$  = base pressure ratio at K from Figure 50

$$K = \frac{M_\infty P_B + M_j P_j}{P_e}$$

$M_j$  = Mach number corresponding to nozzle pressure ratio

$P_B$  = base perimeter exposed to free-stream

$P_j$  = jet perimeter

$P_e$  = perimeter of circle of area equal to the base area

$$C = (.37M_\infty + 0.62) M_{j\text{design}} \frac{2(D_b/D_j) - 1.5}{10} M_{j\text{design}} \frac{A_j}{A_j + A_B} \frac{P_{je}}{P_e}$$

where  $D_b$  = base diameter

$D_j$  = jet exit diameter

$M_{j\text{design}}$  = nozzle design exit Mach number

$A_j$  = jet exit area

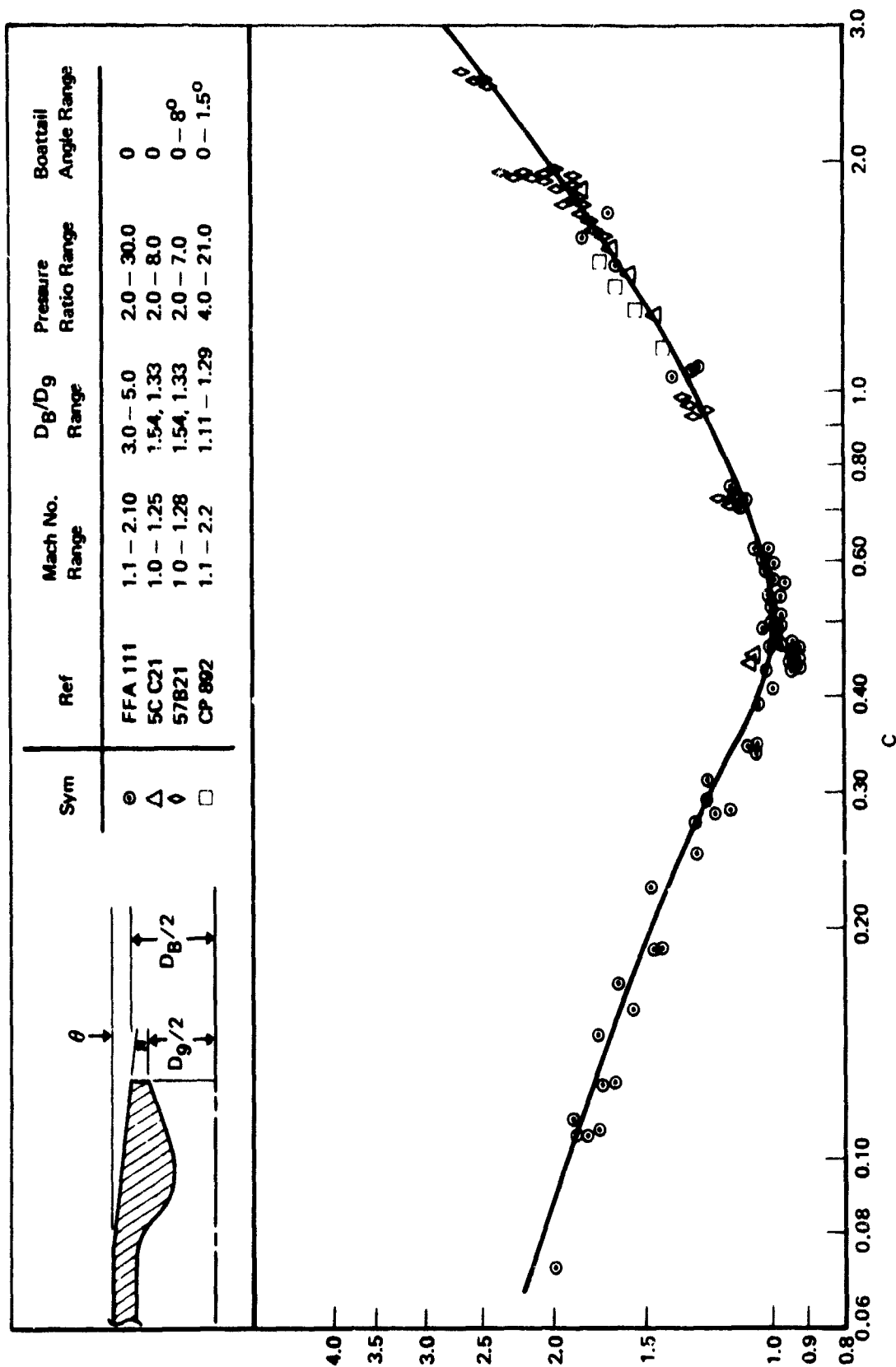


Figure 50: ANNULAR SUPERSONIC BASE PRESSURE CORRELATION

$A_B$  = base area

$P_{j_e}$  = nozzle exit static pressure (just inside the nozzle)

The parameter  $(P_b/P_\infty)_K$  is plotted as a function of  $K$  in Figure 51.  $B$  is plotted as a function of  $C$  in Figure 50.

The procedure for determining base drag is then:

1. Compute  $C$
2. Find the corresponding  $B$  from Figure 49.
3. Compute  $K$
4. Find  $(P_b/P_\infty)_K$  from Figure 50.

5. Compute  $(P_b/P_\infty)_M$  from  $B$  and  $(P_b/P_\infty)_K$

6. 
$$C_{D_{BS}} = \frac{2 A_B}{\gamma M_\infty^2 A_M} \left( 1 - \left( \frac{P_b}{P_\infty} \right)_M \right)$$

A method to account for upstream boundary layer effects has been developed by Nash (Reference 26). Nash proposed a curve of the limiting value of the base pressure coefficient for zero boundary layer thickness as a function of Mach number. Then he obtained an impressive correlation (Figure 52) for the increment in base pressure coefficient due to a finite momentum thickness  $\theta$  approaching a base of effective height  $h$ . Thus the base pressure coefficient in the absence of jet effects can be estimated. The momentum thickness,  $\theta$ , to make use of the correlation can be obtained from experimental data, detailed theoretical calculations, or engineering procedures, as time permits.

#### 5.2.4 Scrubbing Drag

Provisions for scrubbing drag calculations follow the method of Reference 27, which has been used to correct the 747 JT9D engine uninstalled performance for the scrubbing drag due to the fan nozzle flow impinging on the nacelle afterbody.

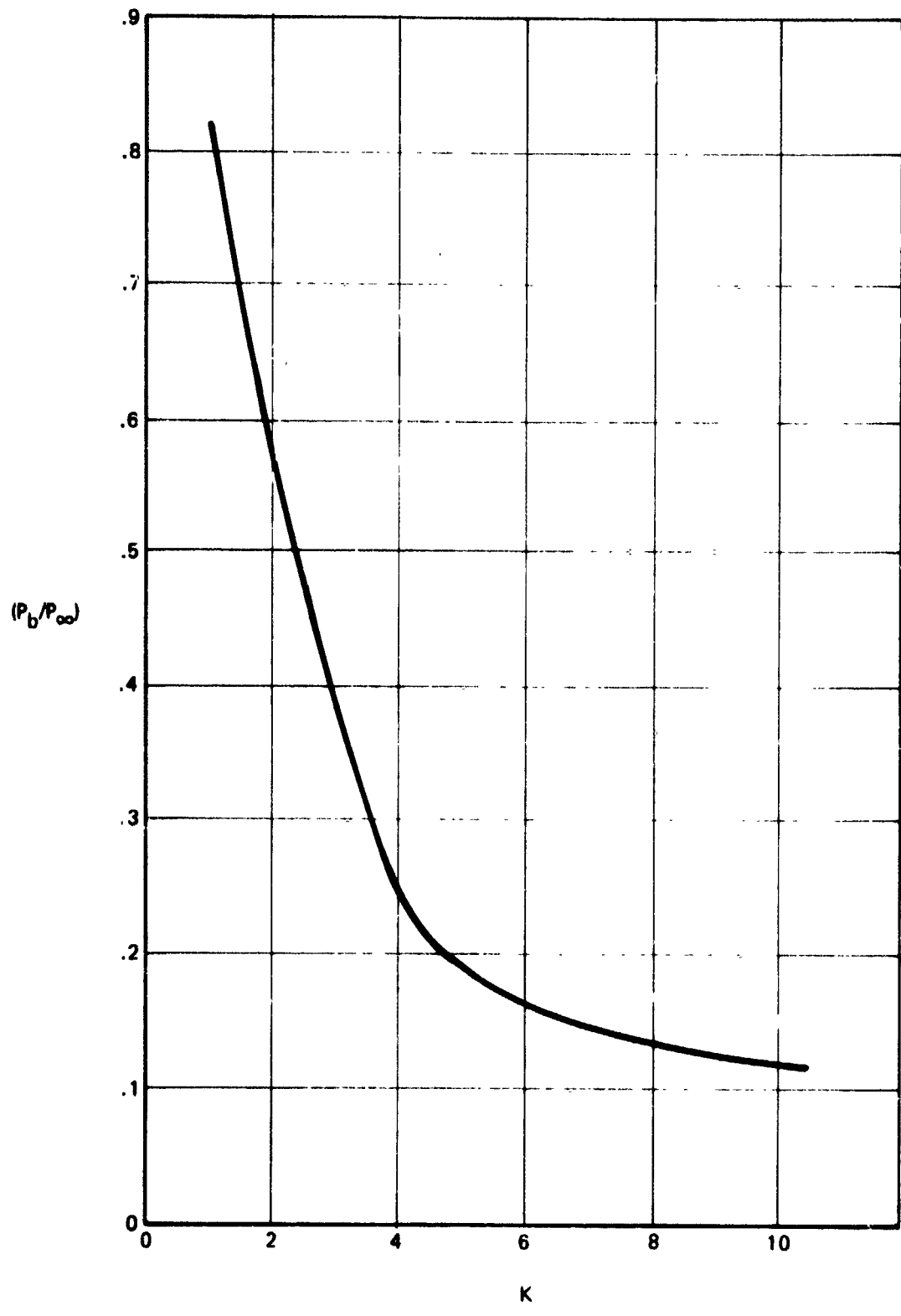


Figure 51: REFERENCE BASE PRESSURE RATIO

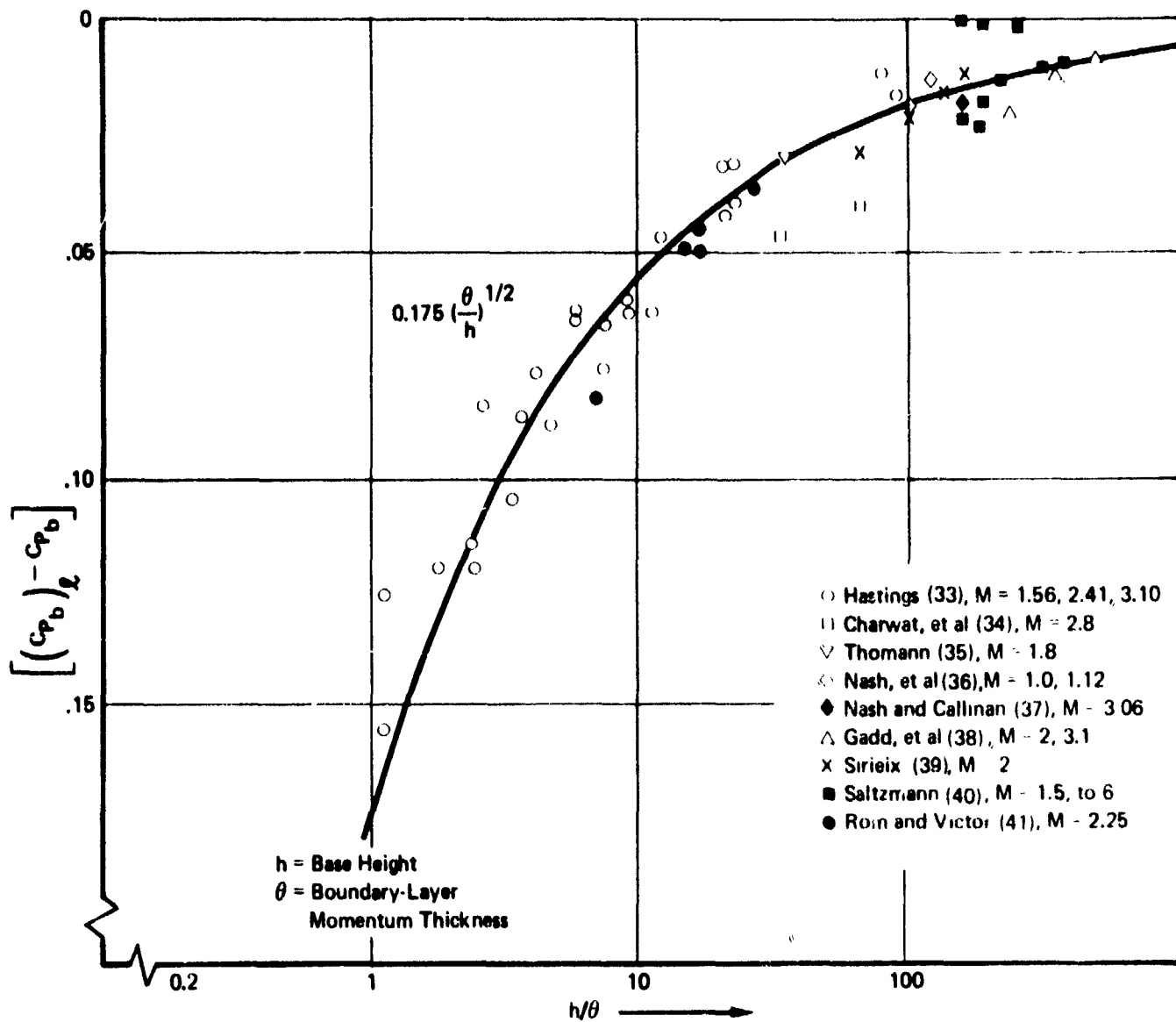


Figure 52: CORRELATION OF BASE PRESSURE DATA FOR SUPERSONIC FLOW

The method divides the calculation of viscous scrubbing drag into two parts: The portion of the flow from the nozzle exit to the end of the core flow, and the portion from the end of the core flow to the end of the afterbody. The flows differ in that the core region has a constant velocity scrubbing the surface, and the latter portion is in a region of velocity decay (Figure 53). For the region of the core the viscous drag is expressed as

$$D_C = 0.036b\rho v^{.2}V_J^{1.8}X_C^{.8}$$

where  $b$  = width

$\rho$  = density

$v$  = kinematic viscosity

$V_J$  = exhaust flow velocity

$X_C$  = core length

For the region beyond the core, the drag is expressed as

$$D = 0.0288b \int_{X_C}^{X_L} V_X \left[ \int_{X_C}^{X_L} \frac{1}{V_X^{.25}} dx + \frac{X_C}{V_J^{.25}} \right]^{.20} dx$$

Where  $V_X$  is the local velocity at station  $X$ .

The core length ( $X_C$ ) and velocity decay ( $V_X = f(X-X_C)$ ) at any point downstream of the core are determined using the method of Lawrence (Reference 27). The maximum velocity downstream of the core was correlated as

$$\frac{V_{MAX} - V_\infty}{V_J - V_\infty} = K \left( \frac{\Delta X}{h} \right)^B$$

Where

$V_{MAX}$  = maximum velocity downstream of  $X_{CORE}$

$V_J$  = fully expanded jet velocity

$V_\infty$  = free-stream velocity

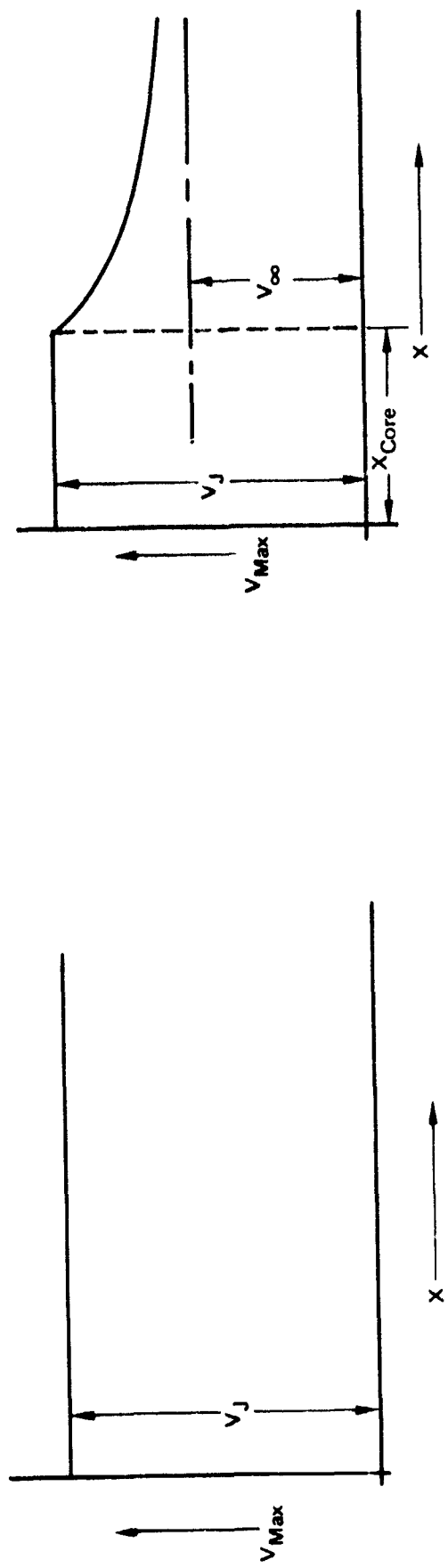
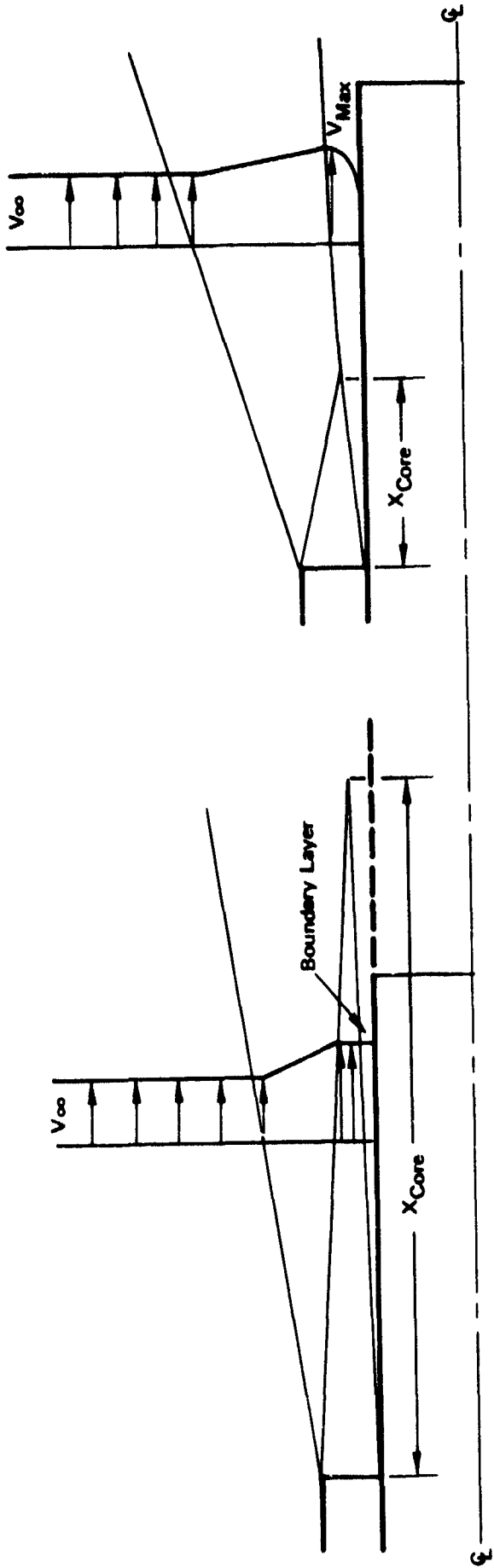


Figure 53: VELOCITY REGIONS FOR SCRUBBING DRAG CALCULATIONS

- K = velocity decay constant
- B = velocity decay exponent
- $\Delta X$  = local station downstream of  $X_{CORE}$
- h = flow height

The constants K and B were developed from wind tunnel data, and are presented in Figure 54. Intermediate values for other Mach numbers are assumed proportional to free-stream ram pressure ratio. Core length is calculated by setting  $V_j = V_{MAX}$  and solving directly for  $X_C$ .

The above method exists now in subroutine form (see Volume II).

### 5.3 ANGLE-OF-ATTACK EFFECTS

Angle-of-attack effects on nozzle internal performance and nozzle/afterbody drag are difficult to predict using techniques suitable for preliminary studies because the existing body of experimental data to show these effects is very limited. In addition, the data available are for specific configurations and cannot readily be generalized. Reference 31 contains experimental nozzle/afterbody data at angle-of-attack for a twin-engine fighter at Mach 0.9. These data show that there is negligible effect of angles-of-attack from -2 to +10 degrees on nozzle/afterbody drag for the tails-off configuration. When the tails are on, however, there is a large increase in drag due to angle-of-attack. There is not enough data, however, to determine how much the angle-of-attack drag increase depends on the particular configuration used.

Variations in angle-of-attack can affect the nozzle thrust coefficient by changing the local pressure field at the nozzle exit, and by introducing asymmetries and interactions into the nozzle exit flow field due to thinning, thickening, or separating the boundary layer ahead of the nozzle. The extent to which these effects alter the nozzle thrust depend on many variables, including nozzle geometry, pressure ratio, afterbody shape, fin location, and angle-of-attack range. No generalized data were located to predict these effects. It can be expected however, that for a choked, underexpanded nozzle at reasonably low area ratio, the effects of moderate changes in angle-of-attack on nozzle thrust coefficient,  $C_{Fg}$ , can be neglected for purposes of preliminary studies.

For most preliminary design studies, steady state cruise performance is emphasized, therefore, the effect of changes

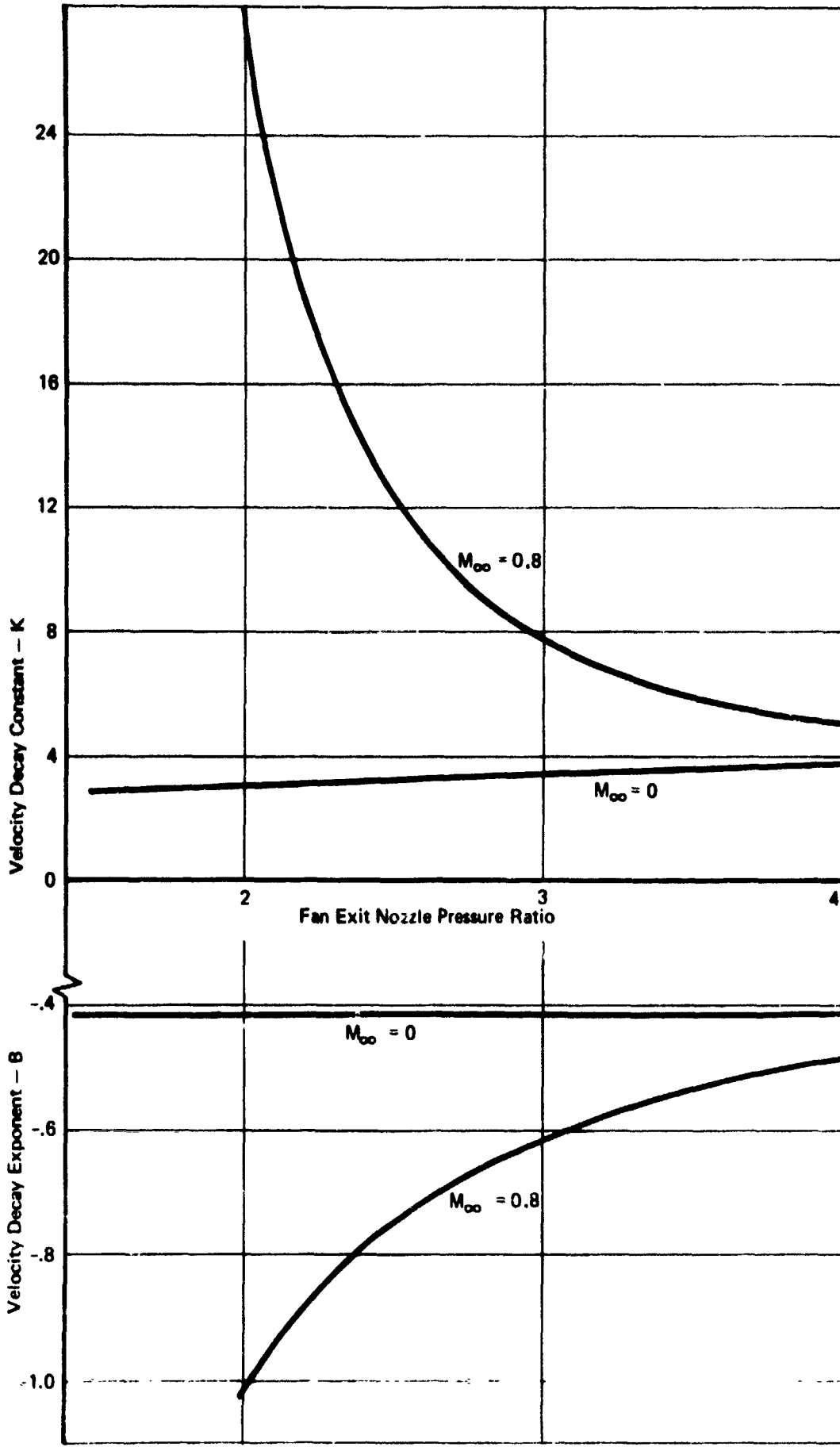


Figure 54: CORE LENGTH AND VELOCITY DECAY CONSTANTS

in angle-of-attack on afterbody drag is not of primary interest and can also be neglected.

If angle-of-attack performance is considered critical to the design, a more extensive study should be made of the particular configuration of interest to determine whether the effect is likely to be large or small.

#### 5.4 INSTALLATION EFFECTS OF THRUST VECTOR CONTROL AND THRUST REVERSERS

The installation of thrust vector control and thrust reverser equipment (in the stowed position) can create losses in internal thrust coefficient, increases in nozzle/afterbody drag, and increases in airplane weight.

To determine the magnitude of these losses and weight increases it is necessary to compare the performance and weight of various airplane design concepts which use thrust/vectoring and reversing installations with similar airplanes that do not have TR/TV installations. Only a limited amount of data are available from studies of this type, and the configurations are mostly of the V/STOL type. The results from recently completed Air Force Contract F33615-71-C-1850, (Reference 29) are used to illustrate the magnitude of the effects involved. The results, presented in Table IV, were obtained using a subsonic STOL transport as a basepoint. Various thrust vectoring and reversing installations were designed for the transport and the final performance and weights were compared with the basepoint to obtain the increments shown in Table IV. For a full description of the configuration, see Reference 29.

TABLE IV

Performance and Weight Changes Due to Thrust Vectoring and Reversing Installations

THRUST REVERSER CONCEPT	* $\Delta C_V$	* $\Delta C_D$	$\Delta Wt.$ lb. (Per Nacelle)
Externally-Blown Flap Systems	FAN 0.0 PRI 0.0	FAN 0.0 PRI +0.035	+730
Cascade Fan Thrust Reverser; Primary Spoiler unmixed flow engine	0.0	0.0	+930
Cascade Fan Thrust Reverser; Cycle Spoiling of Primary Thrust mixed flow engine	-0.024	+0.03	+930
Cascade Thrust Reverser; Clamshell Blocker Door mixed flow engine	+0.008	-0.006	+930
Mechanical Flap and Vectored Thrust Lift Systems	-0.009	-0.006	+1220
Multibearing Vectoring Nozzle; Cascade Fan Thrust Reverser; Cycle Spoiling of Primary Thrust mixed flow engine	+0.016	-0.043	+860

TABLE IV (Continued)

	* $\Delta C_V$	* $\Delta C_D$	$\Delta$ Wt. lb. (Per Nacelle)
Lobstertail Ext. Deflector; Cascade Fan Thrust Reverser; Cycle Spoiling of Primary Thrust mixed flow engine	+0.024	-0.030	+800
Two-Dimen. Vectoring Nozzle; Cascade Fan Thrust Reverser; Cycle Spoiling of Primary Thrust mixed flow engine	+0.002	-0.088	+1470
Rotating Nozzles; Thrust Vectoring and Reversing unmixed flow engine	FAN +0.012 PRI +0.005	FAN -0.014 PRI -0.041	+1260
Multibearing Vectoring/Reversing Nozzle mixed flow engine	+0.002	-0.036	+770
External Deflector/Target TR/TV System mixed flow engine	+0.013	-0.014	+720
Multibearing Vectoring Nozzle Cascade Fan Thrust Reverser unmixed flow engine	FAN +0.011 PRI 0.0	FAN -0.010 PRI 0.0	+2680
External Deflector Thrust Vectoring; Cascade Fan Thrust Reverser; No Primary Reverser or Spoiler unmixed flow engine	FAN +0.011 PRI 0.0	FAN -0.010 PRI 0.0	+1900
External Deflector/Target TR/TV System (Dual Pod) mixed flow engine	-0.002	-0.037	+830

TABLE IV (Continued)

	* $\Delta C_V$	* $\Delta C_D$	$\Delta Wt.$ lb. (Per Nacelle)
Upper Surface Flowing Lift Systems			
Cascade Fan Thrust Reverser;	FAN 0.0	FAN 0.0	+840
Primary Thrust Spoiler unmixed flow engine	PRI 0.0	PRI -0.035	
External Target Thrust Reverser mixed flow engine	-0.02	0.0	+620

\* $C_V$  = Thrust Coefficient

$C_D$  = Discharge Coefficient

$$\Delta C_V = \frac{\Delta F}{F_i}; \Delta C_D = \frac{\Delta F'}{W_{Initial}} \text{Ideal}$$

Based on the data presented in Table IV, it appears that the installation of thrust vectoring and reversing equipment can change the nozzle internal thrust coefficient by as much as  $-0.024$  to  $+0.024$  and increase the weight from 620 to 2680 lb. for a typical subsonic STOL airplane. Since the weight effect appears to be the most significant effect, it is expected that the effect of these installations in supersonic aircraft would result in somewhat more severe penalties to the mission range due to the decreased L/D ratios as design Mach number is increased.

## REFERENCES

1. Keenan, J. H., and Kaye, J., Gas Tables, John Wiley and Sons, New York, 1954.
2. Johnson, T. J., and Huff, J. H., Propulsion System Integration and Test Program (Steady State), Part IV. Inlet Drag Tests, AFAPL-TR-69-44, Air Force Aero Propulsion Laboratory, June 1969.
3. Johnson, T. J., and Young, L. C., Summary of Methods for Calculating Inlet Performance Losses, TFD-67-767, North American Rockwell Corp., L. A. Division, 1967.
4. Ball, W. H., Design Studies of a Supersonic Transport Propulsion System with Dual-Inlet/Engine Pods, D6A11445-1, The Boeing Company, Seattle, Washington, October 1970.
5. 2707-300PPD Airplane Propulsion System Validation Document, Section 3, Intake System, The Boeing Company, Seattle, Washington, 1969.
6. Young, L. C., Design Concepts for Inlets and Exhaust Nozzles, TFD-64-170, North American Rockwell Corp., Los Angeles, California, 1964.
7. Peterson, M. W., and Tamplin, G. C., Experimental Review of Transonic Spillage Drag of Rectangular Inlets, AFAPL-TR-66-30, Air Force Aero Propulsion Laboratory, WPAFB, Ohio, May 1966.
8. Osmon, R. V., Supersonic Inlet Performance Prediction for Single-Cone, and Two-Dimensional Inlets, ASNF-69-1-Vol. I, Aeronautical Systems Division, Wright-Patterson Air Force Base, Ohio, March, 1970.
9. Ross, P. A., Lightweight Fighter Propulsion System Development, D180-14475-1 TN, The Boeing Company, Seattle, Washington, January 1973.
10. Bernstein, A., Heiser, W., and Hevenor, C., Compound-Compressible Nozzle Flow, AIAA Paper No. 66-663, 1966.
11. Hiatt, D. L., Supersonic Boattail Wave Drag, Coordination Sheet ME-RES-593, The Boeing Company, 1969.

12. Mercer, C. E., and Berrier, B. L., Effect of Afterbody Shape, Nozzle Type, and Engine Lateral Spacing on the Installed Performance of a Twin-Jet Afterbody Model, NASA TM X-1855, September 1969 (Confidential).
13. Miller, S. R., and Salemann, V., Twin Engine Fighter Afterbody and Nozzle Tests, Mach 0.85 to 2.2, Report No. 1, Document D6-18088, The Boeing Company, Seattle, Washington, 1966.
14. Phase II Oral Review, Program for Experimental and Analytical Determination of Integrated Airframe-Nozzle Performance, Report LR 25153, Lockheed-California Company, February 29, 1972.
15. Misoda, P., SST Twin Engine Propulsion Pod Nozzle Study, Document D6A11701-1, The Boeing Company, Seattle, Washington, 1971.
16. Maiden, D. L., and Runckel, J. F., Effect of Nozzle Lateral Spacing on Afterbody Drag and Performance of Twin-Jet Afterbody Models with Convergent Nozzles at Mach numbers up to 2.2, NASA TM X-2099, 1970.
17. Salemann, V., Twin-Engine-Fighter Afterbody and Nozzle Wind Tunnel Tests, Mach 0.85 to 0.95, Report No. 2, Document D6-60033, The Boeing Company, Seattle, Washington, 1966.
18. Miller, S. R., Installation Effects on Plug Nozzle Performance at Subsonic Speeds, Document D162-10184-1, The Boeing Company, Seattle, Washington, 1971.
19. Blaha, B. J., and Mikkelson, D. C., Wind Tunnel Investigation of Airframe Installation Effects on Underwing Engine Nacelles at Mach Numbers from 0.56 to 1.46, NASA TM X-1683, 1968.
20. Mikkelson, D. C., and Head, V. L., Flight Investigation of Airframe Installation Effects on a Variable Flap Ejector Nozzle of an Underwing Engine Nacelle at Mach Numbers from 0.6 to 1.3, NASA TM X-2010, 1970.
21. Blaha, B. J., Effect of Underwing Engine Nacelle Shape and Location on Boattail Drag and Wing Pressures at Mach Numbers from 0.56 to 1.46, NASA TM X-1979, 1970.
22. Shrewsbury, G. D., Effect of a Simulated Wing on the Pressure-Drag Coefficients of Various 15 Degree Boattails at Mach Numbers from 0.56 to 1.00, NASA TM X-1662, 1968.

23. Bergman, D., "Effects of Engine Exhaust Flow on Boattail Drag", *Journal of Aircraft*, Vol. 8, No. 6, 1970.
24. McDonald, H., and Hughes, P. F., "A Correlation of High Subsonic Afterbody Drag in the Presence of a Propulsive Jet or Support Sting", *Journal of Aircraft*, Vol. 2, No. 3, 1965.
25. Miller, S. R., Prediction of Supersonic Axisymmetric Base Drag in the Presence of a Supersonic Jet, Memo METM 69-6, The Boeing Company, Seattle, Washington, 1969.
26. Nash, J. F., A Discussion of Two-Dimensional Turbulent Base Flows, NPL Aero Report 1162, 1965.
27. Lawrence, R. L., "Afterbody Flow Fields and Skin Friction on Short Duct Fan Nacelles", *Journal of Aircraft*, Vol. 2, No. 4, 1965.
28. Postlewaite, J. E., "Thrust Performance of Suppression Nozzles", *AIAA Journal of Aircraft*, July 1966.
29. Petit, J. E., and Scholey, M. B., STOL Transport Thrust Reverser/Vectoring Program, AFAPL-TR-72-109 Vol. 2, Air Force Aero Propulsion Laboratory, WPAFB, Ohio, December 1972.
30. Byrd, K. F., Oller, T. I., and Lichtman, E. A., Military High Mach Exhaust System Design Philosophy, Paper Presented at the AIAA/SAE 8th Propulsion Joint Specialists Conference, New Orleans, Louisiana, November 29 - December 1, 1972.
31. Castells, O. T., et al, Twin Jet Exhaust System Interaction Test, Report No. R72AEG235, General Electric Company, Evandale, Ohio, August 4, 1972.
32. Connors, J. F., and Meyer, R. C., Design Criteria for Axisymmetric and Two-Dimensional Supersonic Inlets and Exits, NACA TN 3589, 1956.
33. Hastings, R. C., Turbulent Flow Past Two-Dimensional Bases in Supersonic Streams, R. A. E. Tech Note Aero 2931, December 1963. Also A. R. C. 26117 - F. M. 3496-Perf. 2336, August 7, 1964.
34. Charwat, A. F., et al, "An Investigation of Separated Flows; Part 1. The Pressure Field," *Journal of Aero/Space Sciences*, Vol. 28, p. 457, June 1961.

35. Thomann, H., Measurements of Heat Transfer and Recovery Temperature in Regions of Separated Flow at a Mach Number of 1.8, F. F. A. Rep. 82, 1959.
36. Nash, J. F., et al, Experiments on Two-Dimensional Base Flow at Subsonic and Transonic Speeds, N. P. L. Aero Report 1070, January 1963. A. R. C. 25070-F. M. 3356 - Perf. 2226 - P. A. 955. January 21, 1963.
37. Nash, J. F., and Callinan, J., The Use of a Ventilated Cavity as a Means of Increasing Base Pressure at Supersonic Speeds, NPL Paper, 1965.
38. Gadd, G. E., et al, Base Pressures in Supersonic Flow, A. R. C. C. P. 271, March 1955.
39. Sirieix, M., "Pression de Culot et Processus de Mélange Turbulent en Écoulement Supersonique Plan", La Recherche Aeronautique, No. 78, p. 13, September/October, 1960.
40. Saltzman, E. J., Base Pressure Coefficients Obtained from the X-15 Airplane for Mach Numbers up to 6, NASA TN D-2420, August 1964.
41. Rom, J., and Victor, M., "Base Pressure Behind Two-Dimensional and Axially-Symmetric Backward Facing Steps in a Turbulent Supersonic Flow", Israel. J. M. Tech. Vol. 2., No. 1, February 1964.
42. Bryson, A. E., An Experimental Investigation of Transonic Flow Past Two-Dimensional Wedge and Circular-Arc Sections Using a Mach-Zehnder Interferometer, NACA TN 2560, 1951.
43. Thornock, Russel L., Experimental Investigation of the Flow Through Convergent Conical Nozzles, D6-20375, The Boeing Company, Seattle, Washington, Sept. 1968.
44. Salemann, V., Exhaust System Interaction Program, Fifth Quarterly Report, D162-10467-2, The Boeing Company, Seattle, Washington, July 1971.

APPENDIX

ENGINEERING FLOW CHARTS

\* Tables indicated by arabic numbers (in Figures 55 - 59) such as Table 7, refer to the tables sketched in Figures 9 and 10.

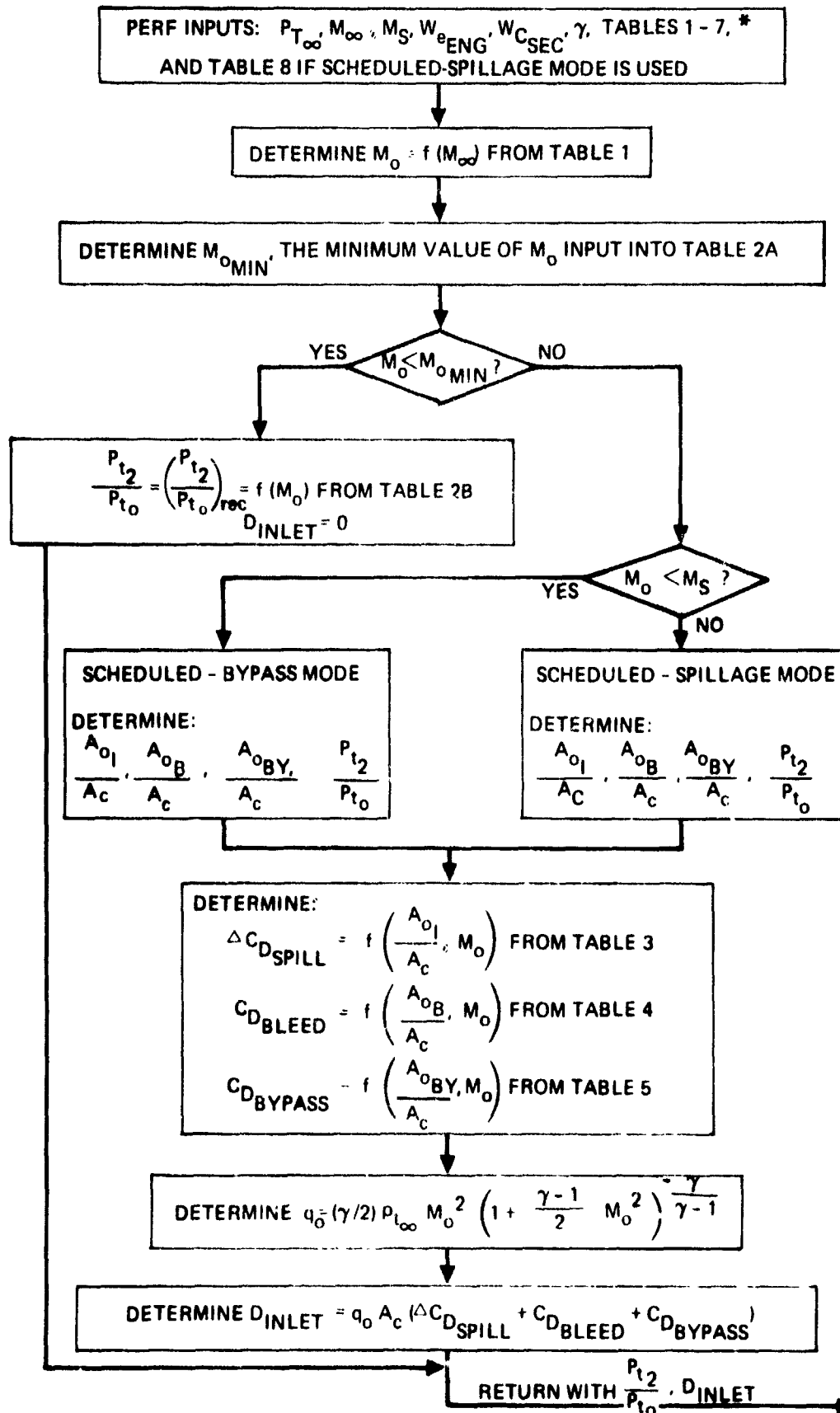


Figure 55. FLOW CHART FOR INLET PERFORMANCE

AREA FUNCTION  $F_1 (M, \gamma)$ :

$$F_1 (M, \gamma) = (0.013858) \frac{\left(1 + \left[\frac{\gamma-1}{2}\right] M^2\right)^{\frac{\gamma+1}{2(\gamma-1)}}}{M \sqrt{\gamma}}$$

AIRFLOW DEMAND FUNCTION  $F_2 \left( \frac{P_{t2}}{P_{t0}}; M_0, W_{cENG}, W_{cSEC}, A_c, \gamma \right)$ .

$$\frac{A_{0ENG}}{A_c} = \frac{F_1 (M_0, \gamma)}{A_c} \left\{ W_{cENG} \right\} \left( \frac{P_{t2}}{P_{t0}} \right)$$

$$\frac{A_{0BY}}{A_c} = f \left( \frac{A_{0ENG}}{A_c}, M_0 \right) \text{ FROM TABLE 7}$$

$$F_2 = \frac{F_1 (M_0, \gamma)}{A_c} \left\{ W_{cENG} + W_{cSEC} \right\} \left( \frac{P_{t2}}{P_{t0}} \right) + \frac{A_{0BY}}{A_c}$$

Figure 56: INLET FUNCTIONS

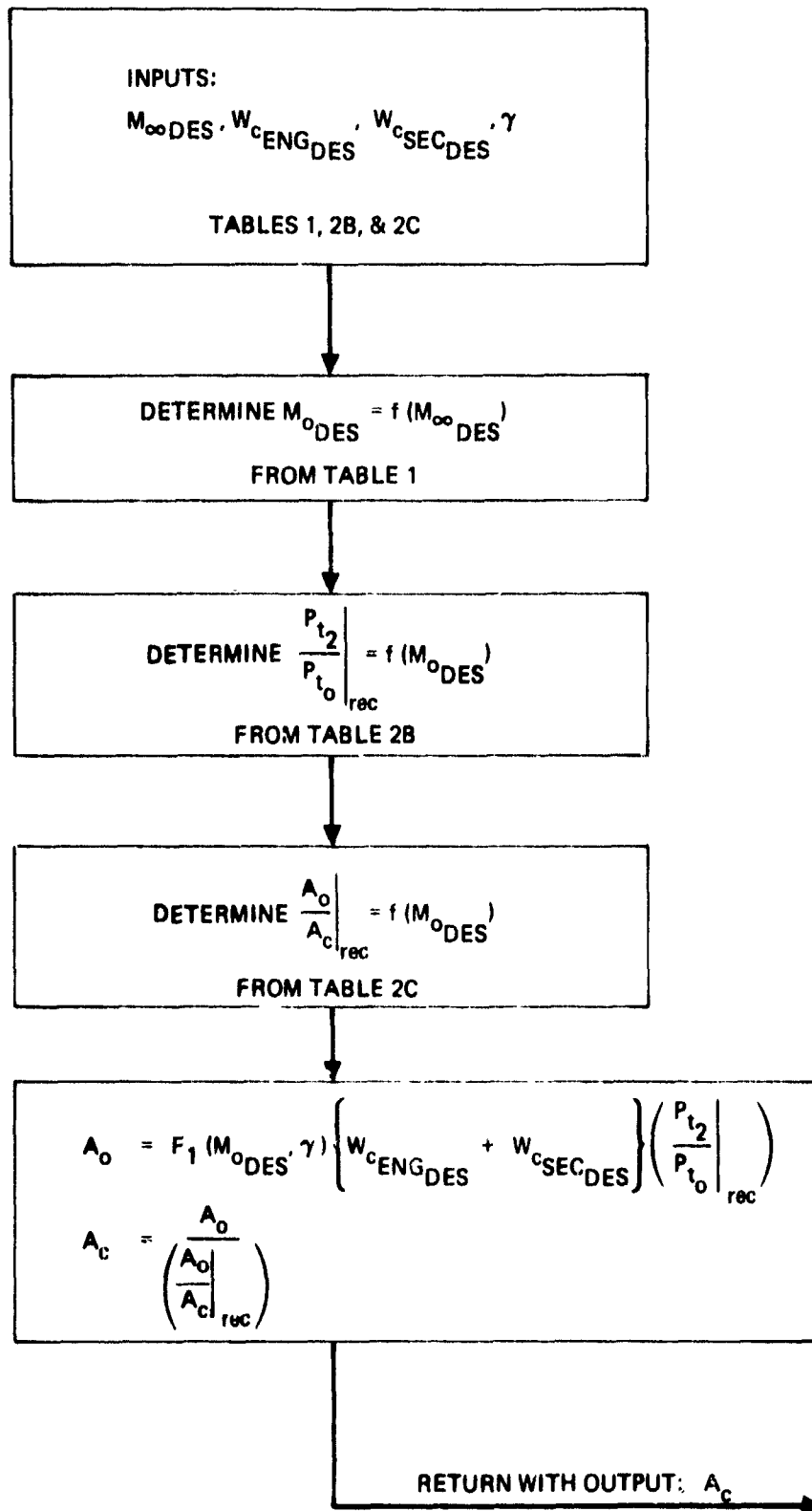


Figure 57: FLOW CHART FOR INLET SIZING SUBROUTINE

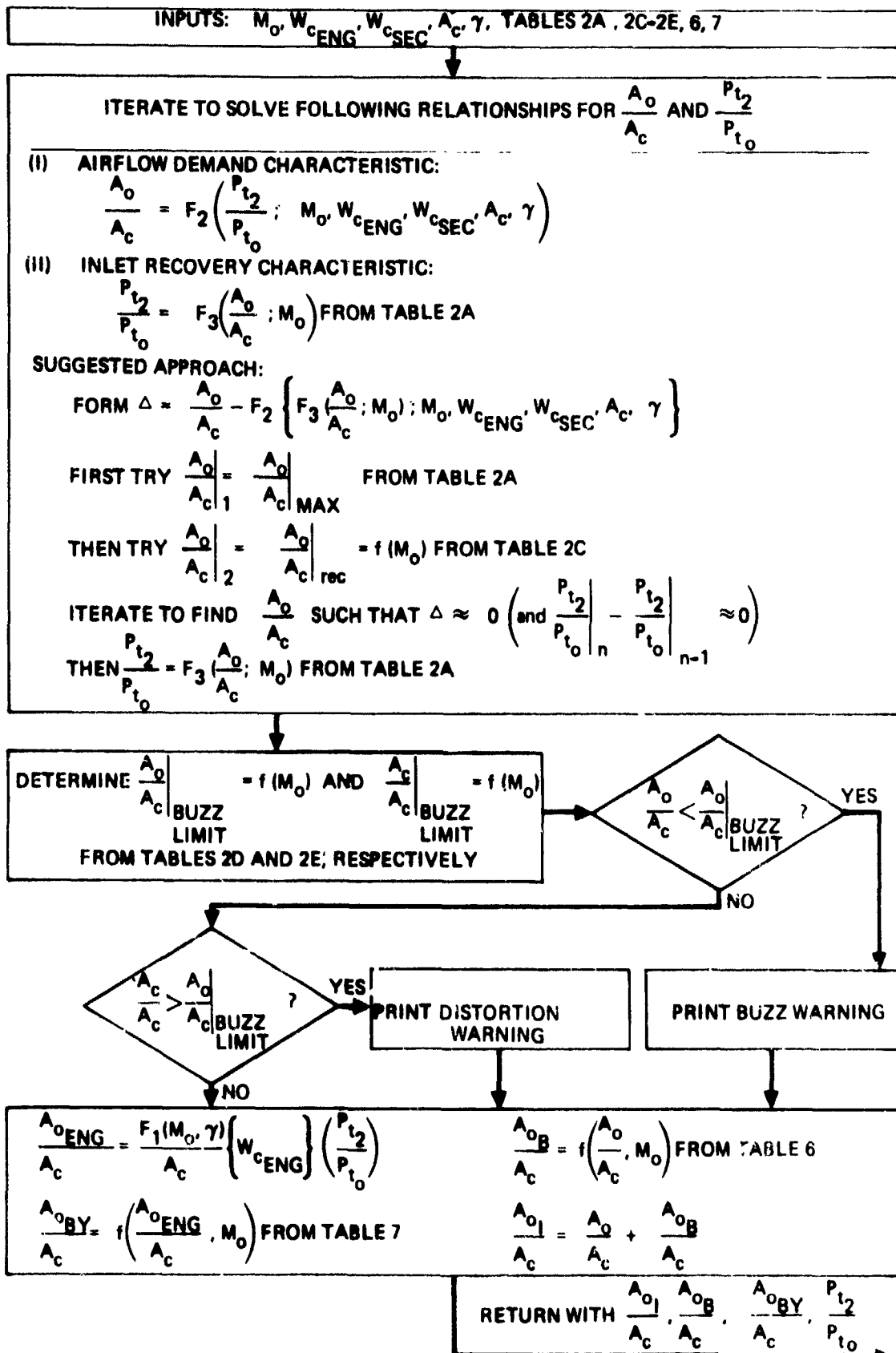


Figure 58: FLOW CHART FOR SCHEDULED-BYPASS MODE

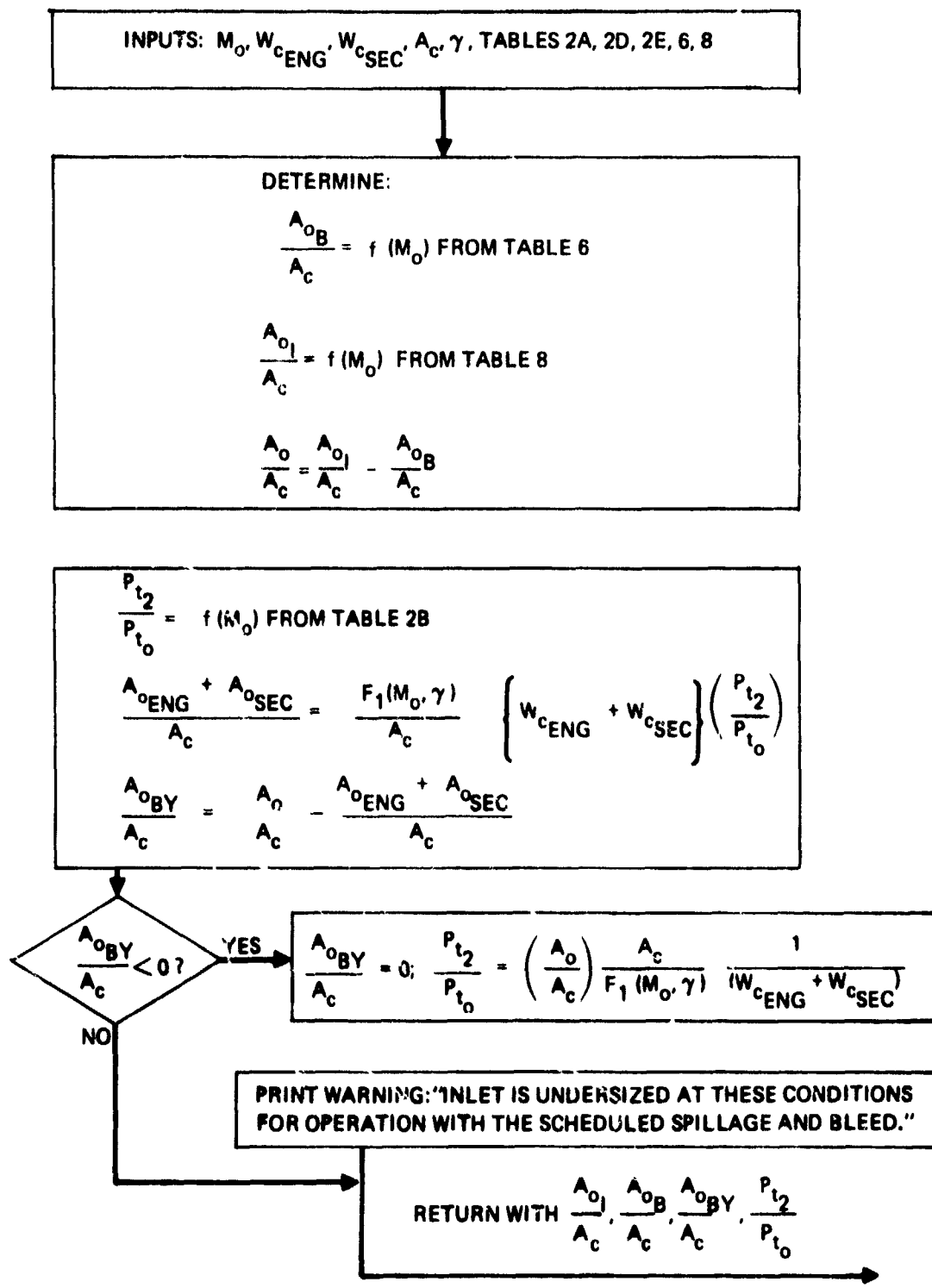


Figure 59: FLOW CHART FOR SCHEDULED-SPILLAGE MODE

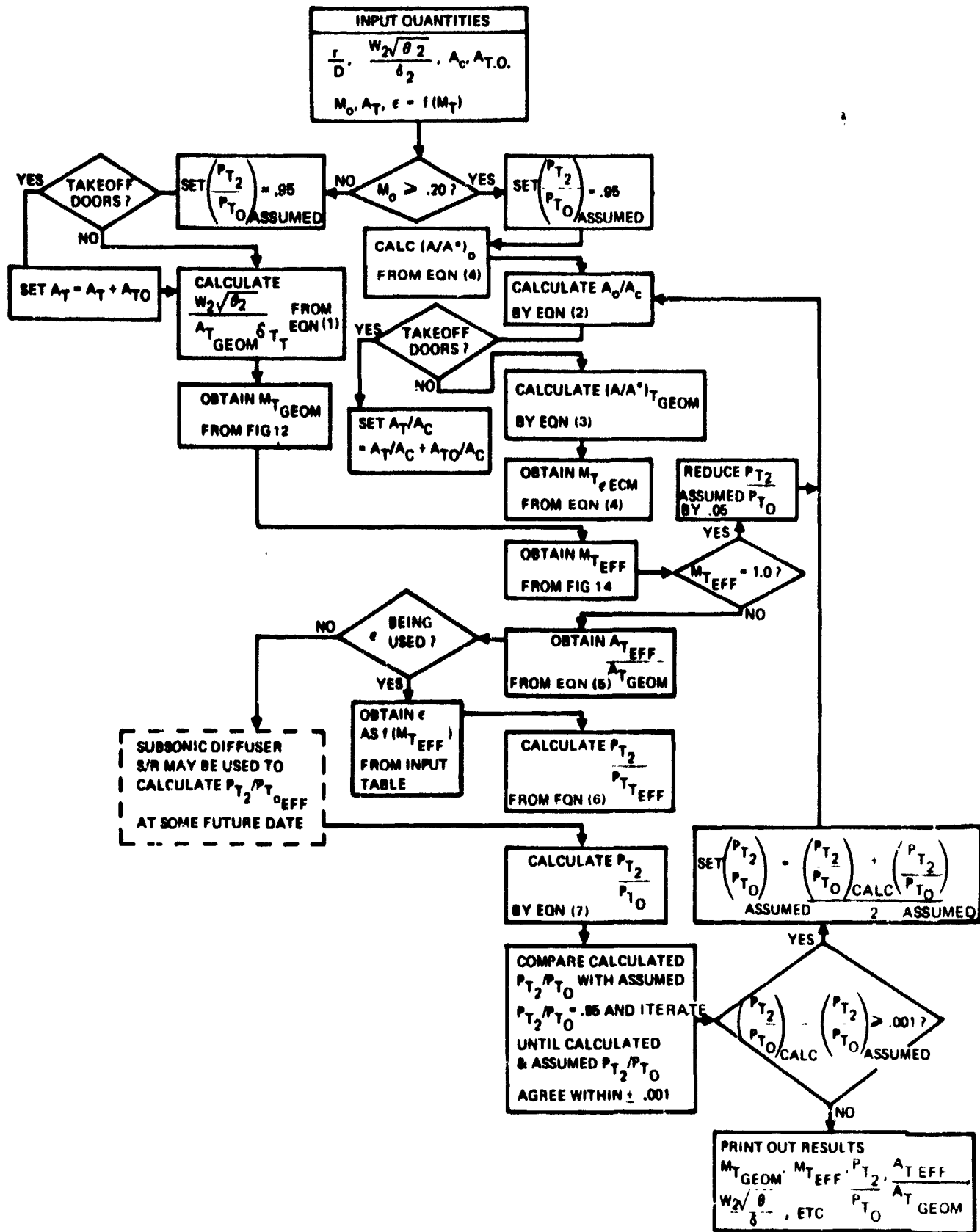


Figure 60: FLOW CHART FOR LOW SPEED INLET PERFORMANCE CALCULATION

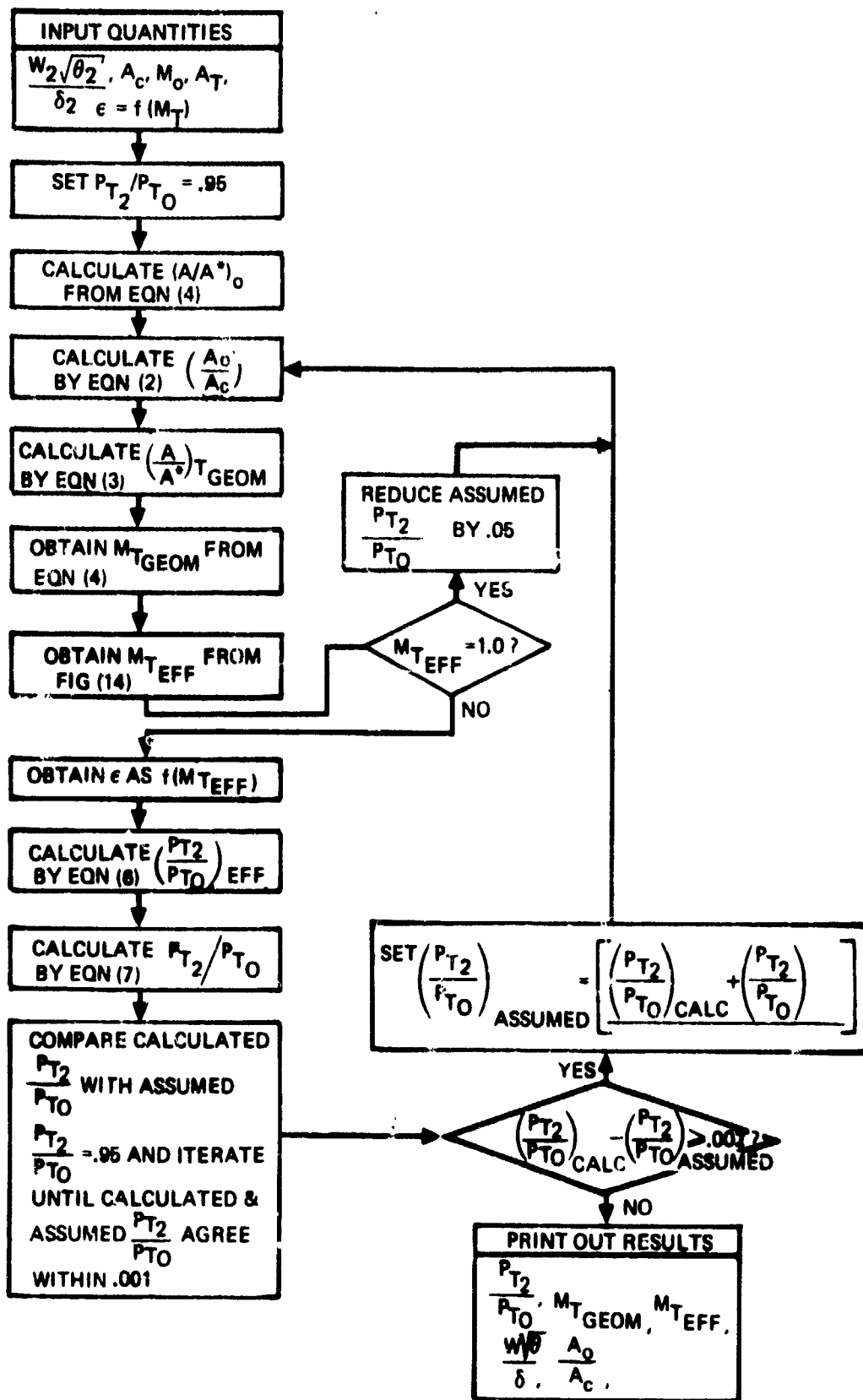


Figure 61: FLOW CHART FOR SUBSONIC AND TRANSONIC INLET INTERNAL PERFORMANCE CALCULATION





(CAN BE USED FOR BOUNDARY LAYER BLEED OR BYPASS)

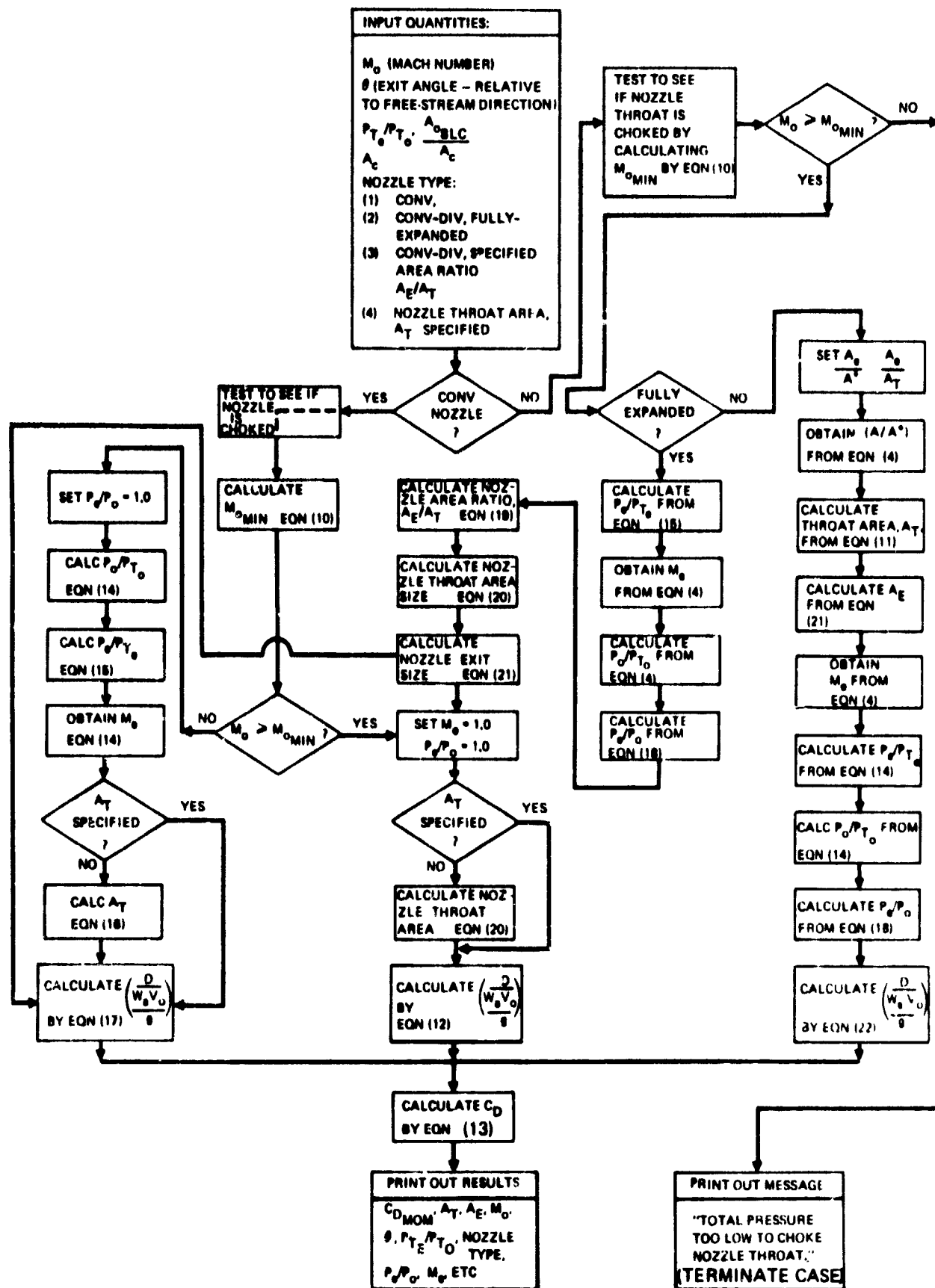


Figure 64: FLOW CHART FOR MOMENTUM DRAG CALCULATION

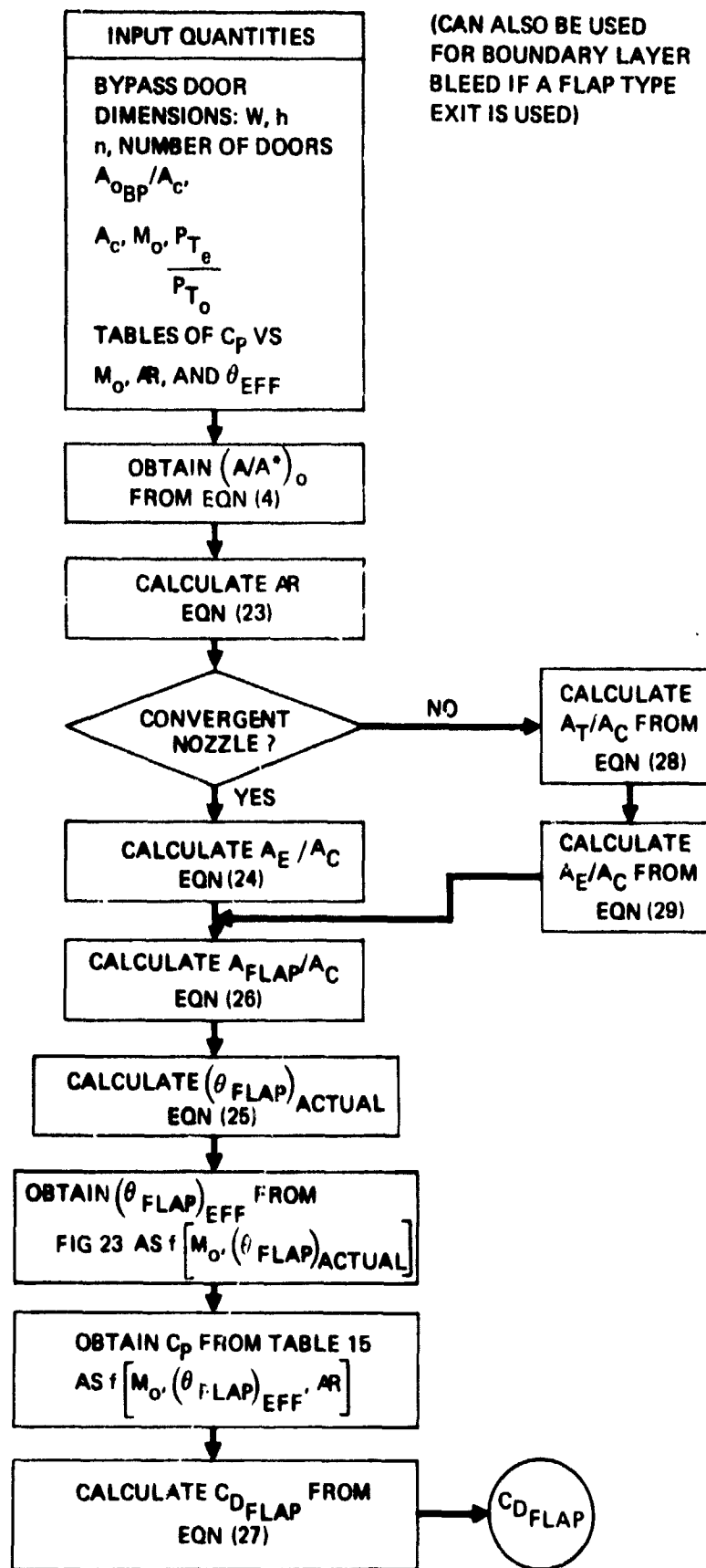


Figure 65: FLOW CHART FOR BYPASS FLAP DRAG CALCULATION

Unclassified

Security Classification

DOCUMENT CONTROL DATA - R & D

(Security classification of title, body of abstract and indexing annotation must be entered when the overall report is classified)

1. ORIGINATING ACTIVITY (Corporate author) The Boeing Company P. O. Box 3999 Seattle, WA 98124		2a. REPORT SECURITY CLASSIFICATION Unclassified	
		2b. GROUP	
3. REPORT TITLE Propulsion System Installation Corrections Volume I: Engineers Manual			
4. DESCRIPTIVE NOTES (Type of report and inclusive dates) Final Report 31 December 1971 to 31 December 1972			
5. AUTHOR(S) (First name, middle initial, last name) William H. Ball			
6. REPORT DATE December 1972	7a. TOTAL NO OF PAGES xvi + 140 = 156	7b. NO OF REFS 44	
8a. CONTRACT OR GRANT NO F33615-72-C-1580	9a. ORIGINATOR'S REPORT NUMBER(S) AFFDL-TR-72-147		
b. PROJECT NO 1366	9b. OTHER REPORT NO(S) (Any other numbers that may be assigned this report)		
c.			
d.			
10. DISTRIBUTION STATEMENT Distribution limited to U.S. Government agencies only; test and evaluation; statement applied 29 December 1972. Other requests for this document must be referred to Air Force Flight Dynamics Laboratory, (PTB), Wright-Patterson Air Force Base, Ohio 45433			
11. SUPPLEMENTARY NOTES		12. SPONSORING MILITARY ACTIVITY Flight Dynamics Laboratory Air Force Systems Command Wright-Patterson Air Force Base, OH	
13. ABSTRACT This report presents the results of a research program to develop a procedure for use in calculating propulsion system installation losses. These losses include inlet and nozzle internal losses and external drag losses for a wide variety of subsonic and supersonic aircraft configurations up to Mach 4.5. The calculation procedure, which was largely developed from existing engineering procedures and experimental data, is suitable for preliminary studies of advanced aircraft configurations. Engineering descriptions, equations, and flow charts are provided to help in adapting the calculation procedures to digital computer routines. Many of the calculation procedures have already been programmed on the CDC 6600 computer. Program listings and flow charts are provided for the calculation procedures that have been programmed. The work accomplished during the program is contained in four separate volumes. Volume I contains an engineering description of the calculation procedures. Volume II is a programmers manual containing flow charts, listings, and subroutine descriptions. Volume III contains sample calculations and sample input data. Volume IV contains bookkeeping definitions and data correlations.			

KEY WORDS	LINK A		LINK B		LINK C	
	ROLE	WT	ROLE	WT	ROLE	WT
Afterbody Drag						
Boattail Drag						
Bookkeeping Aero-Propulsion Forces						
Boundary Layer Bleed Drag						
Bypass Drag						
Inlet Performance						
Inlet Shock Losses						
Nozzle/Afterbody Installation Losses						
Nozzle Interference Drag						
Nozzle Thrust Coefficient						
Propulsion Installation Losses						
Spillage Drag						
Subsonic Diffuser Losses						
Supersonic Inlets						
Total Pressure Recovery						